Analysis of inhibition effects on deep hydrodesulfurization using model reactions

Edgar Mauricio Morales Valencia

Tesis presentada como requisito para acceder al Título de: Doctor en Ingeniería Química

Director

Víctor Gabriel Baldovino Medrano

Ph.D. en Ingeniería Química.

Co-director

Carlos Omar Castillo Araiza

Ph.D. en Ingeniería Química

Universidad Industrial de Santander

Facultad de Ingenierías Fisicoquímicas

Escuela de Ingeniería Química

Doctorado en Ingeniería Química

Bucaramanga

2019

AGRADECIMIENTOS

¡Pero gracias a Dios, que nos da la victoria por medio de nuestro Señor Jesucristo! 1 Corintios 15:57.

A Colciencias por su apoyo económico en el marco del Programa de Doctorados Nacionales Convocatoria 511.

A la Universidad Industrial de Santander por su apoyo económico.

A los profesores Aristóbulo Centeno y Sonia A. Giraldo por haberme iniciado en este fascinante mundo de la catálisis.

A mis directores, profesores Víctor Gabriel Baldovino y Carlos Omar Castillo, por su apoyo constante y palabras de aliento cuando más lo necesitaba, por ser un ejemplo de hombres de ciencia y calidad humana.

Al Laboratorio de Catálisis e Hidrocarburos del Centro de Nanociencias y Nanotecnología de la Universidad Nacional Autónoma de México (UNAM), y al Grupo de Procesos de Transporte y Reacción en Sistemas Multifásicos de la Universidad Autónoma Metropolitana (UAM)-Unidad Iztapalapa, por su colaboración durante la realización de mi pasantía doctoral.

A los miembros del Centro de Investigaciones en Catálisis de la Universidad Industrial de Santander (CICAT-UIS).

A todos los amigos que me dejó este trasegar, especialmente a Iván Mora, Edwing Velasco y Carlos Santolalla quienes me animaron siempre a seguir adelante.

A mis compañeros de vida, Sandra y Emi, regalos de Dios, por todo su amor y paciencia, por ser mí soporte y compañía en este camino.

A mi maravillosa familia, a mi mamá quien siempre ha confiado en mí y me ha brindado todo su amor y apoyo incondicional, a mis hermanos y sobrinos quienes han luchado a mi lado y me brindan su amor y ayuda.

Dedicatoria

Porque todas las cosas proceden de él, y existen por él y para él. ¡A él sea la gloria por siempre! Amén. Romanos 6:36.

El camino no fue fácil, hubo mementos de angustia y preocupación, sin embargo, mi Dios Todopoderoso en quien creo, nunca me dejó solo, y a través del amor incondicional de mi mamá, mis hermanos, mis sobrinos, Sandra y Emi, y todos mis amigos, siempre me sostuvo y me permitió seguir adelante. Es por eso que todo mi esfuerzo va dedicado a Dios y a cada uno de ellos que nunca dejaron de confiar en mí y siempre estuvieron a mi lado.

Y de manera especial en la memoria de mi papá, quien en su paso por nuestra vida nos demostró su gran amor y ejemplo, sueño con el día en que pueda abrazarlo de nuevo y darle las gracias también.

¡Los amo!,

Edgar Mauricio Morales Valencia

Content

Page.

Introduction 22

1. Reactivity of Olefins and Inhibition Effect on the Hydrodesulfurization of a Model FCC Naphtha 31

1.1 Catalytic Tests 33

1.2 Results and discussion 36

1.2.1 Inhibition effect of the olefins on the reactivity of 2-MT. 36

1.2.2 Reactivity of 2,5-dimethyl-2,4-hexadiene (2,4C_6diene) in the presence of cyclohexene. 41

1.2.3 Effect of 2,4C_6diene on the reactivity of cyclohexene. 45

1.2.4 Reactivity of 1-octene in the presence of TMPs. 47

1.2.5 Reactivity of TMPs in the presence of 1-octene. 48

1.3 Conclusions 52

2. Kinetic Assessment of the Simultaneous Hydrodesulfurization of Dibenzothiophene and the Hydrogenation of Diverse Polyaromatic Structures 53

2.1 Catalytic Tests 58

2.2 Kinetic modeling 61

2.2.1 Hydrodesulfurization of dibenzothiophene 61

2.2.2 Hydrodesulfurization of dibenzothiophene simultaneous to the hydrogenation of aromatic compounds. 65

2.2.2.1 Hydrogenation of naphthalene simultaneous to the hydrodesulfurization of dibenzothiophene (DBTNP). 65
2.2.2.2 Hydrogenation of fluorene simultaneous to the hydrodesulfurization of dibenzothiophene (DBTFL). 68
2.2.2.3 Hydrogenation of phenanthrene simultaneous to the hydrodesulfurization of dibenzothiophene (DBTPHE). 69
2.2.3 Estimation of model parameters. 71
2.2.3.1 Physicochemical tests on the parameters of the models. 73
2.3 Results 75
2.3.1 Experimental evaluation 75
2.3.1.1 Hydrodesulfurization of dibenzothiophene in the absence and in the presence of aromatic compounds. 75
2.3.1.2 Hydrogenation of naphthalene, fluorene, and phenanthrene in the absence and in the presence of dibenzothiophene. 77
2.3.2 Kinetic modeling 78
2.3.2.1 Hydrodesulfurization of dibenzothiophene 78
2.3.2.1 Simultaneous HDS of DBT and hydrogenation of aromatics. 82
2.4 Discussion 87
2.4.1 Kinetics of the hydrodesulfurization of dibenzothiophene 87
2.4.1.1 Comparison of the kinetic model presented herein with previous works. 87
2.4.1.2 Nature of the active sites. 90
2.4.1.3 Considerations about the reaction mechanism. 92

2.4.2 Kinetics of the hydrodesulfurization of dibenzothiophene and hydrogenation of aromatics 95
2.4.2.1 Simultaneous hydrodesulfurization of dibenzothiophene and hydrogenation of naphthalene 95
2.4.2.1.1 Reactivity of dibenzothiophene and naphthalene. 95
2.4.2.1.2 Considerations about the reaction mechanism DBTNP. 97
2.4.2.2 Simultaneous hydrodesulfurization of dibenzothiophene and hydrogenation of fluorene 98
2.4.2.2.1 Reactivity of dibenzothiophene and fluorine. 98
2.4.2.2.2 Considerations about the reaction mechanism DBTFL. 98
2.4.2.3 Simultaneous hydrodesulfurization of dibenzothiophene and hydrogenation of phenanthrene 99
2.4.2.3.1 Reactivity of dibenzothiophene and phenanthrene. 99
2.4.2.3.2 Considerations about the reaction mechanism DBTPHE. 100
2.5 Conclusions 101
3. Effect of Nitrogen-Containing Compounds on the Hydrodesulfurization of Dibenzothiophene 102
3.1 Catalytic Tests 107
3.2 Kinetic Modeling 108
3.3 Results 109
3.3.1 Hydrodesulfurization of Dibenzothiophene. 109
3.3.2 Hydrodenitrogenation of Quinoline. 110
3.3.3 Hydrodenitrogenation of Indole. 112

3.3.4 Hydrodesulfurization of Dibenzothiophene in the Presence of Nitrogen Compounds..... 114

3.3.5 Hydrodenitrogenation of Quinoline and Indole in the Presence of Dibenzothiophene. 117

3.3.6 Kinetic Modeling. 119

3.3.6.1 Hydrodesulfurization of Dibenzothiophene Simultaneous to the Hydrodenitrogenation of Quinoline. 119

3.3.6.2 Hydrodesulfurization of Dibenzothiophene Simultaneous to the Hydrodenitrogenation of Indole. 124

3.4 Discussion 129

3.4.1 Effect of quinoline and indole on the hydrodesulfurization of dibenzothiophene..... 129

3.4.1.1 Inhibition effect of nitrogen compounds on the Hydrodesulfurization of Dibenzothiophene. 129

3.4.1.2 Promotion effect of the DDS pathway and overall conversion of Dibenzothiophene.... 131

3.5 Conclusions 139

4. General Conclusions 140

References 144

Appendices 168

List of Figures

Page.

Figure 1. Quality of the crude oil produced around the word. 23

*Figure 2***.** Typical catalytic hydrotreating units within a refinery. 25

Figure 3. Typical aromatic and heterocycles molecules containing S or N found on crude oil... 28

*Figure 4***.** Reaction scheme for the HDS of 2-MT proposed by Peréz-Martinez et al. 37

*Figure 5***.** Selectivity to 2-MT products as a function of the conversion of 2-MT and different temperatures. Pressure= 50 bar, liquid-flow rate of 20 mLh^{-1} and H_2/liquid feed ratio of 500.... 37

Figure 6. Reaction scheme of 2,4C_6diene 42

*Figure 7***.** Conversion of the 2,4C_6diene in the presence of 2-MT (Feed 2 and 3) and in the presence of 2-MT and cyclohexene (Feed 6-8) at different temperatures. P= 50 bar, liquid-flow rate of 20 mLh^{-1} and H_2/liquid feed ratio of 500. 43

*Figure 8***.** Conversion of cyclohexene in the presence of 2-MT (Feed 4 and 5) and in the presence of 2-MT and 2,4C_6diene (Feed 6-8) at different temperature. P= 50 bar, liquid-flow rate of 20 mLh^{-1} and H_2/liquid feed ratio of 500. 45

Figure 9. Hydrogenation of cyclohexene as a function of 2-MT conversion. P= 50 bar, liquid-flow rate of 20 mLh^{-1} and H_2/liquid feed ratio of 500. 46

*Figure 10***.** Reaction scheme for HYDO of 1-octene proposed by Pérez-Martinez et al. (Pérez-Martínez et al., 2010) 47

*Figure 11***.** Reaction scheme of HYDO of TMPs. 49

*Figure 12***.** 1/T dependence of the rate constant of the conversion of Feeds 2, 5, 9 and 10. Pressure= 50 bar, liquid-flow rate of 20 mLh-1 and H2/liquid feed ratio of 500..... 51

Figure 13. Reaction network for the hydrodesulfurization of dibenzothiophene..... 54

*Figure 14***.** Reaction network for the hydrogenation of polyaromatic compounds: a) Naphthalene, b) Fluorene, and c) Phenanthrene. 66

Figure 15. Parity diagrams for comparing experimental with calculated conversion of DBT ($\%X_{DBT}$) and the yields of BP ($\%Y_{BP}$) and CHB ($\%Y_{CHB}$), for the three kinetic models the HDS of DBT: a) DBT1S, b) DBT2S, and c) DBTBP2S. *p*=5 MPa, T=260-300°C, liquid-flow rate of 30 $mL \cdot h^{-1}$ and H_2/liquid feed ratio of 500. 79

*Figure 16***.** Parity diagram for comparing experimental with the calculated conversion of DBT ($\%X_{DBT}$) and NP ($\%X_{NP}$), and the yields of their reaction products ($\%Y_{BP}$, $\%Y_{CHB}$, $\%Y_{TTL}$). The simulated values were calculated from the model DBTNP that describe the simultaneous HDS of DBT and hydrogenation of NP. *p*=5 MPa, T=260-300°C, liquid-flow rate of 30 $mL \cdot h^{-1}$ and H_2/liquid feed ratio of 500. 82

*Figure 17***.** Parity diagram for comparing experimental with the calculated conversion of DBT ($\%X_{DBT}$) and FL ($\%X_{FL}$), and the yields of their reaction products ($\%Y_{BP}$, $\%Y_{CHB}$, $\%Y_{HHFL}$). The simulated values were calculated from the model DBTFL that describe the simultaneous HDS of DBT and hydrogenation of FL. *p*=5 MPa, T=260-300°C, liquid-flow rate of 30 $mL \cdot h^{-1}$ and H_2/liquid feed ratio of 500. 83

*Figure 18***.** Parity diagram for comparing experimental with the calculated conversion of DBT ($\%X_{DBT}$) and PHE ($\%X_{PHE}$), and the yields of their reaction products ($\%Y_{BP}$, $\%Y_{CHB}$, $\%Y_{OHPHE}$, $\%Y_{DHPHE}$, $\%Y_{THPHE}$). The simulated values were calculated from the model DBTPHE that

describe the simultaneous HDS of DBT and hydrogenation of PHE. *p*=5 MPa, T=260-300°C, liquid-flow rate of 30 mL·h^{-1} and H_2/liquid feed ratio of 500. 84

*Figure 19***.** Illustration of the adsorption of DBT on the two routes of HDS on NiMoS/γ-Al_2O_3.The rectangular box represents brim regions, and the oval marks the CUS-like sites. Color scheme: green, nickel; blue, molybdenum; yellow, sulfur. 92

*Figure 20***.** Conversion of DBT and yields of BP, CHB, and THDBT at different $WcatFDBT0-1$. Conditions: *p* = 5 MPa, T = 300°C, liquid-flow rate of 30 mL·h^{-1} and H_2/liquid feed ratio of 500..... 110

*Figure 21***.** Reaction network of the HDN of quinoline. Conversion of quinoline and yields of products in the absence (bold data) and in the presence of DBT (underlined data). Conditions: Q=0.24 wt %, DBT= 1.7 wt %, *p*=5 MPa, T=300°C, liquid-flow rate of 30 mL·h^{-1} and H_2/liquid feed ratio of 500. 111

*Figure 22***.** Reaction network of the HDN of indole. Conversion of indole and products yields in the absence (bold data) and in the presence of DBT (underlined data). Conditions: IND=0.22 wt%, DBT=1.7 wt %, *p*=5 MPa, T=300°C, liquid-flow rate of 30 mL·h^{-1} and H_2/liquid feed ratio of 500. 113

*Figure 23***.** Impact factors on the HDS of DBT of: a) Quinoline, and b) Indole. The reactions were carried out at a fixed molar ratio sulfur/nitrogen of 5, *p*=5 MPa, liquid-flow rate of 30 mL·h^{-1} and H_2/liquid feed ratio of 500. 115

*Figure 24***.** Parity diagram for comparing experimental with the calculated conversion of DBT and Q, and the yields of their reaction products. The simulated values were calculated from the model DBTQ that describe the simultaneous HDS of DBT and hydrogenation of quinoline. Conditions: *p* = 5 MPa, T = 260−300 °C, and space-time velocity= 40-88 $WcatFDBT0-1.$ 124

Figure 25. Parity diagram for comparing experimental with the calculated conversion of DBT and IND, and the yields of their reaction products. The simulated values were calculated from the model DBTIND that describe the simultaneous HDS of DBT and hydrogenation of indole. Conditions: p = 5 MPa, T = 260−300 °C, and space-time velocity= 40-88 $WcatFDBT0 - 1$.. 129

Figure 26. Adsorption equilibrium constants correlate with proton affinity. Data obtained by LaVopa et al. (LaVopa & Satterfield, 1988a) at 360ºC (blue marks) and by Nagai et al.(Nagai et al., 1986) at 260ºC (orange marks), both studied used NiMo/γ-Al_2O_3 catalyst..... 131

List of Tables

Page.

Table 1. *Quality of the crude oil produced in Colombia.* 24

Table 2. *Model feeds used in this study*[a] 35

Table 3. *Effect of the different feeds on the 2-MT conversion and selectivity*[a] 39

Table 4. *Effect of cyclohexene on 2,4C_6diene selectivity*[a] 43

Table 5 *Effect of TMPs on 1-octeno HYDO and selectivity*[a,b] 48

Table 6. *Effect of 1-octeno on TMPs conversion and selectivity*[a] 50

Table 7. *Reaction Mechanism and Catalytic Cycles for the Kinetic Model DBT1S* 62

Table 8. *Reaction Mechanism and Catalytic Cycles for the Kinetic Models DBT2S and DBTBP2S* 63

Table 9. *Reaction Mechanism and Catalytic Cycles for the Kinetic Model DBTNP to Describe the Hydrogenation of NP* 67

Table 10. *Reaction Mechanism and Catalytic Cycles for the Kinetic Model DBTFL to Describe the Hydrogenation of FL* 68

Table 11. *Reaction Mechanism and Catalytic Cycles for the Kinetic Model DBTPHE to Describe the Hydrogenation of PHE* 70

Table 12. *Conversion and selectivity observed at different conditions and obtained evaluating the conversion of DBT or aromatic compound individually or in blend.*[a] 76

Table 13. *Kinetic parameters values and corresponding 95% probability confidence intervals for the kinetic model DBTBP2S used to describe the HDS of DBT.*..... 81

Table 14. *Kinetic parameters values and corresponding 95% probability confidence intervals for the kinetic model DBTNP used to describe the HDS of DBT and hydrogenation of NP.*..... 85

Table 15. *Kinetic parameters values and corresponding 95% probability confidence intervals for the kinetic model DBTFL used to describe the HDS of DBT and hydrogenation of FL.*..... 86

Table 16. *Kinetic parameters values and corresponding 95% probability confidence intervals for the kinetic model DBTPHE used to describe the HDS of DBT and hydrogenation of PHE...* 86

Table 17. *Kinetic expressions for dibenzothiophene hydrodesulfurization based on Langmuir-Hinshelwood-Hougen-Watson approach.*..... 89

Table 18. *Conversion and yield of the products of the HDS of DBT under different feeds. Reaction conditions: T=300°C, p=5 MPa, and fixed molar ratio sulfur/nitrogen of 5.* 116

Table 19. *Conversion of quinoline and product yields in the presence of DBT at different* $WcatFDBT0-1$. *Conditions: T=300°C, p=5 MPa, and fixed molar ratio sulfur/nitrogen of 5.* 118

Table 20. *Conversion of indole and product yields in the presence of DBT at different* $WcatFDBT0-1$. *Conditions: T=300°C, p=5 MPa, and fixed molar ratio sulfur/nitrogen of 5.* 119

Table 21. *Reaction Mechanism and Catalytic Cycles for the Kinetic Model DBTQ to Describe the Hydrogenation of Quinoline.* 121

Table 22. *Values of the Kinetic Parameters and Corresponding 95% Probability Confidence Intervals for the Model DBTQ Used to Describe the HDS of DBT and Hydrogenation of Quinoline*[a]. 123

Table 23. *Reaction Mechanism and Catalytic Cycles for the Kinetic Model DBTIND to Describe the Hydrogenation of Indole* 125

Table 24**.** *Values of the Kinetic Parameters and Corresponding 95% Probability Confidence Intervals for the Model DBTIND Used to Describe the HDS of DBT and HDN of IND*[a] 128

Appendices

Page.

Appendix A. Supplementary Information Chapter 1 168

Appendix B. Supplementary information Chapter 2 170

Appendix C. Supplementary Information Chapter 3 183

Nomenclature

Roman letters

$A_i^{'}$	natural logarithm of pre-exponential factor, mm (g h)$^{-1}$
P_n	partial pressure of component *n*, %
E_A	activation energy, kJ mol^{-1}
F_n^0	inlet molar flow rate of the component *n*, mmol h^{-1}
F_n	molar flow rate of the component *n*, mmol h^{-1}
k_n^F	reaction rate coefficients of the forward, dep.
k_n^B	reaction rate coefficient of the backward, dep.
r_n	specific reaction rate of reaction *n*, mmol (g h)$^{-1}$
R	universal gas constant, kJ (mol K)$^{-1}$
RSS	objective function
S_n	selectivity of component *n*, %
T	temperature, K
Y_n	yield of component *n*, %
w_n	objective function weight factor of each response
W	mass of catalysts, g

Greek letters

*	active sites for the hydrogenation and hydrogenolysis reactions
β	active sites for the H_2 adsorption

ΔH_n^0	standard enthalpy of adsorption for component *n*, kJ mol^{-1}
ΔH_r°	standard enthalpy of reaction, kJ mol^{-1}
ΔS_n^0	standard entropy of adsorption for component *n*, J (mol K)$^{-1}$
ΔS_n^0	standard entropy of adsorption for component *n* used in Eq. (30), kJ (mol K)$^{-1}$
φ	vector of parameters accounted for in the objective function
π	active sites for the hydrogenation reactions
σ	active sites for the hydrogenolysis reactions
θ_i	fraction coverage of vacant of *i* site
λ	impact factor
v_j	Horiuti number

Subscripts

cat	Catalyst
exp	Experiment
g	gas phase
n	component *n*
obs	Observed
tab	Tabulated

Superscripts

^	Calculated
º	inlet, standard

Resumen

TÍTULO: Análisis de los efectos de inhibición en la hidrodesulfuración profunda usando reacciones modelo*.

AUTOR: Edgar Mauricio Morales Valencia**

PALABRAS CLAVE: Hidrodesulfuración profunda, nafta FCC, diésel, efectos de inhibición, modelamiento cinético.

DESCRIPCIÓN:

Esta investigación se enfocó inicialmente en el estudio de los efectos de inhibición sobre la HDS de una carga modelo de nafta FCC, utilizando como catalizador CoMo-S/γ-Al_2O_3. En particular, se estudió la HDS del 2-metiltiofeno y los efectos de inhibición de una olefina lineal , una cicloolefina, una diolefina ramificada plana y unas olefinas planas ramificadas. Los tres tipos de olefinas inhibieron la hidrodesulfuración, y el grado de inhibición dependió tanto del tipo de olefina como de su concentración en la alimentación de reacción.

En la segunda parte del trabajo se evaluó una carga modelo tipo diésel. Se estudió la HDS de dibenzotiofeno y los efectos de la presencia de moléculas con diferentes estructuras aromáticas: naftaleno, fluoreno y fenantreno, así como de compuestos que contienen nitrógeno en su estructura: quinolina e indol, utilizando como catalizador NiMo-S/γ-Al_2O_3. Además, se realizó un modelado cinético de las reacciones simultáneas, el cual se basó en el formalismo de Langmuir-Hinshelwood-Hougen-Watson y se sometió a un análisis de regresión con la forma reparametrizada de las ecuaciones de Arrhenius y van't Hoff. Antes de abordar los efectos de inhibición, se revisó la cinética del HDS de DBT, en este sentido, las observaciones se ajustaron mejor al considerar que las dos rutas paralelas para el HDS de DBT, es decir, las llamadas rutas de desulfuración directa y desulfuración mediada por hidrogenación, tienen lugar en dos tipos diferentes de sitios activos. El modelo desarrollado se utilizó como base para el modelado cinético de la inhibición de compuestos aromáticos y nitrogenados en el HDS de DBT. Los parámetros cinéticos se estimaron en ambos sitios catalíticos y exhibieron consistencia termodinámica. Estos hallazgos son importantes porque proporcionan una idea de los efectos de inhibición o promoción de compuestos poliaromáticos y nitrogenados de diferentes estructuras químicas sobre HDS ultra profunda.

* Tesis Doctoral.

** Facultad de Ingenierías Fisicoquímicas. Escuela de Ingeniería Química. Director: Prof. Víctor Gabriel Baldovino Medrano. Codirector: Prof. Carlos Omar Castillo Araiza.

Abstract

TITLE Analysis of inhibition effects on deep hydrodesulfurization using model reactions*.

AUTHOR: Edgar Mauricio Morales Valencia**

KEYWORDS: Deep hydrodesulfurization, FCC naphtha, diesel, inhibition effects, kinetic modeling.

DESCRIPTION:

This contribution presents in the first part the inhibition effect of olefins on the HDS and hydrogenation of olefins (HYDO) of a model FCC naphtha over CoMo-S/γ-Al_2O_3 catalysts. Particularly, the inhibition effects on the HDS of 2-methylthiophene by a linear olefin (1-octene), a cycloolefin (cyclohexene), a planar branched diolefin (2,5-dimethyl-2,4-hexadiene), and two non-planar branched olefins (2,2,4-trimethyl-1-pentene and 2,4,4-trimethyl-2-pentene) were analyzed. All three kinds of olefins inhibited the hydrodesulfurization, and the degree of inhibition depended on both the type of olefin and on its concentration in the reaction feed.

In the second part of the work, simulating a feedstock diesel, the effects of diverse aromatic structures: naphthalene (NP), fluorene (FL) and phenanthrene (PHE), and N-containing compounds: quinoline (Q) and indole (IND), on the HDS of dibenzothiophene over a sulfided NiMo-S/γ-Al_2O_3 catalyst were studied. Kinetic modeling of the simultaneous reactions was based on the Langmuir-Hinshelwood-Hougen-Watson (LHHW) formalism and was submitted to regression analyses with the reparametrized form of the Arrhenius and van't Hoff equations. Before addressing inhibition effects, the kinetics of the HDS of DBT was revisited. In this sense, observations were better fitted when considering that the two parallel pathways for the HDS of DBT, i.e. the so called direct desulfurization (DDS) and hydrogenation mediated desulfurization (HYD) routes, take place on two different types of active sites. The developed model was used as a basis for the kinetic modeling of the inhibition of aromatics and nitrogen compounds on the HDS of DBT. The kinetic parameters were estimated on both catalytic sites and exhibited thermodynamic consistency. These findings are important because they provide an insight into the inhibition or promotion effects of polyaromatic and N-containing compounds of different chemical structures on ultra-deep HDS.

* Ph.D. Thesis

** Facultad de Ingenierías Fisicoquímicas. Escuela de Ingeniería Química. Director: Prof. Víctor Gabriel Baldovino Medrano. Codirector: Prof. Carlos Omar Castillo Araiza.

Introduction

Oil refinery - between crude oil quality and stringent emission standards

The transportation sector including on-road vehicles and non-road engines is one of the largest sources of air pollution (Colvile, Hutchinson, Mindell, & Warren, 2001). During the combustion of fossil fuels different gaseous pollutants are emitted such as sulfur oxides (SO_X), nitrogen oxides (NO_X), ozone (O_3), carbon monoxide (CO), volatile organic compounds (VOCs), and some gaseous forms of metals (Campbell, Zhang, Yan, Lu, & Streets, 2018; Fan, Perry, Klemeš, & Lee, 2018). Due to its negative impact on health and environment, the governments have adopted more stringent emission standards reducing the maximum concentration allowed of sulfur, nitrogen, and aromatics in the fuels (United States Environmental Protection Agency (EPA)). For instance, in the United States, the Tier 3 program has set since 2017 new emission standards for vehicles reducing the sulfur content in gasoline to a maximum of 10 ppm (United States Environmental Protection Agency (EPA)). For diesel fuel the standards are also strict, currently, the amount of sulfur should not exceed 15 ppm (United States Environmental Protection Agency (EPA)). Similarly, in the European Union, diesel and gasoline have been limited to 10 ppm of sulfur for on-road vehicles since 2009 and for non-road engines since 2011 (European Commission).

The quality of the crude oil to be refined is, however, the main problem that has the petroleum industry to comply with strict environmental standards worldwide (Speight & Ancheyta Juárez, 2007; Speight & Speight, 2013; Stanislaus, Marafi, & Rana, 2010). Two of the most important properties to classify the crude oils are sulfur content and density (Correa Pabón & Souza Filho,

2019; A. Demirbas, Alidrisi, & Balubaid, 2015; Ayhan Demirbas, Bafail, & Nizami, 2016). Crude oil with less than 0.5% sulfur is defined as sweet and crude oil with greater than 0.5% sulfur as sour (Correa Pabón & Souza Filho, 2019). Meantime, density is measured in °API gravity, an inverse of the petroleum liquid's density relative to water. The conventional crude oils can be generally considered as light (°API > 31.1), medium (31.1>°API>22.3), heavy (22.3>°API>10), and extra-heavy (>10) (Ayhan Demirbas et al., 2016). According to the World Oil Review 2018 (ENI (Ente Nazionale Idrocarburi), 2018), a medium and sour crude oil is the most produced around the world (vide Figure 1). Nevertheless, in Colombia for the year 2017, nearly 51% of the crude oil produced was heavy and sour, while ca. 40% was heavy and medium sour (vide Table 1). The heavier and sourer the crude, the larger the concentration of sulfur content in the oil, being harder to treat it to reach ultra-low sulfur levels (~10 ppm S) because of refractory sulfur compounds (Carrillo & Corredor, 2013; Clews, 2016; Laredo et al., 2002). This result in operational and economic challenges for the refining industry (Duayne Whitehurst, Isoda, & Mochida, 1998a; C. Song, 2003).

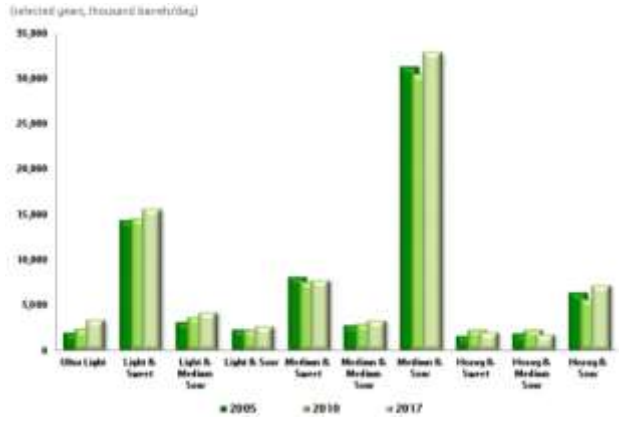

Figure 1. Quality of the crude oil produced around the word. Taken from: (ENI (Ente Nazionale Idrocarburi), 2018)

Table 1**.**

Quality of the crude oil produced in Colombia.

(thousand barrels/day)

	2000	2005	2010	2015	2016	2017	Share of total 2000	Share of total 2017
Colombia	684	526	786	1,006	880	853		
Light & Sweet	340	135	51	49	53	49	49.7%	5.7%
Medium & Sweet	105	74	61	42			15.3%	
Medium & Medium Sour					36	32		3.8%
Heavy & Medium Sour	234	309	416	438	347	337	34.1%	39.5%
Heavy & Sour	6	8	258	476	443	434	0.9%	50.9%

Taken from**:** (ENI (Ente Nazionale Idrocarburi), 2018)

Hydrotreating Units

The hydrotreatment (HDT) of oil fractions has become on one of the main processes in moderns refineries to obtain fuels that meet the stringent environmental requirements (Parkash & Parkash, 2003; Speight & Ancheyta Juárez, 2007; Speight & Speight, 2019). Once the crude is fractionated in the atmospheric distillation unit, the different heteroatoms distributed over the whole boiling range must be removed from the intermediate streams before being fed into another refinery process unit, or before blending into a finished refined product (vide Figure 2) (Alkandari, Mujtaba, & Arellando-Garciaa, 2017). In the hydrotreating units, simultaneous reactions of hydrodesulfurization (HDS), hydrodesnitrogenation (HDN), hydrodesoxygenation (HDO), hydrodemetallization (HDM) take place to remove out of the oil sulfur, nitrogen, oxygen and heavy metals, respectively. Furthermore, other reactions may occur during the HDT such as isomerization, and hydrogenation of aromatics and olefins (Bandyopadhyay & Upadhyayula, 2018; Moreau & Geneste, 1990; Stanislaus et al., 2010). However, depending on the oil stream, the type and concentration of compounds vary considerably during the HDT (Al-Barood & Stanislaus, 2007).

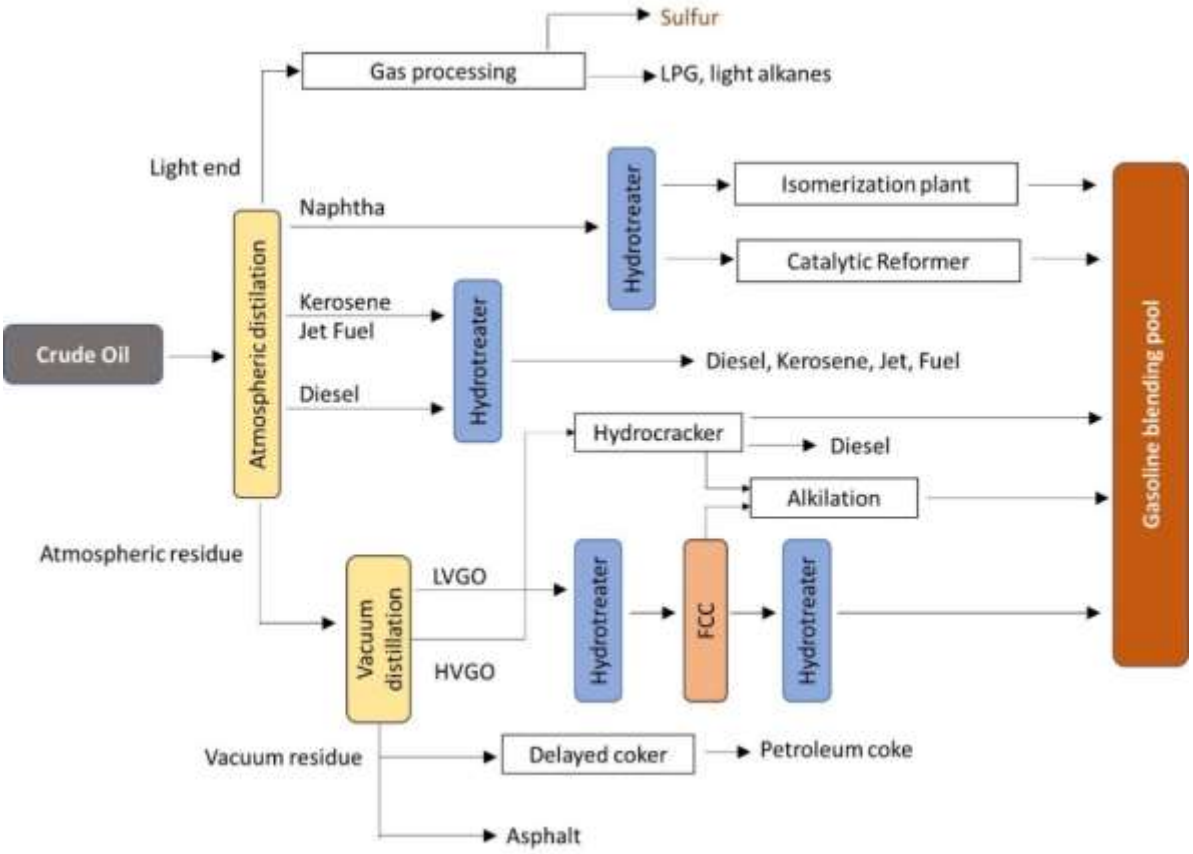

Figure 2. Typical catalytic hydrotreating units within a refinery (Speight & Ancheyta Juárez, 2007).

Hydrotreating of Fluid Catalytic Cracking (FCC) gasoline

Commercial gasoline is a blending pool of different fractions coming mainly from isomerization, catalytic reformer, and mainly fluid catalytic cracking (FCC) units (Babich & Moulijn, 2003; Brunet, Mey, Pérot, Bouchy, & Diehl, 2005; Kaufmann, Kaldor, Stuntz, Kerby, & Ansell, 2000; Speight & Ancheyta Juárez, 2007). Before the reforming and isomerization units, the naphtha is hydrotreated and, therefore, the sulfur content in gasoline from these streams is not higher than 15%. Besides, FCC contributes from 30-40% to the total pool of gasoline, containing a larger concentration of sulfur that, in turns, comes from atmospheric residue or vacuum distillates which contain a high concentration of sulfur compounds (0.5-1.5 wt.%) (Choi et al., 2004; Pérez-

Martínez, Eloy, Gaigneaux, Giraldo, & Centeno, 2010). Thus, this gasoline is the most important stream to be treated by HDT in terms of sulfur content (Celis-Cornejo, Granados-Zarta, Bravo-Villarreal, Pérez-Martínez, & Giraldo-Duarte, 2013; Miller, Reagan, Kaduk, Marshall, & Kropf, 2000). The sulfur compounds on this stream are mainly thiophene and its alkylderivatives, and benzothiophene (Wen, Wang, Xu, & Gao, 2012; Yin, Zhu, & Xia, 2002). The hydrodesulfurization of these S-containing compounds under typical conditions of hydrotreating (P = 1.5-6 MPa and T = 260-320 °C) and using conventional catalysts (Co/Ni-promoted MoS_2) is not difficult (Brunet et al., 2005). Nevertheless, due to FCC gasoline has a high concentration of olefins (20-40 wt.%) to improving its octane number, it is mandatory to reduce the sulfur content at a maximum keeping the olefin saturation at a minimum (Lamic et al., 2008; Pérez-Martínez, Gaigneaux, & Giraldo, 2012; Tu et al., 2016). Therefore, for the hydrotreating of FCC gasoline, the simultaneous reactions of hydrodesulfurization and hydrogenation of the different olefins present in the feedstock must be taken into account.

Hydrotreating of Diesel

The production of ultra-low sulfur diesel requires a catalytic hydrotreatment process at more severe conditions than for the production of gasoline with ultra-low sulfur. Most of the sulfur contained in the molecules, including the most refractory compounds, such as alkyl dibenzothiophenes must be removed (Schulz, Böhringer, Waller, & Ousmanov, 1999; Shafi & Hutchings, 2000). One of the main problems of this removal process relates to the presence of inhibitory molecules such as aromatic and nitrogen compounds, H_2S, NH_3 (vide Figure 3) (Lamic et al., 2008; Rana, Navarro, & Leglise, 2004; C. Song & Ma, 2003; Tao et al., 2017; Zeuthen, Knudsen, & Whitehurst, 2001). Nevertheless, the inhibition effect generated by the aforementioned compounds negatively affects the two known routes for the hydrodesulfurization

of dibenzothiophenes and alkyl substituted dibenzothiophenes, the direct desulfurization route (DDS) and the hydrogenation route (HID). In this regard, contradictory trends have been reported (Dorneles de Mello, de Almeida Braggio, da Costa Magalhães, Zotin, & Pereira da Silva, 2017; Duayne Whitehurst, Isoda, & Mochida, 1998b; Egorova & Prins, 2004a, 2004b; Logadóttir et al., 2006). Some authors (Duayne Whitehurst et al., 1998b; Logadóttir et al., 2006) observed that aromatics inhibited the HYD route of desulfurization to a larger extent, compared to the DDS route; whereas other reports observed that DDS and HID were inhibited to the same extent (Egorova & Prins, 2004a; Farag, Sakanishi, Mochida, & Whitehurst, 1998). To this end, the influence of the basicity of nitrogen compounds during hydrodesulfurization has also been discussed. Most of the authors (Beltramone, Crossley, Resasco, Alvarez, & Choudhary, 2008; García-Martínez, Castillo-Araiza, De los Reyes Heredia, Trejo, & Montesinos, 2012; Wei et al., 2015) found that basic nitrogen inhibits more than weakly basic compounds, while other researchers presented evidence showing that weakly basic compounds exert either stronger or similar inhibition effect over hydrodesulfurization (Ho, 2003; Laredo, Altamirano, & De los Reyes, 2003; Laredo S, De los Reyes H, Luis Cano D, & Jesús Castillo M, 2001; Xiang, Chai, Liu, & Liu, 2008). Therefore, the joint effect of aromatic, nitrogen and sulfur compounds on their simultaneous reactions is not clear yet during hydrotreating.

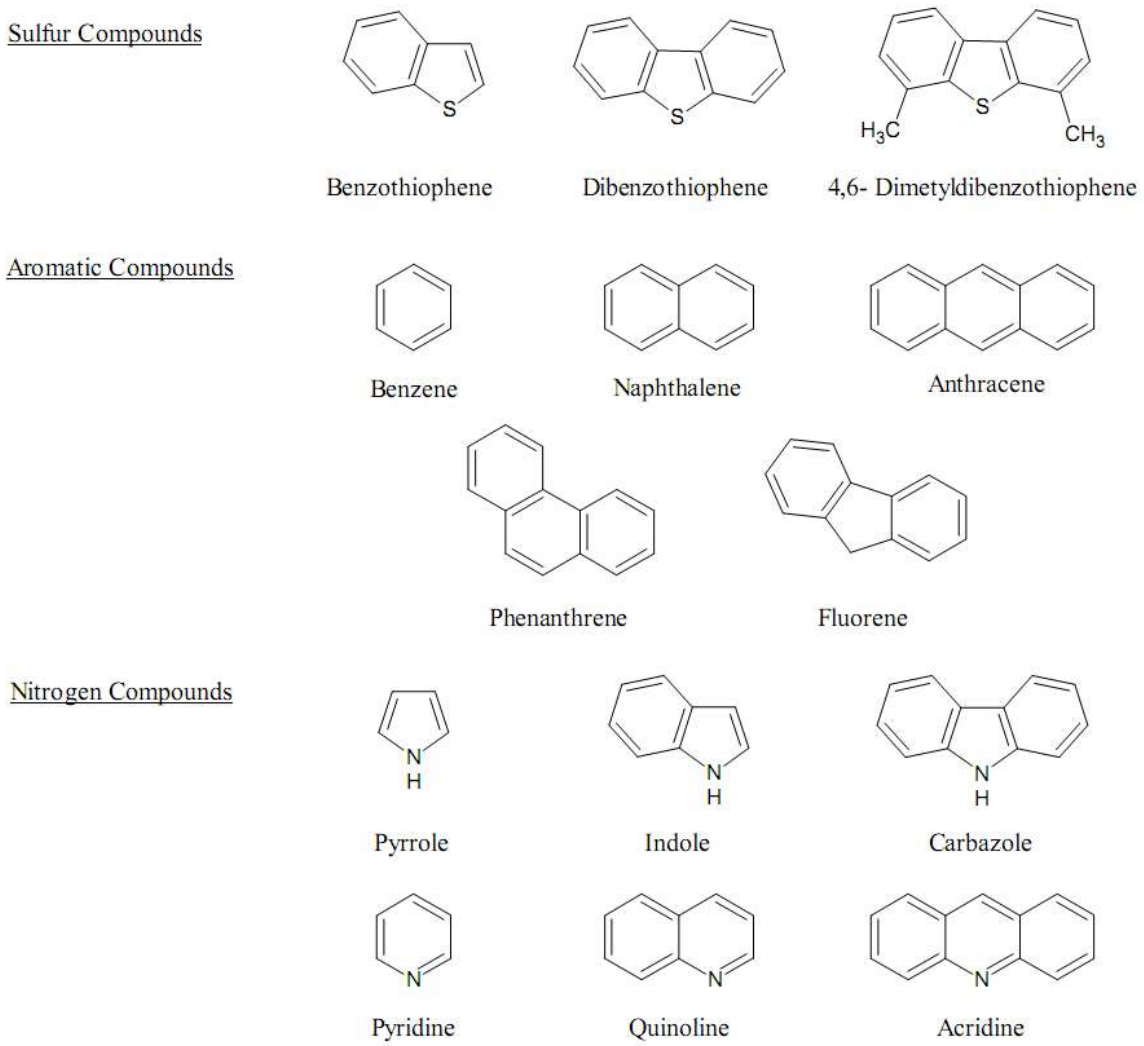

Figure 3. Typical aromatic and heterocycles molecules containing S or N found on crude oil (Stanislaus et al., 2010).

The feedstock of hydrotreating is, as mentioned before, a mixture of hundreds of compounds being converted simultaneously via hydrogenolysis, isomerization, cracking and de/hydrogenation reactions, leading to hydrodearomatization, hydrodesulfurization, and hydrodenitrogenation. The kinetics of these reactions is, particularly, analyzed by formulating either power law expressions or pseudo-first-order rate equations and molecular lumping striving to reduce the complexity of the mathematical expressions inherent to modelling. (Bhaskar, Valavarasu, Sairam, Balaraman, &

Balu, 2004; Jiménez, Kafarov, & Nuñez, 2007; Koltai et al., 2002; M. A. Rodríguez & J. Ancheyta, 2004; T. Song et al., 2006). These approaches have produced models capable of fitting experimental observations satisfactorily. However, they fall short to provide chemical insights at molecular level during the catalytic cycles performed at the catalytic surface (de Oliveira, Hudebine, Guillaume, & Verstraete, 2016). More insightful approaches to molecular level kinetic modelling are often achieved by studies made accounting for model feeds (Castillo-Araiza et al., 2015; Romero, Thybaut, & Marin, 2008; Vanrysselberghe & Froment, 1996); nevertheless, such results are not easily scalable to industrial hydrotreating where some effects are neglected, and the influence of mass and heat transport cannot be ruled out. Rigorous kinetic models for the simultaneous reactions of hydrodearomatization, hydrodesulfurization, and hydrodenitrogenation based on a reaction mechanism with chemical and thermodynamic consistency are scarce (García-Martínez et al., 2012).

Scope of the thesis

For the production of gasoline and diesel with ultra-low sulfur content it is necessary to eliminate the sulfur of the different compounds including the least reactive ones. However, in the feedstocks the sulfur compounds are present with other compounds such as olefins, aromatics, and nitrogen compounds that react simultaneously. Bases on this, there is a need to analyze the reactivity of the sulfur molecules in the presence of the other compounds found in the feed. In the first chapter, the hydrotreating of a model FCC naphtha is analyzed. The hydrodesulfurization of 2-methylthiophene was studied in the presence of olefins with different structure and geometry. Thus, 1-octene was selected as linear olefin, cyclohexene as cyclic olefin, 2,4,4-trimethylpentenes as branched and non-planar olefin, and 2,5-dimethyl-2,4-hexadiene as branched planar olefin. The effect of the olefins on the conversion and product yields of the hydrodesulfurization of 2-

methylthiophene, and the mutual effect between them were evaluated at different temperatures and concentrations.

In Chapter 2 and 3, the hydrotreating of a model feed for the production of diesel is evaluated. Chapter 2 accounts for the hydrodesulfurization of dibenzothiophenes in the absences of other compounds. Different kinetic models were proposed assuming one or two catalytic centers involved in the reaction. All models were submitted to regression analyses with the reparametrized form of the Arrhenius and van´t Hoff equations. Owing to the latter, activation energies and pre-exponential factors as well as the adsorption enthalpies and entropies were estimated. The statistical significance of the overall regression for each model and of the corresponding individual parameters was tested by means of an F-test and of a t-test, respectively. Then, the simultaneous reactions of hydrodesulfurization and hydrogenation of aromatic compounds were evaluated. As representative aromatic compounds, naphthalene with two fused aromatic, phenanthrene with three fused aromatic rings, and fluorene with a chemical structure identical to dibenzothiophene were selected. Kinetic models for the simultaneous hydrodesulfurization of dibenzothiophene and the hydrogenation of each aromatic compounds were developed with the same statistical and thermodynamic rigor used in the model for the hydrodesulfurization of dibenzothiophene. In the same line, in the Chapter 3 the hydrodesulfurization of dibenzothiophene was assessed in the presences of N-containing compounds with different basicity. Because of their proton affinity, quinoline (953.2 kJ mol^{-1}) and indole (933.4 kJ mol^{-1}) were selected as basic and weakly basic compounds, respectively. These reactions were carried out at different temperatures and different space-time velocities. Following the same methodology used during the development of kinetic models for the simultaneous reactions of hydrodesulfurization and hydrogenation, kinetic models

were proposed for the simultaneous reactions of dibenzothiophene and hydrodenitrogenation of quinoline and indole. Finally, in Chapter 4, the general conclusions are presented.

1. Reactivity of Olefins and Inhibition Effect on the Hydrodesulfurization of a Model FCC Naphtha

Fluid Catalytic Cracking (FCC) naphtha constitutes 30 to 40% of the total gasoline pool and contributes importantly to the octane number of the fuel which is associated to its olefin content. Normally, FCC naphtha is composed by 20-40% olefins. However, FCC naphtha also contributes 85 to 95% of the total sulfur content of gasoline. By reasons of public domain, sulfur must be removed from the fuel to comply with environmental regulations (Brunet, Mey, Pérot, Bouchy, & Diehl, 2005; Gilbert, 2014; Liu et al., 2014a; Zhang, Liu, Liu, Jiang, & Li, 2019). The elimination of sulfur from FCC naphtha is conventionally done through catalytic hydrodesulfurization (HDS). The most important sulfur compounds present in FCC gasoline are thiophene and its alkyl derivatives (Anabtawi, Alam, Ali, Ali, & Siddiqui, 1995; Dos Santos, Dulot, Marchal, & Vrinat, 2009). However, the interaction between the olefins and such S-compounds along with simultaneous and competitive reactions between these compounds on the catalysts surface are difficult to avoid. The challenge of the refiner is thus to reduce at maximum the sulfur content of the fuel while keeping a high octane number. To do the latter, olefin saturation must be kept at minimum (Badawi, Vivier, & Duprez, 2010; Liu et al., 2014b; Song, 2003).

In order to achieve low sulfur gasoline, the inhibition effect of olefins on HDS must be firstly understood. Some authors have studied the reactivity of various olefins during the HDS of a model FCC gasoline (Anabtawi et al., 1995; Badawi et al., 2010; Dos Santos et al., 2009; Gilbert, 2014; Liu et al., 2014b; Song, 2003). Nevertheless, the influence of the structure of the olefins on their reactivity under HDS conditions is still debated and remains mostly speculative. Badawi et al. (Badawi et al., 2010) studied the hydrogenation of olefins (HYDO) of different types over CoMo-S/Al_2O_3 and NiMo-S/Al_2O_3 catalysts. For CoMo-S/Al_2O_3, these authors concluded that "the olefin with the highest steric hindrance is less adsorbed than the others". Conversely, for NiMo-S/Al_2O_3 they reported that there is no influence of the olefin structure on the reactivity. Toba et al. (Toba, Miki, Matsui, Harada, & Yoshimura, 2007) and Liu et al. (Liu et al., 2014b) found that methyl groups bonded to olefinic carbons limit the adsorption of the olefins on the active sites of the catalyst and, in addition, influence the hydrogenation of the olefin. Hatanaka et al. (Hatanaka, Yamada, & Sadakane, 1997b) studied the inhibition effect of cyclohexene, 1-octene, 1-hexene and TMPs on the HDS of thiophene over CoMo-S/Al_2O_3 catalysts. They postulated that the strength of the inhibiting effect does not depend on the steric effects of the olefin molecules but on the strength of its interaction with the catalyst active sites.

As previously mentioned, FCC naphtha is composed of a mixture of several olefins of different nature (Viswanadham et al., 2007) and, HYDO is, of course, not exempt of being influenced by the simultaneous presence of these different olefins. However, detailed studies regarding the hydrogenation effect between olefins are scarce in open literature (Badawi et al., 2010; Liu et al., 2014b; Toba et al., 2007).

In this chapter, the reactivity of 2-methylthiophene (2-MT) in the presence of different kinds of olefins and the effects of the nature and concentration of these olefins over such reactivity were

studied. For this purpose, a linear olefin (1-octene), a cycloolefin (cyclohexene), a planar branched diolefin (2,5-dimethyl-2,4-hexadiene), and two non-planar branched olefins (2,2,4-trimethyl-1-pentene and 2,4,4-trimethyl-2-pentene) were selected as model olefins typically present in FCC naphtha. In order to further elucidate the mutual influence of these olefins on their own reactivity under HDS conditions, their hydrogenation was analyzed in detail.

1.1 Catalytic Tests

Reactions were carried out in a high-pressure fixed-bed continuous flow reactor. A CoMo/γ-Al_2O_3 commercial catalyst *Procatalyse* with a BET specific surface area of 174 $m^2 \cdot g^{-1}$, BJH pore volume of 0.46 $g \cdot cm^{-1}$, and average BJH pore diameter of 10.6 nm was employed in the catalytic tests. Catalyst extrudates were grinded and sieved so as to obtain particles within the diameter range: 300-600 µm. For the catalytic tests, 0.3 g of catalyst were dried *in situ* under N_2 flow (100 $mL \cdot min^{-1}$) at 120°C for 1 h. Afterwards, the catalyst was sulfided under a flow of 15% of H_2S in H_2 (100 $mL \cdot min^{-1}$) at atmospheric pressure and 400°C for 3 h. After sulfidation, the reactant liquid was fed to the reactor at a rate of 20 $mL \cdot h^{-1}$, the reactor pressure was increased with H_2 to 1.7 MPa, and the reactor temperature was decreased to the reaction temperature (230-280°C). A H_2/(liquid feed) rate ratio of 500 $NL \cdot L^{-1}$ was fixed for all tests. Under these conditions, the absence of any diffusion limitations was previously demonstrated (Pérez-Martínez, Eloy, Gaigneaux, Giraldo, & Centeno, 2010). Samples of the liquid products from the reactor were collected every hour. Reactions were conducted until reaching a steady state. Such a steady state was defined from the criterion of not observing changes in the conversion of reactants for at least three consecutive liquid products samples. The identification and quantification of liquid reaction products were made by the gas

chromatography (GC) and GC mass spectroscopy (GC-MS) techniques. Gas chromatography analyses were carried out with a HP 6890 chromatograph equipped with an FID detector and an automatic injector. The columns HP-1 (Agilent J&W) (100 m × 0.25 mm × 0.5 μm) and HP-5 MS (Agilent J&W) (50 m × 0.20 mm × 0.5 μm) were used in the GC and GC-MS analyses, respectively. In both cases, the following routine for the analyses was employed: the oven was programmed with a heating ramp of 8 °C min^{-1} starting from 40 °C (2 min) and up to 100 °C (3 min), then heating to 150 °C (6 min) was achieved with a temperature ramp of 33 °C min^{-1}, and, finally, the oven was heated to 260 °C (7 min) at a temperature ramp of 35 °C min^{-1}. Helium (99.99%, Linde Colombia S.A) at a 19 cm s^{-1} linear velocity (1.1 mL min^{-1}, at constant flow) was always used as carrier gas, with. The MS identification of the reaction products was done by means of a computer matching method, comparing their spectra with those of Wiley, NIST and QUADLIB spectral libraries. Finally, the quantification of the identified reaction products was performed by making use of calibration curves for each compound. The experimental error in the mass balance was found to be below ±15%.

The reaction feed consisted of mixtures of 2 wt.% 2-methylthiophene (Sigma-Aldrich, 98%), as a model sulfur compound, 2 wt.% dodecane (Sigma-Aldrich, ≥ 99%), as internal standard for the chromatographic analysis, and n-heptane (J. T. Baker, 99.4%), as solvent, with different olefins. The following olefins were used: 2,5-dimethyl-2,4-hexadiene (2,4C_6diene) (Sigma-Aldrich, 96%), cyclohexene (Sigma-Aldrich, ≥ 99%), 1-octene (Sigma-Aldrich, 98%) and a mixture of 2,4,4-trimethylpentenes (TMPs), 2,4,4-trimethyl-1-pentene (TM1P) and 2,4,4-trimethyl-2-pentene (TM2P) (3:1 approximately) (Merck, 90%). These olefins were selected as representatives of diolefins, cycloolefins, linear olefins, and terminal and external non-planar

branched olefins typically present in FCC gasoline. A summary of the reaction feeds prepared is shown in Table 2.

Table 2.

Model feeds used in this study[a]

	Feed No. (wt. %)											
	1	**2**	**3**	**4**	**5**	**6**	**7**	**8**	**9**	**10**	**11**	**12**
2-MT (sulfur compound)	2	2	2	2	2	2	2	2	2	2	2	2
2,5-dimethyl-2,4-hexadiene (2,4C$_6$diene)	-	1.2	3	-	-	1.2	2	3.2	-	-	-	-
Cyclohexene (cycloolefin)	-	-	-	3.2	8	3	5	8	-	-	-	-
1-octene (linear olefin)	-	-	-	-	-	-	-	-	5	-	5	6.4
TMPs (non-planar branched olefins)	-	-	-	-	-	-	-	-	-	11.5	11.5	14.4

[a] Dodecane (2 wt. %) was used as an internal standard for chromatographic analysis and n-heptane was used as solvent.

Catalytic results were expressed in terms of: the conversion of 2-MT (%C$_{2\text{-MT}}$), the hydrogenation activity of olefins (%HYDO) and selectivity (%S) to 2-MT, 2,4C$_6$diene, cyclohexene, 1-octene, TM1P or TM2P, as follows:

$$\%C_{2-MT} = \frac{n^0_{(2-MT)} - n_{(2-MT)}}{n^0_{(2-MT)}} \times 100 \qquad (1.1)$$

Where, $n^0_{(2-MT)}$ and $n_{(2-MT)}$ are the initial and final moles of 2-methylthiophene (2-MT), respectively.

$$\%HYDO_i = \frac{n^0_{o_i} - n_{o_i}}{n^0_{o_i}} \times 100 \qquad (1.2)$$

Where, $n^0_{o_i}$ and n_{o_i} are the initial and final moles of the olefin *i*, respectively.

$$\%Selectivity_j = \frac{n_j}{\alpha_{ij}(n_i^0 - n_i)} * 100 \qquad (1.3)$$

Where, n_i^0 and n_i are the initial and final moles of reactant i and n_j are the final moles of the product j. α_{ij} is the ratio between the stoichiometric coefficients of the product j and the reactant i.

1.2 Results and discussion

Section 1.2.1 discusses the results of the conversion of 2-MT in the absence and presence of the studied olefins. Obtained product distributions are analyzed in order to clarify the inhibition role of the olefins on the HDS of 2-MT. Section 1.2.2 discusses the conversion and selectivity of 2,4C_6diene in the presence of cyclohexene as a function of cyclohexene concentration and reaction temperature. Section 1.2.3 presents the effect of 2,4C_6diene over the hydrogenation of cyclohexene. Section 1.2.4 discusses the influence of non-planar branched olefins (TMPs) over the conversion and selectivity of the linear olefin (1-octene). Finally, section 1.2.5 analyzes the conversion and products distribution from the HYDO of TM1P and TM2P in the absence and presence of 1-octene.

1.2.1 Inhibition effect of the olefins on the reactivity of 2-MT. The reaction of 2-MT in the absence of olefins was carried out in order to identify the products distribution of the HDS reaction by itself. Such products distribution is schematically represented in the reaction network showed in Figure 4. The desulfurization of 2-MT involves two reaction routes. The first one is the hydrogenation (HYD) mediated pathway in which 2-methyltetrahydrothiophene (2-MTHT) is firstly produced as a partially hydrogenated reaction intermediate which is further desulfurized to:

1-pentene, 2-pentene, and/or pentane. The second pathway is the direct removal of the sulfur heteroatom (DDS) from 2-MT to form 1,3-pentadiene (1,3Penta). The latter can be further hydrogenated to the same kind of products as those obtained via the HYD route.

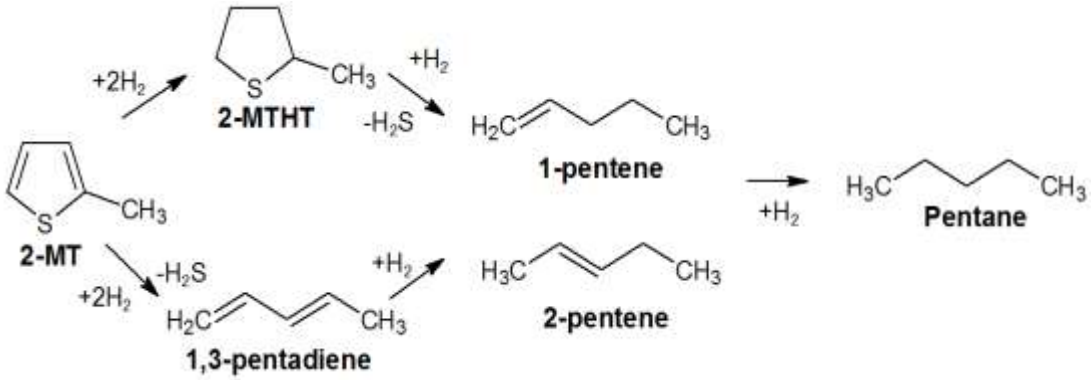

Figure 4. Reaction scheme for the HDS of 2-MT proposed by Peréz-Martinez et al. (Pérez-Martínez et al., 2010)

Figure 5 shows the selectivity to the products of 2-MT HDS as a function of 2-MT conversion and temperature.

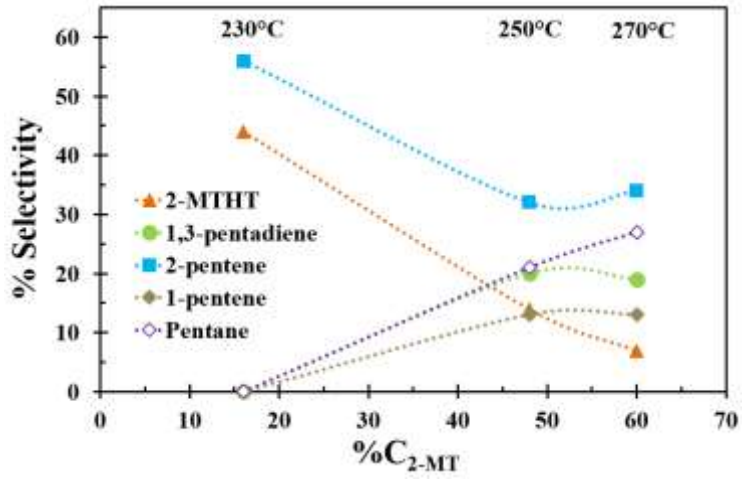

Figure 5. Selectivity to 2-MT products as a function of the conversion of 2-MT and different temperatures. Pressure= 50 bar, liquid-flow rate of 20 mLh^{-1} and H_2/liquid feed ratio of 500.

The reactivity of 2-MT increased with temperature. At 230°C, the conversion of 2-MT was 16% and only 2-THMT and 2-pentene were detected as reaction products. At 250 and 270°C, %C-2MT increased to 48 and 60%, respectively. Such a conversion increase changed the products distribution. The selectivity to 2-THMT and 2-pentene diminished while 1,3Penta, 1-pentene and pentane were produced. When the reaction temperature was risen from 230 to 270°C, the selectivity to 2-MTHT, a reaction intermediate of the HYD route, decreased considerably dropping from 44 to 7%. Conversely, the selectivity to desulfurized products: 1,3-pentadiene, 1-pentene, and pentane, increased from 0 to 19, 13, and 27%, respectively. 2-pentene was the only desulfurized product whose selectivity decreased with temperature. A possible explanation for this trend is its isomerization to 1-pentene or its hydrogenation to pentane. On the other hand, the hydrogenolysis reaction resulting on the C-S bond scission of 2-MT is not limited thermodynamically as in contrast to the hydrogenation of the aromatic ring of the 2-MT before sulfur removal. Aromatics hydrogenation reactions are highly exothermic and reversible (Stanislaus & Cooper, 1994). For that reason, the production of 2-MTHT is affected at higher temperatures whereas the production of desulfurized products is favored. A similar behavior was observed by Zhao et al. (Zhao, Oyama, & Naeemi, 2010) who successfully correlated experimental results with values of theoretical equilibrium constants for HDS and HYD reactions. Furthermore, in this work, the calculated apparent activation energy of 2-MT HDS is 96 $kJmol^{-1}$ which is fairly close to values reported in literature (Celis-Cornejo, Granados-Zarta, Bravo-Villarreal, Pérez-Martínez, & Giraldo-Duarte, 2013).

The effect of the four kinds of olefins tested herein on the conversion of 2-MT and on selectivity are shown in Table 3.

Table 3.

Effect of the different feeds on the 2-MT conversion and selectivity[a]

Feed	%$C_{2\text{-MT}}$	Selectivity of 2-MT products[b]				
		2-MTHT	1,3-pentadiene	2-pentene	1-pentene	pentane
1	60	7	19	34	13	27
2	44	5	20	40	9	26
3	22	6	21	41	11	21
4	20	15	23	36	15	11
5	15	19	23	33	17	8
9	37	11	22	34	15	18
10	39	6	22	37	14	21

[a] Reaction condition: T=270°C, P= 50 bar, liquid-flow rate of 20 mLh^{-1} and H_2/liquid feed ratio of 500.

[b] 2-MT: 2-methylthiophene; 2MTHT: 2-methyltetrahidrothiophene; 1,3Penta: 1,3-pentadiene.

In general, the conversion of 2-MT was affected by the presence of all of the studied olefins. The degree of inhibition depended on the type of olefin and on its concentration in the reaction feed. In particular, %C-2MT dropped from 60 to 44% with 1.2 wt. % of 2,4C_6diene (Feed 2) and to 22% with 3 wt. % of the same olefin (Feed 3). When doubling the concentration of 2,4C_6diene, the inhibition effect on %C-2MT was also doubled. On the other hand, the selectivity to 2-MTHT and 1,3Penta did not change significantly. Meanwhile, the selectivity to 2-pentene increased whereas the selectivity to 1-pentene and pentane decreased. This indicates that the presence of a branched diolefin may either inhibit the hydrogenation of 2-pentene to pentane or its isomerization to 1-pentene.

The influence of cyclohexene was analyzed at two different concentrations: 3.2 and 8 wt. %. Cyclohexene inhibited 2-MT HDS. However, the increase in cyclohexene concentration in the

reaction feed was not directly proportional to the observed decrease in the conversion of 2-MT (Table 3). This trend differed from that encountered for 2,4C_6diene. For such a case, an increment in the concentration of 2,4C_6diene strongly inhibited 2-MT HDS. Hatanaka et al. (Hatanaka et al., 1997b) studied the effect of the olefin content on the HDS of thiophene and found a similar tendency as the one obtained herein. On the other hand, the presence of cyclohexene, which is a non-branched olefin, had a distinct detrimental effect on the conversion of 2MTHT and on the production of pentane. The selectivity to 2MTHT increased considerably from 7% for the cyclohexene-free reaction (Feed 1) to 15 and to 19% with 3.2 (Feed 4) and 8 wt. % (Feed 5) of cyclohexene in the feed, respectively. Furthermore, the selectivity to pentane dropped from 27 (Feed1) to 11 (Feed 4) and 8% (Feed 5) in this case.

At a similar concentration, 2,4C_6diene (branched olefin) and cyclohexene (non-branched olefin) showed a comparable effect on the conversion of 2-MT. There were noticeable differences in selectivity, nonetheless. While cyclohexene strongly inhibited the conversion of 2-MTHT to the desulfurized products, 2,4C_6diene did not present any effect on the conversion of 2-MTHT. Particularly, in this instance, the selectivities to 2-MTHT were 6% and 15% for Feeds 3 and 4, respectively. On the other hand, the selectivity to pentane dropped from 21% in the presence of 2,4C_6diene and to 11% in the presence of cyclohexene. These results showed that the two olefins, 2,4C_6diene and cyclohexene, had the same inhibition effect on the conversion of 2-MT, but they affected the selectivity in the HDS reaction differently. Indeed, the desulfurization of the partially hydrogenated 2-MTHT intermediate was more affected by the non-branched olefin, i.e. cyclohexene.

The inhibition effect of 1-octene (linear non-branched olefin) and TMPs (branched olefins) on the HDS of 2-MT is analyzed next. In spite of the higher concentration of TMPs (11.5 wt.%)

in respect to the concentration of 1-octene (5 wt.%), the inhibition effect on 2-MT conversion by TMPs was slightly higher than in the presence of the linear olefin. Concerning the selectivity of the HDS of 2-MT, results showed that 1-octene, the non-branched olefin, affected negatively the desulfurization of 2-MTHT whereas TMPs did not seem to have an effect on this same reaction. Hatanaka et al. (Hatanaka et al., 1997b) suggested that 1-octene is strongly adsorbed on the HDS active site whereas TMPs are weakly adsorbed. However, the existence, nature and the number of the active centers involved in hydrogenation and hydrodesulfurization reactions remains unclear yet (Brunet et al., 2005; Dos Santos et al., 2009).

In general, 1-octene, TMPs, 2,4C_6diene, and cyclohexene showed a very strong inhibition effect on the HDS of 2-MT. This inhibition effect increased as the follows: cyclohexene ≈ 2,4C_6diene > 1-octene > TMPs. From the observed products distribution (Table 3), the inhibition effect of the olefins on the desulfurization of 2-MT, i.e. only desulfurized products taken into account, followed the trend: cyclohexene ≈ 1-octene >> 2,4C_6diene ≈ TMPs. Hatanaka et al. (Hatanaka et al., 1997b) reported that the strength of the inhibition is not to be considered dependent on steric effects from the olefins. From the results presented herein, such a conclusion seems arguable because the non-branched olefins (cyclohexene and 1-octene) presented a strong inhibition effect on the HDS of 2-MT while branched olefins (2,4C_6diene and TMPs) did not affect hydrodesulfurization. In view of this, inhibition effects are rather related to a steric hindrance induced by the methyl groups of the branched olefins that impede an adsorption on the catalytic active sites.

1.2.2 Reactivity of 2,5-dimethyl-2,4-hexadiene (2,4C_6diene) in the presence of cyclohexene. Olefins may undergo various reactions. Under the reaction conditions employed

herein, 2,4C_6diene underwent only double bond isomerization and hydrogenation reactions. Skeletal isomerization was negligible. This reaction requires a strongly acidic catalyst which is not the case of a CoMo-S/γ-Al_2O_3 catalyst (Brunet et al., 2005). Figure 6 shows the hydrogenation of 2,4C_6diene based on the determined products distribution.

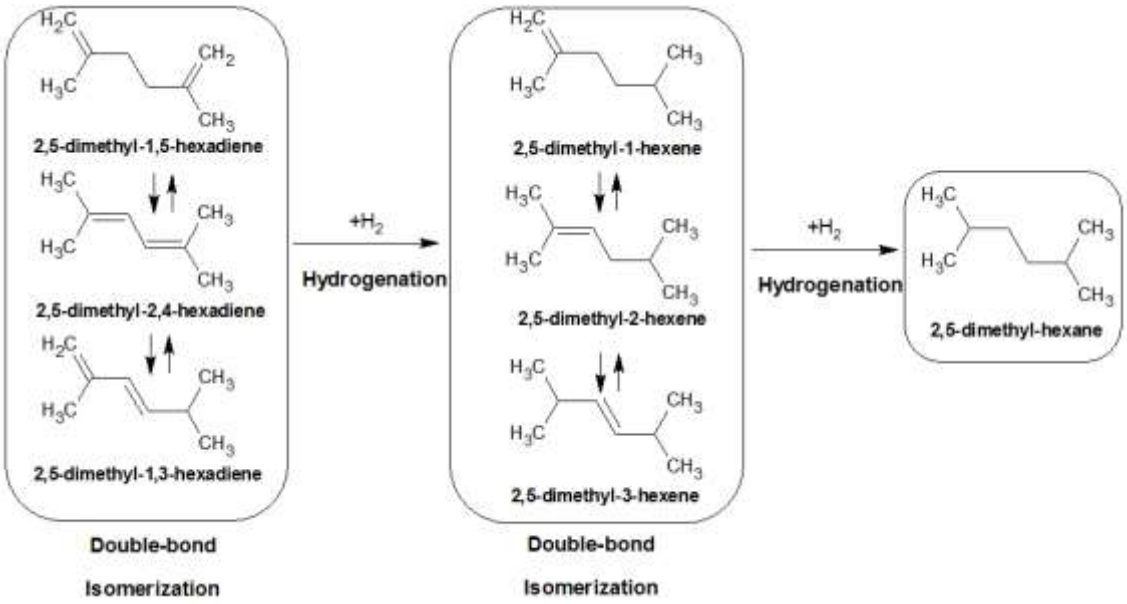

Figure 6. Reaction scheme of 2,4C_6diene

Isomerization products were: 2,5-dimethyl-1,5-hexadiene and 2,5-dimethyl-1,3-hexadiene. For convenience, these two products will be referred to as C_6dienes. The hydrogenation of 2,4C_6diene could proceed in three ways to form: 2,5-dimethyl-1-hexene (1Hexene), 2,5-dimethyl-2-hexene (2Hexene) and 2,5-dimethyl-3-hexene (3Hexene). The fully saturated product was 2,5-dimethyl-hexane (Hexane).

Figure 7 summarizes 2,4C_6diene conversion at different temperatures while Table 4 shows the obtained products distribution.

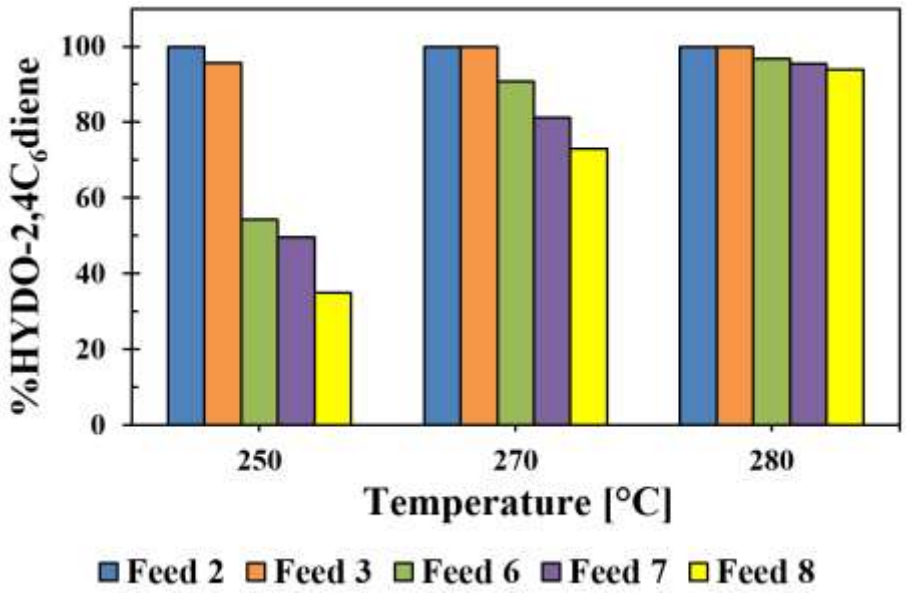

Figure 7. Conversion of the 2,4C_6diene in the presence of 2-MT (Feed 2 and 3) and in the presence of 2-MT and cyclohexene (Feed 6-8) at different temperatures. P= 50 bar, liquid-flow rate of 20 mLh^{-1} and H_2/liquid feed ratio of 500.

Table 4**.**

Effect of cyclohexene on 2,4C_6diene selectivity[a]

Feed[c]	Selectivity to 2,4C_6diene products[b]					Total products	
	C_6dienes	1Hexene	2Hexene	3Hexene	Hexane	Unsaturated	Saturated
2	0	10	59	8	23	77	23
3	0	12	59	12	17	83	17
6	0	13	61	23	3	97	3
7	2	12	61	25	2	98	2
8	2	12	59	26	1	99	1

[a] Reaction conditions: T=270°C, P= 50 bar, liquid-flow rate of 20 mLh^{-1} and H_2/liquid feed ratio of 500.

[b] 2,4C_6diene: 2,5-dimethyl-2,4-hexadiene; C_6dienes: isomers of 2,4C_6diene; 1Hexene: 2,5-dimethyl-1-hexene; 2Hexene: 2,5-dimethyl-2-hexene; 3Hexene: 2,5-dimethyl-3-hexene; Hexane: 2,5-dimethylhexane.

[c] Vide Table 3.

According to results, when 2,4C_6diene was the only olefin present (Feeds 2 and 3), the %HYDO-2,4C_6diene was a 100 or very close to a 100 % regardless of temperature. For all reactions, the main product was 2-hexene. This result is in agreement with results reported by Itatani et al. (Itatani & Bailar, 1972) who found that 2-hexene is the most stable product because of hyperconjugative stability. For cyclohexene-free reactions, results showed a higher production of the saturated product (Hexane); 23% for Feed 2 and 17% for Feed 3. Isomerization products were not found. Therefore, the experiments performed herein indicate the HDS environment of the reaction does not affect the HYDO of 2,4C_6diene. For Feeds 2 and 3, the conversions of 2-MT were 44 and 22%, respectively. Consequently, the partial pressure of H_2S inside the reactor was higher during the catalytic test carried out with Feed 2. Nevertheless, the products distribution and the conversion of 2,4C_6diene did not change significantly during these tests. Several authors have studied the effect of the partial pressure of H_2S on HYDO (Badawi, Vivier, Pérot, & Duprez, 2008; Daudin, Brunet, Perot, Raybaud, & Bouchy, 2007; Hatanaka, Yamada, & Sadakane, 1997a; LI, 2013). Liu et al. (Liu et al., 2014b) found that the inhibition effect caused by H_2S on HYDO is much stronger at lower reaction temperatures, and that such inhibition increased with the number of substituents of the olefin double bond. Hatanaka et al. (Hatanaka et al., 1997b) found that the hydrogenation of 1-octene and 1-hexene are retarded by the presence of H_2S whereas the hydrogenation of 2,4,4-trimethyl-2-pentene is promoted.

For Feeds 6 to 8, which are a mixture of 2-MT, cyclohexene, and 2,4C_6diene, the ratio between cyclohexene and 2,4C_6diene was fixed at 2.5. In general, the hydrogenation of 2,4C_6diene decreased as with its concentration. At 250°C, a comparison of the results obtained for those feeds with the same diolefin concentration, a strong inhibition effect from cyclohexene was clearly observed. The %HYDO-2,4C_6diene dropped from 100 for Feed 2 to 54 % for Feed 6, and from 96

for Feed 3 to 35 % for Feed 8. The inhibition effect of cyclohexene was negligible when temperature was raised. On the other hand, the selectivity to 1-hexene and 2-hexene were not affected by the presence of cyclohexene. In cases where the selectivity to 3-hexene increased, the selectivity to hexane decreased. Reactions carried out with Feeds 7 and 8; which had the highest content of olefins, showed low production of isomerization products (C_6dienes). The presence of cyclohexene changed the products distribution and, in addition, inhibited the complete saturation of 2,4C_6diene. Particularly, hexane selectivity dropped from 23 for Feed2 to 3% for Feed 6.

1.2.3 Effect of 2,4C_6diene on the reactivity of cyclohexene. Cyclohexene was hydrogenated to cyclohexane without the formation of other reaction products. Figure 8 shows cyclohexene conversion in the absence and presence of 2,4C_6diene.

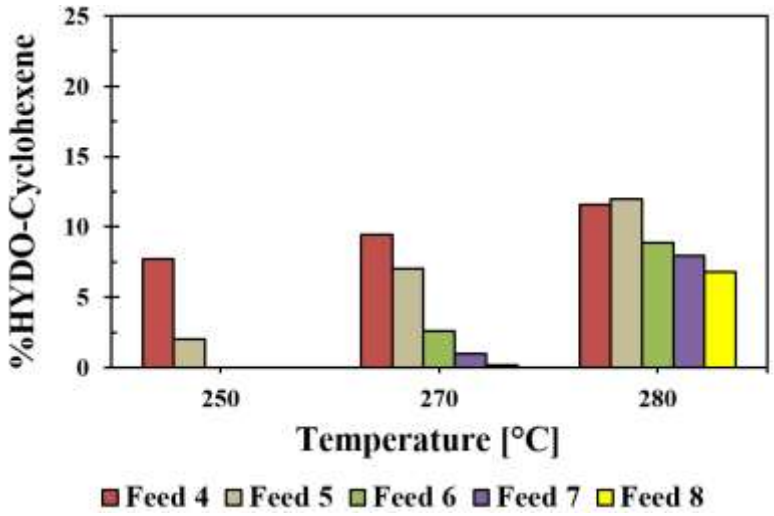

Figure 8. Conversion of cyclohexene in the presence of 2-MT (Feed 4 and 5) and in the presence of 2-MT and 2,4C_6diene (Feed 6-8) at different temperature. P= 50 bar, liquid-flow rate of 20 mLh^{-1} and H_2/liquid feed ratio of 500.

The hydrogenation of cyclohexene was very low. For all instances, cyclohexane conversion remained below 15%. When the concentration of cyclohexene in the feed was increased its conversion decreased. For reactions performed with mixed feeds, i.e. Feeds 6-8, and at 250°C, cyclohexene was not hydrogenated, but instead it must be recalled that it strongly inhibited the HDS of 2-MT and the hydrogenation of 2,4C_6diene. The observed inhibition effect of 2,4C_6diene over the conversion of cyclohexene decreased at higher temperatures. At 280°C, for example, %C-Cyclohexene dropped from 11% for Feed 4 to 9% for Feed 6 and from 8% for Feed 5 to 7% for Feed 8.

Figure 9 shows the effect of the conversion of 2-MT over the hydrogenation of cyclohexene.

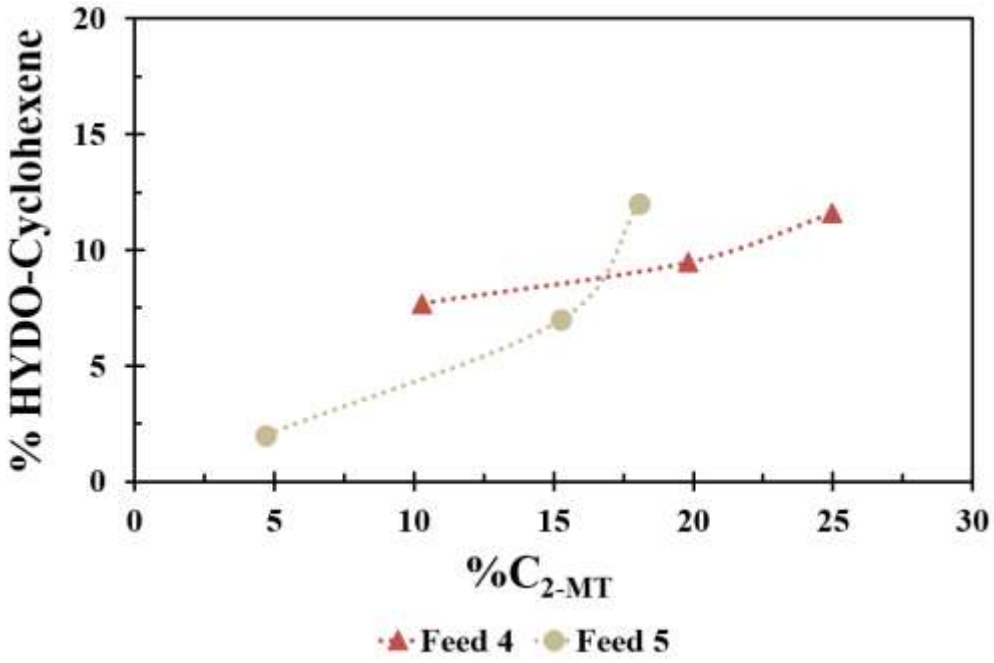

Figure 9. Hydrogenation of cyclohexene as a function of 2-MT conversion. P= 50 bar, liquid-flow rate of 20 mLh^{-1} and H_2/liquid feed ratio of 500.

An increase in cyclohexene conversion with 2-MT conversion was evidenced. This trend can be related to an increase in the partial pressure of H_2S. Yamada et al. (Yamada, Saito, Wakatsuki,

& Obara, 1987) studied the effect of H_2S on the reactivity of aromatic hydrocarbons over CoMo-S/Al_2O_3 catalysts. These authors found that an increase in the H_2S partial pressure inhibited the hydrogenation of benzene but, conversely, promoted the hydrogenation of o-xileno. Accordingly, they proposed that, at low partial pressure, H_2S plays a beneficial role on maintaining the sulfided state of the CoMo catalyst and may, in some cases, enhance hydrogenation.

1.2.4 Reactivity of 1-octene in the presence of TMPs. Figure 10 shows the observed reaction scheme for the hydrogenation of 1-octene. The main reactions that this linear olefin underwent were: the migration of its double bond from the positions 1 to the positions 2, 3, and 4; i.e. the isomerization of the molecule from an external to an internal olefin. Besides, a hydrogenation of the internal and external olefins to octane was observed.

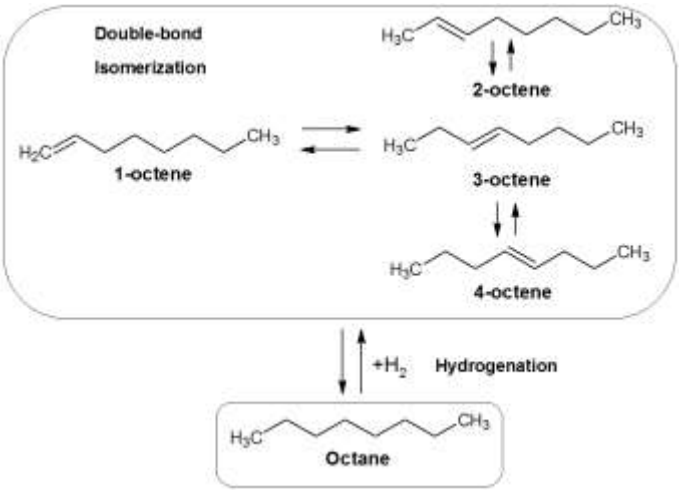

Figure 10. Reaction scheme for HYDO of 1-octene proposed by Pérez-Martinez et al. (Pérez-Martínez et al., 2010)

Table 5 shows the conversion and products distribution for 1-octene as a function of temperature. In all reaction tests, 1-octene was almost completely converted. For Feeds 11 and 12,

in which TMPs were present, the conversion and products distribution of 1-octene did not change significantly. Hence, the reactivity of 1-octene under those conditions was not affected by the presence of branched olefins.

Table 5

Effect of TMPs on 1-octeno HYDO and selectivity[a,b]

Feed[c]	230°C			250°C			270°C		
	%HYDO	nC8s	Octane	%HYDO	nC8s	Octane	%HYDO	nC8s	Octane
9	95	68	32	97	51	49	97	32	68
11	96	61	39	97	49	51	98	34	66
12	94	66	34	96	59	41	97	45	55

[a] Reaction condition: P= 50 bar, liquid-flow rate of 20 mLh^{-1} and H_2/liquid feed ratio of 500.

[b] nC8s: isomers of 1-octene.

[c] Vide Table 3.

Regarding products distribution, at 230°C, the selectivity to octane was 32%. When temperature was increased to 270°C, the selectivity to octane increased to 68%. Therefore, a significant effect of temperature over the hydrogenation of 1-octene and its isomers was evidenced. In this respect, Toba et al. (Toba et al., 2007) found that the hydrogenation of internal olefins increased with temperature whereas the conversion of a terminal olefin remained constant. Henceforth, this work demonstrates that an increment of the reaction temperature promotes the HYDO of 1-octene, especially, of its isomers (internal olefins).

1.2.5 Reactivity of TMPs in the presence of 1-octene. The observed reaction scheme for the hydrogenation of TMPs is shown in Figure 11. An isomerization of the double-bond between both kinds of branched olefins (TM1P and TM2P) occurred. The hydrogenated product was isooctane

and the cracking products were isobutene and isobutane (iC4s). Products from skeletal isomerization were not observed, at least not in quantifiable concentrations.

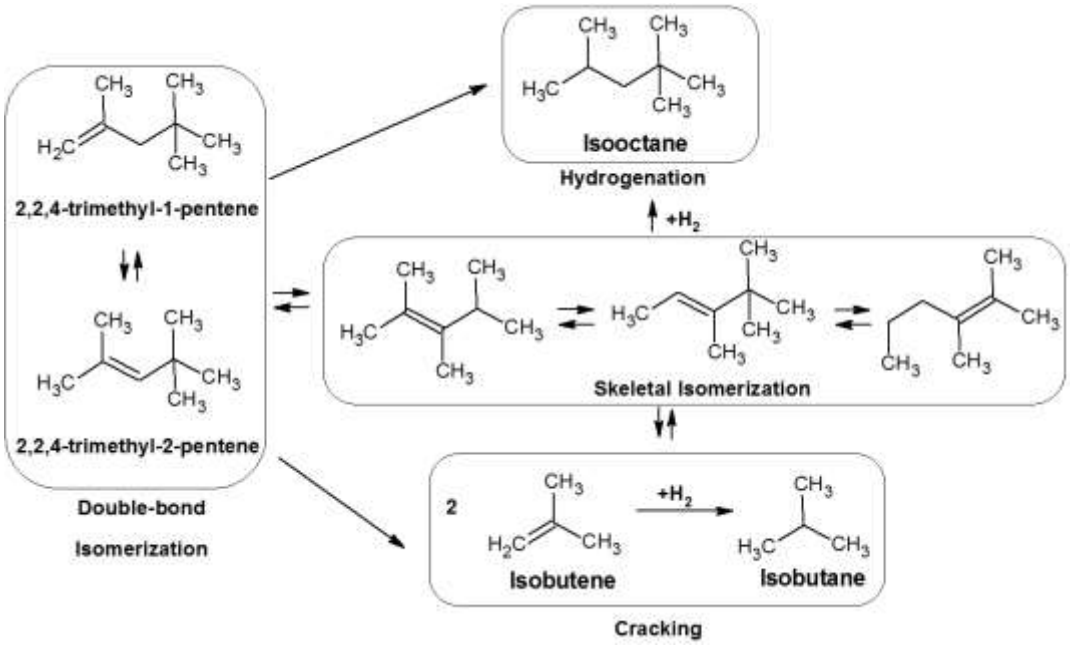

Figure 11. Reaction scheme of HYDO of TMPs.

Table 6 shows the conversions of TM1P and TM2P and the corresponding products distribution for the performed reaction tests.

Table 6.

Effect of 1-octeno on TMPs conversion and selectivity[a]

Feed[b]	%HYDO-TM1P	%HYDO-TM2P	Selectivity of TMPs products[c]	
			iC4s	Isooctane
10	42	16	16	84
11	44	18	19	81
12	26	-9	3	97

[a] Reaction condition: T=250°C, P= 50 bar, liquid-flow rate of 20 mLh^{-1} and H_2/liquid feed ratio of 500.

[b] Vide Table 3.

[c] TMPs: TM1P+TM2P; TM1P: trimethyl-1-pentene; TM2P: trimethyl-2-pentene; iC4s: isobutene + isobutene.

As expected, the conversion of the terminal olefin (TM1P) was much higher than the conversion of the internal olefin (TM2P). The negative value on TM1P conversion was produced as a result of TM2P double-bond isomerization. In all of the reactions, isooctane was the main reaction product. In order to study the effect of 1-octene on the hydrogenation of TMPs, the results of the reactions conducted with Feed 10 (1-octene-free reaction) and Feeds 11 and 12 were compared. Comparing the results obtained with Feeds 10 and 11, which had the same concentration of the TMPs, it is noted that 1-octene did not affect the reactivity of the TMPs since both the conversion and products distribution did not change. For Feed 12, the concentration of the TMPs was increased hence the conversion decreased. Moreover, the production of cracking products (iC4s) decreased sharply.

In section 1.2.4., it was found that TMPs did not affect the reactivity of 1-octene and in the present section the inhibition effect by 1-octene on TMPs hydrogenation was discarded. In the light of these results, both TMPs (branched olefins) and 1-octene (linear olefin) were not affected

by each other's presence hence, it seems safe to conclude that a competition between branched and linear olefins does not occur under HDS conditions. Hatanaka et al. (Hatanaka et al., 1997b) found similar results and suggested the existence of three different active sites on the surface of CoMo-S/γ-Al_2O_3 catalysts: namely, one site for HDS, another site for linear olefins hydrogenation, and a third site for branched olefins hydrogenation. However, more in-depth studies are still required to confirm such a hypothesis.

The hydrogenation of olefins has been described by a pseudo-first-order reaction kinetics. Figure 12 presents Arrhenius plots obtained after reactions tests carried out with Feeds 2, 5, 9 and 10, which contain 2,4C_6diene, cyclohexene, 1-octene, and TMPs, respectively.

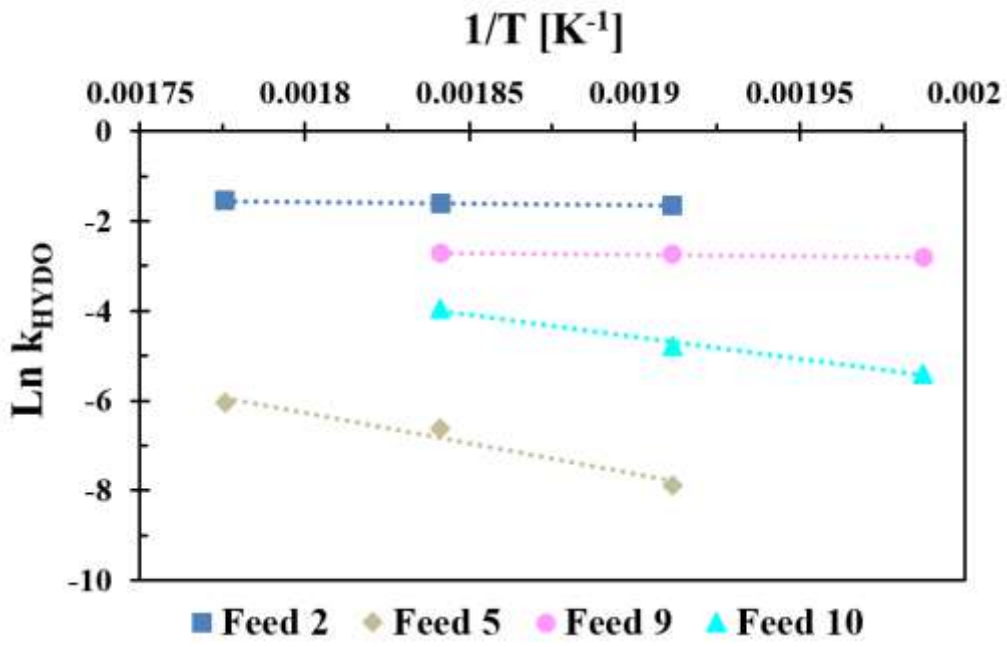

Figure 12. 1/T dependence of the rate constant of the conversion of Feeds 2, 5, 9 and 10. Pressure= 50 bar, liquid-flow rate of 20 mLh-1 and H2/liquid feed ratio of 500.

The obtained reaction rate constants were higher for the HYDO of the planar branched diolefin (Feed 2) and the linear olefin (Feed 9). Reaction rate constants obtained for TMPs (Feed 10), the

non-planar branched olefins, were lower than those for 1-octene (Feed 9) and 2,4C_6diene (Feed 2). Cyclohexene showed the lowest HYDO activity. A similar behavior was reported recently by Liu et al. (Liu et al., 2014b). These authors studied the reactivity of different groups of olefins and S-compounds typical from an FCC gasoline, and found a connection between the structure of the olefins and their reactivity. Olefins with the highest steric hindrance around de double bond (C=C) are less adsorbed on the active site than the others. TMPs are non-planar branched olefins, and for this reason, they are less reactive than 2,4C_6diene and 1-octene.

1.3 Conclusions

In this contribution, the inhibition effect of different kinds of olefins over the HDS of a model FCC naphtha on CoMo-S/γ-Al_2O_3 catalyst was assessed. In general, all olefins, linear, cyclic, and branched inhibited HDS. As branched olefins had a weaker inhibiting effect on HDS, the degree of inhibition of the olefins in HDS was associated to the existence of steric effects. An analysis of the effect of temperature on the selectivity of the HDS of 2-MT in the presence of the selected olefins showed that non-branched olefins (cyclohexene and 1-octene) have a strong inhibition effect on the desulfurization of 2-MT whereas branched olefins (2,4C_6diene and TMPs) do not affect the removal of sulfur. On the other hand, the reactivity of olefins under HDS conditions was also analyzed. In general, linear olefins, branched or non-branched, were more reactive as compared to a cyclic olefin. Furthermore, evidence was found on a positive effect of the H_2S atmosphere on the hydrogenation of the cyclic olefin. A comparison of the results from reactions performed with feeds containing a mix of olefins showed that an inhibition effect between non-

branched and branched linear olefins does not take place. Finally, it is important noticing that the cyclic olefin presented both the lowest reactivity and the strongest inhibition effect on HDS.

2. Kinetic Assessment of the Simultaneous Hydrodesulfurization of Dibenzothiophene and the Hydrogenation of Diverse Polyaromatic Structures

Increasingly stringent environmental requirements for fuels result in operational and economic challenges for the petroleum refining industry (Agency European Environment; Chevron Corporation). Hydrodesulfurization (HDS) of fuel fractions is one of the major catalytic processes coping with environmental statutes for sulfur content. For instance, the maximum allowed concentration of sulfur in diesel fuels in the European Union is 10 ppm (Transport Policy), 15 ppm in the U.S.A. (United States Environmental Protection Agency (EPA)), 10 ppm in Japan (Research Institute of Economy Trade and Industry (RIETI)), and 50 ppm on overage in South America (DieselNet). When the sulfur content in fuels is around 10 ppm, refiners refer to ultra-deep HDS. Such demands drive constant research efforts for the development of new catalysts and processes. HDS catalysts, normally, sulfided CoMo/γ-Al_2O_3 and/or NiMo/γ-Al_2O_3, face ultra-deep HDS aiming to remove sulfur from refractory dibenzothiophenes (DBTs) (Chandak et al., 2014; Duayne Whitehurst, Isoda, & Mochida, 1998; van Looij, van der Laan, Stork, DiCamillo, & Swain, 1998).

It is rather well established that DBTs react on the catalytic surface via the two parallel pathways shown in Figure 13, namely, via the direct desulfurization (DDS), which yields biphenyl (BP), and via the hydrogenation mediated desulfurization (HYD) pathways. HYD comprises

intermediate steps in which one of the benzene rings of DBT is first hydrogenated to tetra-hydro-dibenzothiophene (THDBT) and then to hexa-hydro-dibenzothiophene (HHDBT). These hydrogenation reactions are followed by the scission of the C-S-C bond to yield cyclohexylbenzene (CHB) (Egorova & Prins, 2004b; Houalla, Nag, Sapre, Broderick, & Gates, 1978; Shafi & Hutchings, 2000; Antony Stanislaus, Marafi, & Rana, 2010).

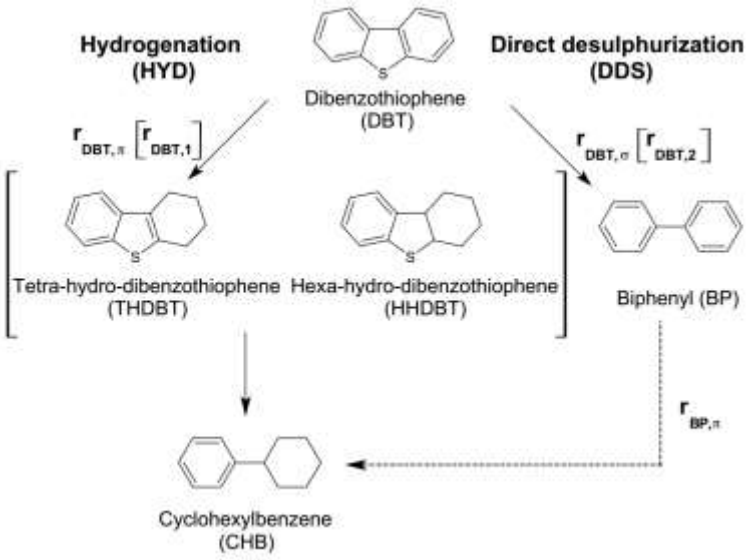

Figure 13. Reaction network for the hydrodesulfurization of dibenzothiophene.

On the other hand, the question of the number and nature of the active sites involved in DDS and HYD is not clear yet. Some authors have proposed a common di-hydro-dibenzothiophene (DHDBT) intermediate for both the DDS and HYD reaction pathways (Bataille et al., 2000; Meille, Schulz, Lemaire, & Vrinat, 1997; Mijoin et al., 2001; Singhal, Espino, Sobel, & Huff, 1981). They suggest that this intermediate could be hydrogenated or desulfurized on the same active site. The difference in reactivity between the two pathways would thus be related to the different reaction rates to the transformation of DHDBT. Kinetic models based on this hypothesis have proposed one site on which DBT and its reaction products competitively adsorb and a second

site for H_2 adsorption (Singhal et al., 1981; Vrinat, 1983; Y. Wang et al., 2004). However, a strong argument against this mechanism is that di-hydro-dibenzothiophene has not ever been detected in HDS reactions under standard operational conditions. Other studies have suggested that the HDS pathway is determined by the adsorption mode of the dibenzothiophene molecules. Particularly, two modes of adsorption can be taken into account. For the DDS and the final C-S-C bond scission in the HYD reaction route, adsorption is considered to occur by the direct attachment of the sulfur heteroatom in an σ adsorption mode. Meanwhile, HYD is considered to occur via π type adsorption of the aromatic structure of the molecule on the active site (Cristol et al., 2004; Valencia, Peña, & García-Cruz, 2012). These two different modes of adsorption require different active sites and different adsorption and kinetic constants for the DDS and HYD routes (Besenbacher et al., 2008; Moses, Hinnemann, Topsøe, & Nørskov, 2007; Tuxen et al., 2012). However, these two adsorption modes for the transformation of DBTs and its derivatives have only been shown to be feasible via molecular simulations without being proven experimentally (Meille et al., 1997). Assuming more than one active site for the adsorption of hydrocarbons increases the complexity of kinetic modeling by augmenting the number of kinetic and adsorption parameters to be estimated. Kinetic expressions for the hydrodesulfurization of dibenzothiophene assuming that the hydrogenolysis and the hydrogenation reactions take place on two different active sites have been modeled scarcely. In this regard, pseudo-first-order order models (Farag, 2006) and the Langmuir-Hinshelwood-Hougen-Watson (LHHW) formalism have been used for the modeling kinetics mainly over CoMo/γ-Al_2O_3 catalysts (Broderick & Gates, 1981; Edvinsson & Irandoust, 1993; Vanrysselberghe & Froment, 1996). Less attention has been given to the study of kinetic models for the HDS of DBT over NiMo/γ-Al_2O_3 (Ho & Sobel, 1991). Nevertheless, at present, owing to the high hydrogenation activity exhibited at high hydrogen partial pressure, NiMo catalysts are

preferred for ultra-low sulfur diesel production (Choi, Kunisada, Korai, Mochida, & Nakano, 2003; Antony Stanislaus et al., 2010) and for the pretreatment stage of the feed for hydrocracking units (Rayo, Ramírez, Torres-Mancera, Marroquín, & Maity, 2012; Sahu, Song, Im, Jeon, & Lee, 2015). For that reason, more rigorous kinetic modeling of the hydrodesulfurization over NiMo/γ-Al_2O_3 catalyst are required to approach the molecular level description of hydrotreating reactions.

In ultra-deep HDS, DBTs must be desulfurized in the presence of highly complex aromatic structures (Koltai et al., 2002; Lecrenay, Sakanishi, & Mochida, 1997; H. Wang & Prins, 2009). Several authors have studied the hydrodesulfurization of dibenzothiophene in the presence of aromatic compounds (Baldovino-Medrano, Giraldo, & Centeno, 2008; Koltai et al., 2002; Song et al., 2006). Aromatic compounds with two and three fused rings have been found to inhibit HDS catalysts (Beltramone, Resasco, Alvarez, & Choudhary, 2008; Song et al., 2006; Antonymuthu Stanislaus & Cooper, 1994). The inhibiting effect on the aforementioned reaction routes is far from being understood, nonetheless. The studies, undertaken to determine possible inhibition effects of aromatics over the hydrodesulfurization of DBTs, often limit themselves to describing relative impacts of the presence of the aromatics on the conversion and selectivity of a selected model molecule (Egorova & Prins, 2004a; Koltai et al., 2002; Song et al., 2006). Furthermore, some contradictory trends have been reported since some authors observe that aromatics may inhibit the HYD route of desulfurization to a larger extent as compared to the DDS route (Duayne Whitehurst et al., 1998; Logadóttir et al., 2006), whereas some others report that both reaction routes are inhibited to the same extent (Egorova & Prins, 2004a; Farag, Sakanishi, Mochida, & Whitehurst, 1998; van Looij et al., 1998).

Kinetic studies for the HDS of DBTs in the presence of aromatic compounds are limited. The pseudo-first-order model has been frequently used to correlate the inhibition effect of the aromatic

compounds (Duayne Whitehurst et al., 1998; Farag et al., 1998; Song et al., 2006). Nevertheless, with this approach, the adsorption equilibrium constants for all the compounds involved in the reaction are not determined, which does not allow the elucidation of a reaction mechanism (Antonymuthu Stanislaus & Cooper, 1994). A simplified LHHW model assuming one site on which DBTs, aromatics, and the reaction products competitively adsorb has also been used (Koltai et al., 2002). However, physicochemical and statistical criteria were not employed to evaluate the estimated kinetic and adsorption parameters. To the best of our knowledge, a rigorous kinetic modeling that describes the competitive adsorption of aromatic compounds and dibenzothiophene assuming the existence of two types of active sites, one for the hydrogenation reactions and the other for the C-S-C bond scission has not been published yet for NiMo/γ-Al_2O_3.

Considering the above, the main objectives of this chapter were: first, to revisit the kinetic model for the hydrodesulfurization of dibenzothiophene over NiMo/γ-Al_2O_3 to elucidate the role of the number of the catalytic centers involved in the reaction. Second, to propose kinetically viable reaction pathways for the mutual inhibition effects present in the simultaneous hydrodesulfurization of dibenzothiophene and hydrogenation of aromatics with different chemical structures: naphthalene (NP), phenanthrene (PHE), and fluorene (FL). To achieve the first objective, three kinetic models were developed. The first one was based on the assumption that HYD and DDS occur on the same type of active sites. The second assumed that the HYD and DDS routes take place on two different active sites. And, the third model also assumed that hydrocarbons are adsorbed on the two different active sites, but included the hydrogenation of biphenyl to cyclohexylbenzene in the reaction network. For the second objective, different kinetic models were developed to elucidate the structural effects of the polyaromatics on the simultaneous reactions of hydrogenation and HDS of DBT. Naphthalene and phenanthrene were used as models of aromatics

with two and three fused rings, respectively. Fluorene was selected as a model for aromatics with a structure equivalent to that of dibenzothiophene, i.e. aromatics with a five-carbon-membered thiophenic ring. All models were based on the Langmuir-Hinshelwood-Hougen-Watson formalism and submitted to regression analyses with the reparametrized form of the Arrhenius and van´t Hoff equations. Owing to the latter, activation energies and pre-exponential factors, as well as the adsorption enthalpies and entropies of each compound were estimated. Statistical tests were performed to determine the overall significance of the regression and for the individual significance of the parameters (Froment, De Wilde, & Bischoff, 2011; Jae Lee & Froment, 2008; Vannice, Hyun, Kalpakci, & Liauh, 1979). The study provided robust kinetic modeling for the inhibition of aromatics on the hydrodesulfurization of dibenzothiophene.

2.1 Catalytic Tests

Catalytic tests were carried out in two different reaction set-ups; namely, Catatest (I) and Catatest (II), vide Appendix B Figure S2.1, provided with high-pressure fixed-bed continuous flow reactors operated in integral mode. Reactors were packed with a 8 wt.% Mo and 1.8 wt.% Ni NiMo/γ-Al_2O_3 commercial catalyst (Procatalyse, BET specific surface area ≈ 150 $m^2 \cdot g^{-1}$, BJH pore volume ≈ 0.42 $cm^3 \cdot g^{-1}$, and average BJH pore diameter ≈ 11.2 nm). Extrudates of the catalyst were ground and sieved to obtain particles with diameters ranging from 300 to 600 µm. For the catalytic tests, ca. 0.30 g (Catatest I) or ca. 0.15 g (Catatest II) of catalyst, were dried in situ under N_2 flow (100 $mL \cdot min^{-1}$) at 120°C for 1 h. Afterwards, the catalyst was sulfided during 4 h using a volumetric flow rate of 100 $mL \cdot min^{-1}$ containing 15% of H_2S in H_2 at atmospheric pressure and 400°C. After sulfidation, reactants were fed to the reactor at a volumetric flow rate of 30 $mL \cdot h^{-1}$. Then, the

reactor pressure was increased with H_2 to 5 MPa and a hydrogen/(liquid feed) rate ratio of 500 $NL \cdot L^{-1}$ was fixed for the experiments. Reaction temperatures were programmed to start at 300°C, to stabilize the catalyst. Afterwards, temperature was decreased to 260°C followed by its increase to 280°C and finally to 300°C again. Such conditions were applied to rule out possible deactivation effects. Some reactions were performed independently at each one of the aforementioned temperatures using fresh catalyst at every run. Such conditions were applied to check for possible deactivation of the catalyst during the experiments. Reactions were conducted until reaching steady state, considered herein as measurements where catalytic conversion and selectivity did not change more than ±2% over time on stream. The absence of heat and mass transport limitations was verified as stated elsewhere (Baldovino-Medrano, Eloy, Gaigneaux, Giraldo, & Centeno, 2009; Baldovino-Medrano et al., 2008).

The reaction feedstock accounted for the following compounds employed either individually or in blends: dibenzothiophene (Sigma-Aldrich, 98%), as a model sulfur compound in ultra-deep HDS, naphthalene (Laboratorios León, 98%), fluorene (Merck, 95%), and phenanthrene (Sigma-Aldrich, 98%), as model aromatic compounds. Hexadecane (Sigma-Aldrich, ≥ 99%) was used as an internal standard for chromatography and cyclohexane (commercial grade) was used as solvent.

Two sets of experiments were carried out to evaluate the kinetic and inhibiting effect of aromatic compounds on the hydrodesulfurization of dibenzothiophene. In the first set of experiments, tests were performed in the absence of aromatic compounds. Temperature was varied between 260 - 330°C, and space-time velocity ($W_{cat}F_{DBT_0}^{-1}$) between 33 - 242 $kg_{cat}kmol_{DBT}^{-1}h$, and, hence, the concentration of DBT was between 1.0 - 3.7 wt.%. The second set of experiments was conducted in the presence of naphthalene, fluorene or phenanthrene. These experiments were carried out at a fixed space-time velocity of DBT of 122 $kg_{cat}kmol_{DBT}^{-1}h$; i.e. 2 wt.% DBT. The

space-time velocity of the aromatic compounds was changed between 28-118 $kg_{cat}kmol^{-1}h$; i.e. between 2.0 – 6.0 wt.%. Reaction temperatures were between 260 - 300°C. Consequently, the total number of experiments for the hydrodesulfurization of dibenzothiophene in the absence and presence of aromatic compounds amounted to 80. There were thus ca. 446 observations took into account during modeling.

Liquid products identification was made with gas chromatography (GC) and mass spectroscopy (MS). Gas chromatography analyses were performed with a HP 6890 chromatograph equipped with an FID detector and an automatic injector. An HP-1 column (Agilent J&W, 100 m × 0.25 mm × 0.5 μm) was used for both GC and GC-MS. Analysis conditions were as follows: the GC oven temperature was programmed from 90 to 180°C (17 min) at 60°C min^{-1}, then to 260°C (10 min) using a temperature ramp of 80°C min^{-1}. Helium (Linde Colombia S.A, 99.99%) was used as carrier gas, with 19 cm s^{-1} linear velocity (1.1 mL min^{-1}, at constant flow). Compounds in each sample were identified by means of a computer matching method, comparing their spectra with those provided in the Wiley, NIST, and QUADLIB libraries. The experimental error in the mass balance was found to be ±5%. The carbon balance calculated for each reaction is given in Tables S2.1 – S2.4, Section S2.2, of the Appendix B.

Catalytic results were expressed in terms of conversion (%X_i), products selectivity (%S_j), and yield (%Y_j) percentages. Conversion was calculated as follows:

$$\%X_i = \frac{F_i^0 - F_i}{F_i^0} \times 100\% \qquad (2.1)$$

Where, F_i^0 and F_i are the inlet and outlet molar flow rate of the hydrocarbon, respectively. Selectivity and yields were calculated as follows:

$$\%S_j = \frac{F_j}{F_i^0 - F_i} \times 100\% \qquad (2.2)$$

$$\%Y_j = \frac{F_j}{F_i^0} \times 100\% \qquad (2.3)$$

Where, F_j is the outlet molar flow rate of the product *j*.

2.2 Kinetic modeling

2.2.1 Hydrodesulfurization of dibenzothiophene. Different kinetic models based on the LHHW formalism were developed. The first model; denominated DBT1S, considered a single active site, i.e. * sites, over which DBT and its reaction products adsorb and react via either DDS or HYD routes. The second model; named DBT2S, assumed that the HYD and DDS routes take place on two different active sites, i.e. π sites where the molecules are hydrogenated and σ sites over which the molecules are desulfurized. A third model; denominated DBTBP2S, was based on the same considerations as those made for the DBT2S model, but it included the hydrogenation of biphenyl to cyclohexylbenzene (Egorova & Prins, 2004b; Ho & Sobel, 1991; Vanrysselberghe & Froment, 1996). The three kinetic models assumed the adsorption and heterolytically dissociation of H_2 occurring on β surface sites, which are different from the sites over which hydrocarbons adsorb (García-Martínez, Castillo-Araiza, De los Reyes Heredia, Trejo, & Montesinos, 2012; Schachtl, Kondratieva, Gutiérrez, & Lercher, 2015).

The reaction mechanism for DBT1S is presented in Table 7. Therein, υ_i is the stoichiometric number used for describing the number of times that each adsorption, desorption, and reaction steps must occur in order to complete one catalytic cycle according to the overall reaction *i*, the latter represented by global reactions 1 and 2. The dissociation of H_2 is considered to occur only on β sites; step A. Whereas, dibenzothiophene, biphenyl, and cyclohexylbenzene are considered to adsorb and react over * sites: steps B to F. The direct desulfurization reaction and hydrogenation

pathway are represented by steps C and E, respectively. The formation and later desorption of H_2S from β sites are represented in steps G and H, respectively. The H_2S desorbed from β sites may be re-adsorbed on * sites; steps I and J.

Table 7.

Reaction Mechanism and Catalytic Cycles for the Kinetic Model DBT1S

step	mechanism	v_1	v_2
A	$H_2 + 2\beta \rightleftarrows 2H\beta$	2	5
B	$DBT + * \rightleftarrows DBT*$	1	1
C	$DBT* + 3H\beta \rightarrow BP* + SH\beta + 2\beta$	1	0
D	$BP* \leftrightarrows BP + *$	1	0
E	$DBT* + 9H\beta \rightarrow CHB* + SH\beta + 8\beta$	0	1
F	$CHB* \rightleftarrows CHB + *$	0	1
G	$SH\beta + H\beta \rightleftarrows H_2S\beta + \beta$	1	1
H	$H_2S\beta \rightleftarrows H_2S + \beta$	1	1
I	$H_2S + * + \beta \rightleftarrows SH* + H\beta$	1	1
J	$SH* + H\beta \rightleftarrows H_2S + * + \beta$	1	1
	Global Reactions		
1	$DBT + 2H_2 \rightarrow BP + H_2S$	1	0
2	$DBT + 5H_2 \rightarrow CHB + H_2S$	0	1

Table 8 presents the reaction mechanism proposed for both DBT2S and DBTBP2S models. H_2 is dissociatively adsorbed on β sites; step A. DDS occurs on a single reaction on σ sites; step C. While, HYD is accounted for on π sites; step F (Broderick & Gates, 1981; Vanrysselberghe & Froment, 1996). Steps J to L were considered only for the model DBTBP2S where the hydrogenation of BP to CHB was assumed to occur as presented in step K. The global reaction represented in step 3 and the respective υ_3 are also exclusively for this model. The adsorption and re-adsorption of H_2S on σ and π sites are also taken into account in steps M to P.

Table 8**.**

Reaction Mechanism and Catalytic Cycles for the Kinetic Models DBT2S and DBTBP2S

step	mechanism	v_1	v_2	v_3
A	$H_2 + 2\beta \rightleftarrows 2H\beta$	2	5	3
B	$DBT + \sigma \rightleftarrows DBT\sigma$	1	0	0
C	$DBT\sigma + 3H\beta \rightarrow BP\sigma + SH\beta + 2\beta$	1	0	0
D	$BP\sigma \rightleftarrows BP + \sigma$	1	0	0
E	$DBT + \pi \rightleftarrows DBT\pi$	0	1	0
F	$DBT\pi + 9H\beta + \sigma \rightarrow CHB\sigma + SH\beta + 8\beta + \pi$	0	1	0
G	$CHB\sigma \rightleftarrows CHB + \sigma$	0	1	0
H	$SH\beta + H\beta \rightleftarrows H_2S\beta + \beta$	1	1	0
I	$H_2S\beta \rightleftarrows H_2S + \beta$	1	1	0
J	$BP + \pi \rightleftarrows BP\pi$	0	0	1
K	$BP\pi + 6H\beta \rightarrow CHB\pi + 6\beta$	0	0	1
L	$CHB\pi \rightleftarrows CHB + \pi$	0	0	1
M	$H_2S + \sigma + \beta \rightleftarrows SH\sigma + H\beta$	1	0	0
N	$SH\sigma + H\beta \rightleftarrows H_2S + \sigma + \beta$	1	0	0
O	$H_2S + \pi + \beta \rightleftarrows SH\pi + H\beta$	0	1	0
P	$SH\pi + H\beta \rightleftarrows H_2S + \pi + \beta$	0	1	0
	Global Reactions			
1	$DBT + 2H_2 \rightarrow BP + H_2S$	1	0	0
2	$DBT + 5H_2 \rightarrow CHB + H_2S$	0	1	0
3[a]	$BP + 3H_2 \rightarrow CHB$	0	0	1

[a]Global reaction 3 must only be considered for the DBTBP2S model.

In general, the following assumptions were made: (i) an approximation to pseudo-equilibrium for adsorption and desorption steps; (ii) the concentration of hydrogen is constant during the reaction due to its large partial pressure. In consequence, H_2 concentration and sites β were lumped into the kinetic constant of the corresponding reaction rate; (iii) surface reactions are rate-determining steps (RDS); (iv) the hydrogenolysis of THDBT and HHDBT are fast enough so as

to be immediately desulfurized into cyclohexylbenzene and H_2S; and, (v) all products contribute to kinetic inhibition by competitive adsorption with dibenzothiophene, i.e. biphenyl, cyclohexylbenzene, and H_2S. On the basis of these assumptions, the corresponding kinetic models can be written as follows:

DBT1S

$$r_{DBT,1} = -k_{DBT,1} K_{DBT,*} P_{DBT} \theta_* \qquad (2.4)$$

$$r_{DBT,2} = -k_{DBT,2} K_{DBT,*} P_{DBT} \theta_* \qquad (2.5)$$

DBT2S

$$r_{DBT,\sigma} = -k_{DBT,\sigma} K_{DBT,\sigma} P_{DBT} \theta_\sigma \qquad (2.6)$$

$$r_{DBT,\pi} = -k_{DBT,\pi} K_{DBT,\pi} P_{DBT} \theta_\pi \qquad (2.7)$$

DBTBP2S

$$r_{DBT,\sigma} = -k_{DBT,\sigma} K_{DBT,\sigma} P_{DBT} \theta_\sigma \qquad (2.8)$$

$$r_{DBT,\pi} = -k_{DBT,\pi} K_{DBT,\pi} P_{DBT} \theta_\pi \qquad (2.9)$$

$$r_{BP,\pi} = -k_{BP,\pi} K_{BP,\pi} P_{BP} \theta_\pi \qquad (2.10)$$

Where:

$$\theta_j = \frac{1}{1 + \sum K_{n,j} P_n} \qquad (2.11)$$

Herein, θ_j denotes the fraction of free active sites *j*, $K_{n,j}$ correspond to the adsorption equilibrium coefficient for the component *n* on the site *j*, and P_n the partial pressure of the component *n*.

In general, calculations showed high coverage of DBT on active sites, vide Appendix B (Section S2.3). Therefore, kinetic expressions were assumed to keep a constant order.

2.2.2 Hydrodesulfurization of dibenzothiophene simultaneous to the hydrogenation of aromatic compounds. After analyzing results that will be commented later (Section 2.4.2.1), the considerations proposed for the model DBTBP2S were used for the kinetic modeling of the hydrodesulfurization of dibenzothiophene simultaneous to the hydrogenation of aromatic compounds. Kinetic models were developed assuming that dibenzothiophene, biphenyl, cyclohexylbenzene, and H_2S are adsorbed on both sites, and aromatic molecules and their reaction products react either only on π sites or on both π and σ sites. The reversibility of the hydrogenation of naphthalene, fluorene, and phenanthrene was considered for kinetic modeling. In what follows, only the kinetic models that led to the best results are presented for the sake of brevity. Kinetic models describing the inhibiting effect on the simultaneous hydrodesulfurization of dibenzothiophene and hydrogenation of naphthalene, fluorene, and phenanthrene were named DBTNP, DBTFL, and DBTPHE, respectively. Kinetic expressions for each model were based on the mechanism of the HDS of DBT, i.e. Table 7, integrated with the mechanism of the respective hydrogenation of each aromatic molecule. In general, assumptions for the proposed models were based on both experimental results and literature review. The reader may refer to the Appendix B (Section S2.4) for data concerning other models tested in this work.

2.2.2.1 Hydrogenation of naphthalene simultaneous to the hydrodesulfurization of dibenzothiophene (DBTNP). Figure14 (a) shows a simplified reaction network for naphthalene hydrogenation (Girgis & Gates, 1991; Rautanen, Lylykangas, Aittamaa, & Krause, 2002; Romero, Thybaut, & Marin, 2008).

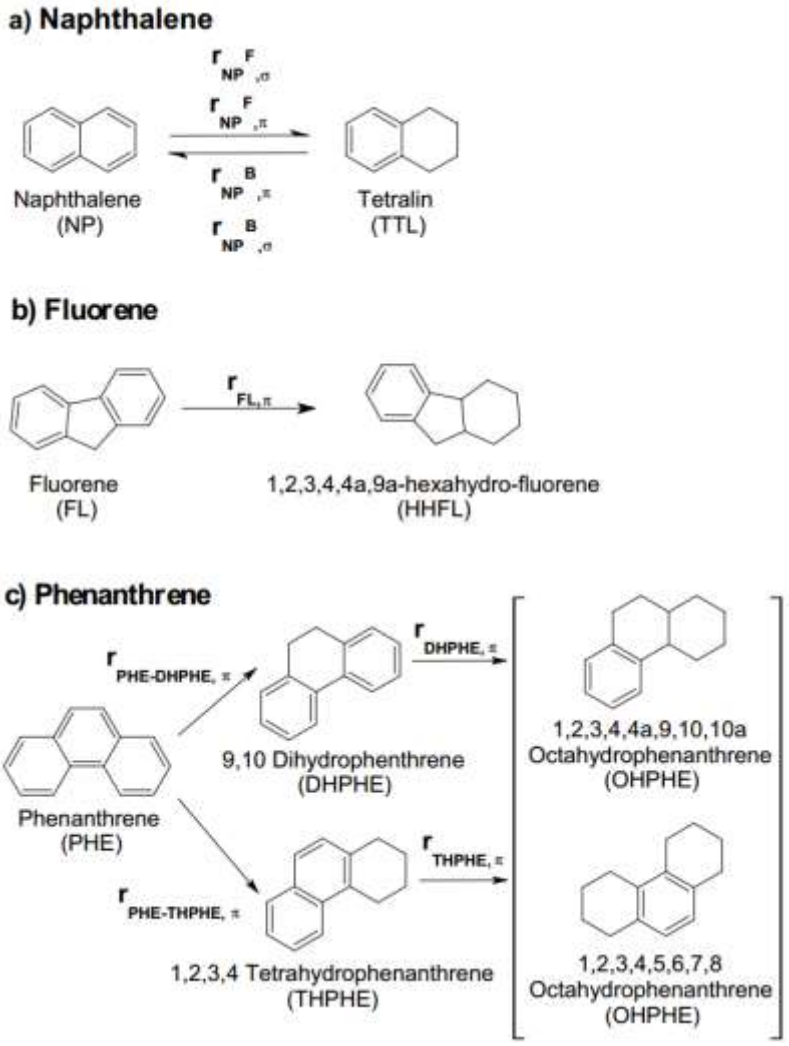

*Figure 14***.** Reaction network for the hydrogenation of polyaromatic compounds: a) Naphthalene, b) Fluorene, and c) Phenanthrene.

In the presence of dibenzothiophene, the modeling of naphthalene hydrogenation was based on the following assumptions: (i) naphthalene is only hydrogenated to tetralin (TTL); (ii) naphthalene and tetralin competitively adsorb and react on both π and σ sites; and, (iii) naphthalene hydrogenation to tetralin is reversible. Table 9 presents the mechanism employed to describe naphthalene hydrogenation. The dissociation of H_2 occurs over β sites; step A. Naphthalene is

adsorbed and hydrogenated on σ sites; steps B and C, and on π sites; steps E and F. Finally, tetralin is desorbed; steps D and G.

Table 9.

Reaction Mechanism and Catalytic Cycles for the Kinetic Model DBTNP to Describe the Hydrogenation of NP

step	mechanism	ν_1	ν_2
A	$H_2 + 2\beta \rightleftarrows 2H\beta$	2	2
B	$NP + \sigma \rightleftarrows NP\sigma$	1	0
C	$NP\sigma + 4H\beta \rightleftarrows TTL\sigma + 4\beta$	1	0
D	$TTL\sigma \rightleftarrows TTL + \sigma$	1	0
E	$NP + \pi \rightleftarrows NP\pi$	0	1
F	$NP\pi + 4H\beta \rightleftarrows TTL\pi + 4\beta$	0	1
G	$TTL\pi \rightleftarrows TTL + \pi$	0	1
	Global Reaction		
1	$NP + 2H_2 \rightleftarrows TTL$	1	1

The rate expressions considered for the simultaneous hydrodesulfurization of dibenzothiophene and hydrogenation of naphthalene were:

$$r_{DBTNP,\sigma} = -k_{DBT,\sigma}K_{DBT,\sigma}P_{DBT}\theta_{DBTNP,\sigma} \quad (2.12)$$

$$r_{DBTNP,\pi} = -k_{DBT,\pi}K_{DBT,\pi}P_{DBT}\theta_{DBTNP,\pi} \quad (2.13)$$

$$r_{BPNP,\pi} = -k_{BP,\pi}K_{BP,\pi}P_{BP}\theta_{DBTNP,\pi} \quad (2.14)$$

$$r_{NP,\sigma} = -\left(k^F_{NP,\sigma}K_{NP,\sigma}P_{NP} - k^B_{NP,\sigma}K_{TTL,\sigma}P_{TTL}\right)\theta_{DBTNP,\sigma} \quad (2.15)$$

$$r_{NP,\pi} = -\left(k^F_{NP,\pi}K_{NP,\pi}P_{NP} - k^B_{NP,\pi}K_{TTL,\pi}P_{TTL}\right)\theta_{DBTNP,\pi} \quad (2.16)$$

Where, k^F_{NP} and k^B_{NP} are the reaction rate coefficients of the forward and backward of naphthalene hydrogenation.

2.2.2.2 Hydrogenation of fluorene simultaneous to the hydrodesulfurization of dibenzothiophene (DBTFL). A simplified hydrogenation network of fluorene based on the proposition by Lapinas et al. (Lapinas, Klein, Gates, Macris, & Lyons, 1991) is presented in Figure14 (b). For the formulation of the kinetic model for fluorene hydrogenation in the presence of dibenzothiophene, the following assumptions were made: (i) only the hydrogenation of the first ring of fluorene to form 1,2,3,4,4a,9a-hexahydrofluorene (HHFL) takes place; (ii) the hydrogenation of fluorene only occurs on π sites; and, (iii) the reversibility of the reaction is neglected. Table 10 presents the mechanism to describe the hydrogenation of fluorene. Hydrogen and fluorene are adsorbed on β and π sites, respectively; steps A and B. Step C summarizes a series of sequential hydrogenation steps. Finally, on step D 1,2,3,4,4a,9a-hexahydrofluo is desorbed.

Table 10**.**

Reaction Mechanism and Catalytic Cycles for the Kinetic Model DBTFL to Describe the Hydrogenation of FL

step	**mechanism**	$\boldsymbol{v_1}$
A	$H_2 + 2\beta \rightleftarrows 2H\beta$	3
B	$FL + \pi \rightleftarrows FL\pi$	1
C	$FL\pi + 6H\beta \rightarrow HHFL\pi + 6\beta$	1
D	$HHFL\pi \rightleftarrows HHFL + \pi$	1
	Global Reaction	
1	$FL + 3H_2 \rightarrow HHFL$	1

The rate expressions for the simultaneous dibenzothiophene hydrodesulfurization and fluorene hydrogenation were thus described by the following equations:

$$r_{DBTFL,\sigma} = -k_{DBT,\sigma} K_{DBT,\sigma} P_{DBT} \theta_{DBTFL,\sigma} \qquad (2.17)$$

$$r_{DBTFL,\pi} = -k_{DBT,\pi}K_{DBT,\pi}P_{DBT}\theta_{DBTFL,\pi} \quad (2.18)$$

$$r_{BPFL,\pi} = -k_{BP,\pi}K_{BP,\pi}P_{BP}\theta_{DBTFL,\pi} \quad (2.19)$$

$$r_{FL,\pi} = -k_{FL,\pi}K_{FL,\pi}P_{FL}\theta_{DBTFL,\pi} \quad (2.20)$$

2.2.2.3 Hydrogenation of phenanthrene simultaneous to the hydrodesulfurization of dibenzothiophene (DBTPHE). Phenanthrene is a polycyclic aromatic hydrocarbon composed of three fused aromatic rings. For the hydrogenation of phenanthrene different networks have been proposed in literature (Beltramone et al., 2008; Ishihara et al., 2003; Korre, Klein, & Quann, 1995; Schachtl, Zhong, et al., 2015; Huibin Yang et al., 2014). Beltramone et al. (Beltramone et al., 2008) and Schachtl et al. (Schachtl, Zhong, et al., 2015) proposed two parallel pathways. The first route is the hydrogenation of phenanthrene to 9,10-dihydrophenanthrene (DHPHE), and the second route is the hydrogenation of phenanthrene to 1,2,3,4-tetrahydrophenanthrene (THPHE). Subsequently, DHPHE and THPHE are supposed to be hydrogenated to octahydrophenanthrene (1,8-OHPHE and 1,10-OHPHE) and thence to perhydrophenanthrene (PHPHE). Conversely, Ishihara et al. (Ishihara et al., 2003) proposed that phenanthrene is hydrogenated exclusively to DHPHE from where DHPHE is hydrogenated to THPHE and OHPHE, and finally to PHPHE. These two reaction networks are modeled herein but the network proposing two parallel pathways for the hydrogenation of phenanthrene in presence of dibenzothiophene led to a better fit of kinetic observations. The details for the other models evaluates are given in Section S2.4 of the Appendix B. Thus, in what follows this reaction network and the corresponding kinetic model are presented. Figure 14 (c) presents the reaction network for the hydrogenation of phenanthrene. 1,8-octahydrophenanthrene and 1,10- octahydrophenanthrene were lumped as octahydrophenanthrene. For the kinetic model, the following assumptions were made: (i) the

hydrogenation of phenanthrene, 9,10-dihydrophenanthrene, and 1,2,3,4-tetrahydrophenanthrene only occur on π sites; and, (ii) the reversibility of the reactions is neglected. The corresponding reaction mechanism is shown in Table 11. Hydrogen and phenanthrene are assumed to adsorb on β and π sites, respectively; steps A and B. Steps C and D represent the hydrogenation of phenanthrene to 9, 10-dihydrophenanthrene and 1,2,3,4-tetrahydrophenanthrene, respectively. The sequential hydrogenation to octahydrophenanthrene from 9,10-dihydrophenanthrene and 1,2,3,4-tetrahydrophenanthrene are represented in steps E and F, respectively. Finally, desorption of products was represented by steps G to I.

Table 11**.**

Reaction Mechanism and Catalytic Cycles for the Kinetic Model DBTPHE to Describe the Hydrogenation of PHE

step	**mechanism**	$\boldsymbol{v_1}$	$\boldsymbol{v_2}$	$\boldsymbol{v_3}$	$\boldsymbol{v_4}$
A	$H_2 + 2\beta \rightleftarrows 2H\beta$	1	2	3	2
B	$PHE + \pi \rightleftarrows PHE\pi$	1	1	0	0
C	$PHE\pi + 2H\beta \rightarrow DHPHE\pi + 2\beta$	1	0	0	0
D	$PHE\pi + 4H\beta \rightarrow THPHE\pi + 4\beta$	0	1	0	0
E	$DHPHE\pi + 6H\beta \rightarrow OHPHE\pi + 6\beta$	0	0	1	0
F	$THPHE\pi + 4H\beta \rightarrow OHPHE\pi + 4\beta$	0	0	0	1
G	$DHPHE\pi \rightleftarrows DHPHE + \pi$	1	0	0	0
H	$THPHE\pi \rightleftarrows THPHE + \pi$	0	1	0	0
I	$OHPHE\pi \rightleftarrows OHPHE + \pi$	0	0	1	1
	Global Reactions				
1	$PHE + H_2 \rightarrow DHPHE$	1	0	0	0
2	$PHE + 2H_2 \rightarrow THPHE$	0	1	0	0
3	$DHPHE + 3H_2 \rightarrow OHPHE$	0	0	1	0
4	$THPHE + 2H_2 \rightarrow OHPHE$	0	0	0	1

The rate expressions for both the simultaneous hydrodesulfurization of dibenzothiophene and hydrogenation of phenanthrene are presented below:

$$r_{DBTPHE,\sigma} = -k_{DBT,\sigma}K_{DBT,\sigma}P_{DBT}\theta_{DBTPHE,\sigma} \quad (2.21)$$

$$r_{DBTPHE,\pi} = -k_{DBT,\pi}K_{DBT,\pi}P_{DBT}\theta_{DBTPHE,\pi} \quad (2.22)$$

$$r_{BPPHE,\pi} = -k_{BP,\pi}K_{BP,\pi}P_{BP}\theta_{DBTPHE,\pi} \quad (2.23)$$

$$r_{PHE-THPHE,\pi} = -k_{PHE-THPHE,\pi}K_{PHE,\pi}P_{PHE}\theta_{DBTPHE,\pi} \quad (2.24)$$

$$r_{PHE-DHPHE,\pi} = -k_{PHE-DHPHE,\pi}K_{PHE,\pi}P_{PHE}\theta_{DBTPHE,\pi} \quad (2.25)$$

$$r_{THPHE,\pi} = -k_{THPHE,\pi}K_{THPHE,\pi}P_{THPHE}\theta_{DBTPHE,\pi} \quad (2.26)$$

$$r_{DHPHE,\pi} = -k_{DHPHE,\pi}K_{DHPHE,\pi}P_{DHPHE}\theta_{DBTPHE,\pi} \quad (2.27)$$

2.2.3 Estimation of model parameters. Kinetic parameters were estimated by minimizing the objective function RSS(φ), which includes the residual sum of squares of the concentration of the different species (Castillo-Araiza et al., 2015; Che-Galicia, Ruiz-Martínez, López-Isunza, & Castillo-Araiza, 2015; Raghuveer, Thybaut, & Marin, 2016):

$$\text{RSS}(\varphi) = \sum_{n=1}^{n_{resp}} w_n \sum_{k=1}^{n_{exp}} \left(F_{k,n} - \hat{F}_{k,n}\right)^2 \xrightarrow{\varphi_1,\varphi_2,\ldots,\varphi_n} min \quad (2.28)$$

Where φ is the optimal parameter vector, n_{exp} is the number of independent experiments, n_{resp} is the number of responses, $F_{k,n}$ and $\hat{F}_{k,n}$ are molar flows of the *n*-th experimental and predicted responses for the *k*-th observations, respectively. And, w_n is the weight factor assigned to the *n*-th response.

The subroutine VODE was used to solve the corresponding set of ordinary differential equations (Brown, Byrne, & Hindmarsh, 1989). The initial minimization of the objective function, vide Eq. 2.28, in the model regression was carried out using the Rosenbrock method (Rosenbrock,

1960). Then the ODRPACK subroutines were called for fitting calculated values to the corresponding experimental data point (Boggs, Donaldson, Byrd, & Schnabel, 1989). These subroutines can perform either weight orthogonal distance regression or nonlinear least square squares for explicit and implicit models using multi-response data with an implementation of the Levenberg-Marquard method (Marquardt, 1963).

The reparameterization of Arrhenius and van´t Hoff expressions led to Eq. (2.29) and Eq. (2.30), respectively. The resulting parameters were used for the regression analysis. The activation energies and pre-exponential factors as well as the adsorption enthalpies and entropies were calculated from the parameter estimation procedure.

$$k_i = \exp\left[A_i^{'} - \frac{E_{A,i}}{R}\left(\frac{1}{T} - \frac{1}{T^*}\right)\right] \qquad (2.29)$$

$$K_n = \exp\left[\frac{\Delta S_n^0}{R} - \frac{\Delta H_n^0}{R}\left(\frac{1}{T} - \frac{1}{T^*}\right)\right] \qquad (2.30)$$

Where, for the *i*-th reaction, $A_i^{'}$ is the natural logarithm of the pre-exponential factor, $E_{A,i}$ is the activation energy, T is the reaction temperature, T^* is the averaged reaction temperature, ΔS_n^0 is the standard adsorption entropy of component n, ΔH_n^0 is the standard adsorption enthalpy of component *n*, and R is the universal gas constant.

The significance of the overall regression for each model was tested after estimating the parameters of the model. This procedure was done by means of an F-test. The F-value for the global significance of the regression was defined as the ratio of the regression sum of squares to the residual sum of squares divided by their respective degrees of freedom.

$$F - value = \frac{\frac{\left[\sum_{n=1}^{n_{rep}} w_n \sum_{n=1}^{n_{rep}} \left(\hat{F}_{k,n}\right)^2\right]}{p}}{\frac{\left[\sum_{n=1}^{n_{rep}} w_n \sum_{n=1}^{n_{rep}} \left(F_{k,n} - \hat{F}_{k,n}\right)^2\right]}{\left(n_{exp} n_{resp} p\right)}} \qquad (2.31)$$

The regression is considered meaningful if the ratio is larger than the tabulated α percentage point (with α = 0.05) of the F distribution with degree of freedom (p, $n_{exp}n_{resp}$-p).

The significance of the individual parameters was evaluated by a *t*-test. Each parameter is tested against a reference t-value:

$$t - value = \frac{\left|b_i - \bar{b_i}\right|}{\sqrt{\left(\sum_{j=1}^{n_{rep}} \sum_{k=1}^{n_{rep}} w_{j,k} J_j^T J_k\right)^{-1}}} \qquad (2.32)$$

Where b_i and $\bar{b_i}$ are the estimated and the reference parameter values, respectively. J_j is the Jacobian matrix of the response j with respect to the parameter b_i. The resulting value of t-value is compared with a tabulated value obtained for $n_{exp}n_{resp}$-p degrees of freedom and a probability level of 1-α, i.e., t-value ($n_{exp}n_{resp}$-p, 1-α/2). The chosen probability is 95%, i.e., α=0.05.

Parity diagrams were also built to visualize the agreement between experimental observations and model fit. The Bayesian information criterion (BIC) was used to avoid model overfitting by introducing a penalty for the number of parameters in the model (Kass & Raftery, 1995; Myung, Tang, & Pitt, 2009; Schwarz, 1978). In other words, the model leading to the lowest BIC was preferred among a finite set of models.

2.2.3.1 Physicochemical tests on the parameters of the models. Typically, testing the fitting of the rate equation to the experimental data and calculating the confidence intervals of the estimated parameters is considered to be enough when developing a kinetic model. However, such a procedure does not provide physical meaning to the parameters of the model. The kinetic and adsorption equilibrium constants contained in the rate expression need to be evaluated to verify whether they are physically reasonable and thermodynamically consistent. Boudart et al. (Boudart & Djega-Mariadassou, 2014) proposed several rules for evaluating kinetic parameters that are

described next. First, since adsorption is, with very few exceptions, exothermic, values for the estimated adsorption enthalpies must satisfy the inequality:

$$-\Delta H_n^0 > 0 \qquad (2.33)$$

Second, the adsorption entropy of the adsorbed species must be higher than zero and lower than the corresponding standard entropy of the corresponding species in the gas phase ($\Delta S_{n,g}^0$):

$$0 < \Delta S_n^0 < \Delta S_{n,g}^0 \qquad (2.34)$$

The following limits for the adsorption entropy must be met:

$$41.8 < -\Delta S_n^0 < 51.04 - 1.4\Delta H_n^0 \qquad (2.35)$$

Finally, another thermodynamic criterion that must be considered is that the standard enthalpy of reaction must be equal to the difference between the change in standard adsorption enthalpies for reactants and products and the activation energies for the forward and backward reactions (Eq. 2.34):

$$\Delta H_r^\circ = \left(\Delta H_R^\circ - \Delta H_P^\circ\right) - (Ea^B - Ea^F) \qquad (2.36)$$

Where, ΔH_r° is the standard enthalpy of reaction, ΔH_R° and ΔH_P° are the standard adsorption enthalpies for reactants and products, and Ea^F and Ea^B are the activation energies for the forward and backward reactions, respectively. Such a relationship is based on the potential energy diagram for the reaction (Mhadeshwar, Wang, & Vlachos, 2003):

2.3 Results

2.3.1 Experimental evaluation

2.3.1.1 Hydrodesulfurization of dibenzothiophene in the absence and in the presence of aromatic compounds. Table 12 displays the conversion of dibenzothiophene and the selectivity to the reaction products as a function of space-time velocity; $W_{cat}F_{DBT_0}^{-1}$. During the hydrodesulfurization of dibenzothiophene, only biphenyl and cyclohexylbenzene were detected. Partially hydrogenated intermediates; i.e. THDBT and HHDBT, of the HYD pathway were only observed as traces. As expected, the conversion of dibenzothiophene increased with space-time and the main reaction product was biphenyl (Egorova & Prins, 2004b; Meille et al., 1997; Vanrysselberghe & Froment, 1996). The selectivity to the DDS route, that is, the selectivity to biphenyl, decreased with space-time velocity, whereas cyclohexylbenzene selectivity increased. This suggests that biphenyl was probably hydrogenated to cyclohexylbenzene, as has been mentioned by other authors (Egorova & Prins, 2004c; Singhal et al., 1981; Vanrysselberghe & Froment, 1996) and corroborated experimentally in this work, vide Appendix B S2.5.

Table 12**.**

Conversion and selectivity observed at different conditions and obtained evaluating the conversion of DBT or aromatic compound individually or in blend.[a]

Feed	$W_{Catal.}F_0^{-1}$	$\%X_{DBT}$	%Selectivity to DBT products		$\%X_{NP}$	$\%X_{FL}$	$\%X_{PHE}$	%Selectivity to PHE products		
			$\%S_{BP}$	$\%S_{CHB}$				$\%S_{THPHE}$	$\%S_{DHPHE}$	$\%S_{OHPHE}$
DBT	46	33.4	87.9	12.1						
	91	57.9	87.5	12.5						
	122	70.8	86.1	13.9						
	182	88.7	85.1	14.9						
NP	56				71.8					
FL	73					12.7				
PHE	73						77.0	19.0	28.1	52.9
DBT+NP[b]	56	72.2	86.7	13.3	38.1					
	28	70.1	86.5	13.5	29.2					
DBT+FL[b]	73	65.3	89.3	10.7		4.5				
	37	58.6	89.1	10.9		3.4				
DBT+PHE[b]	73	56.8	86.3	13.7			42.6	38.8	39.9	21.2
	37	50.7	85.9	14.1			36.4	41.7	40.6	17.6

[a] Reaction conditions: T=300°C, P=5 MPa, liquid-flow rate of 30 mL·h^{-1} and H_2/liquid feed ratio of 500.

[b] The $W_{cat}F_0^{-1}$ is respect of the aromatic compound. $W_{Catal}F_{DBT_0}^{-1}$ is constant and equal to 122 $kg_{cat}kmol_{DBT}^{-1}h$.

The hydrodesulfurization of dibenzothiophene was studied in the presence of naphthalene, fluorene, and phenanthrene at the same space-time of dibenzothiophene, i.e. 122 $W_{cat}F_{DBT_0}^{-1}$, but at different space-times for the aromatic compounds. The conversion of dibenzothiophene and the selectivity to biphenyl and cyclohexylbenzene were not significantly affected by the presence of naphthalene since the standard deviation calculated from these data was ca. 1.1 %. On the other hand, the conversion of dibenzothiophene decreased in the presence of fluorene and phenanthrene. For example, at 37 $W_{cat}F_0^{-1}$, dibenzothiophene conversion dropped from 70.8% to 58.6% and 50.7%, in the presence of fluorene and phenanthrene, respectively. On the other hand, the HYD pathway of the hydrodesulfurization of dibenzothiophene appeared diminished by fluorene, since

the selectivity to biphenyl increased from ca. 86% to 89%. Whereas, phenanthrene seemed not to affect selectivity. To this end, phenanthrene seems to inhibit the DDS and HYD pathways to the same extent, while fluorene seems to inhibit the HYD route stronger than the DDS route.

2.3.1.2 Hydrogenation of naphthalene, fluorene, and phenanthrene in the absence and in the presence of dibenzothiophene. Besides analyzing dibenzothiophene reactivity in the presence of the aromatics, it is also convenient to follow aromatics reactivity in the absence and in the presence of dibenzothiophene; Table 12 shows the corresponding results. In the absence of dibenzothiophene, aromatics conversion followed the order: $\%C_{PHE} = 77 > \%C_{NP} = 71.8 >> \%C_{FL}=12.7$. Therefore, fluorene exhibited a much lower hydrogenation conversion than the other aromatics. The conversion of the aromatics was significantly affected by the presence of dibenzothiophene. The conversion of both naphthalene and phenanthrene dropped ca. 47% from the values observed in the absence of dibenzothiophene. On the other hand, the conversion of fluorene was affected more strongly as it dropped ca. 65%. The selectivity to phenanthrene products also varied in the presence of dibenzothiophene. THPHE and DHPHE, i.e. the products with one hydrogenated aromatic ring, increased their selectivity significantly. Particularly, selectivity to THPHE increased from 19 to 38.8% whereas the selectivity to DHPHE increased from 28.1 to 39.9%. Meanwhile, the selectivity to OHPHE, the product with two hydrogenated aromatic rings, dropped ca. 60%. In conclusion, it is evident that the hydrogenation of naphthalene, fluorene, and phenanthrene was strongly inhibited by the presence of dibenzothiophene which in turn affected products distribution.

2.3.2 Kinetic modeling

2.3.2.1 Hydrodesulfurization of dibenzothiophene. Figure 15 depicts parity diagrams for the HDS of DBT over the NiMo/γ-Al_2O_3 comparing the experimental with the calculated conversion of dibenzothiophene, and the yields of biphenyl and cyclohexylbenzene, for the three developed kinetic models: DBT1S, DBT2S, and DBTBP2S. The DBT1S model which assumes a single site for both HYD and DDS showed the worst fitting (Figure 15a). Conversely, the models assuming two different sites for the HYD and DDS pathways, DBT2S (Figure 15b) and DBTBP2S (Figure 15c), fitted adequately the experimental observations within an error margin lower than 10%. Between DBT2S and DBTBP2S, the latter fitted better the yield of cyclohexylbenzene. The global significance of the performed regressions for each model was assessed via calculation of the corresponding F and BIC-values. Although all models led to a statistically significant regression; i.e. F-value >> tabulated F-value ≈ 2.79, DBTBP2S presented the largest F-value = 29274 and the lower BIC = 1297 which implies a better fitting of the experimental data.

a)

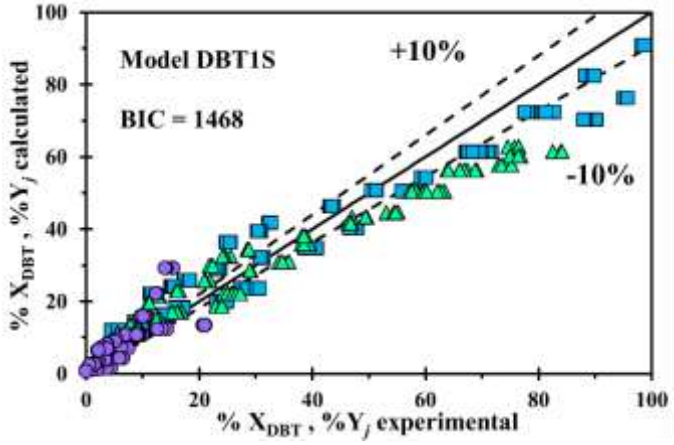

b)

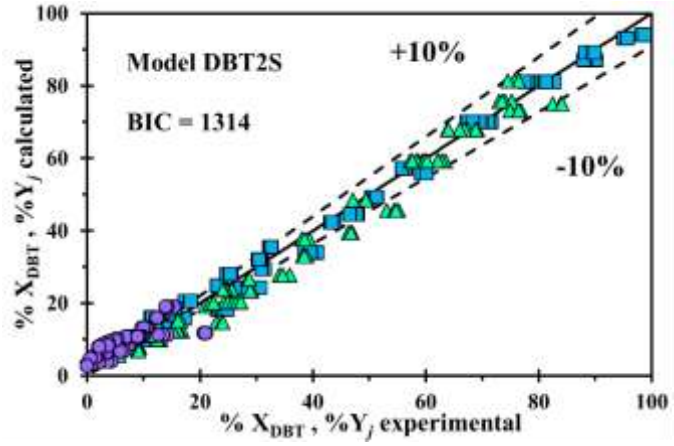

c)

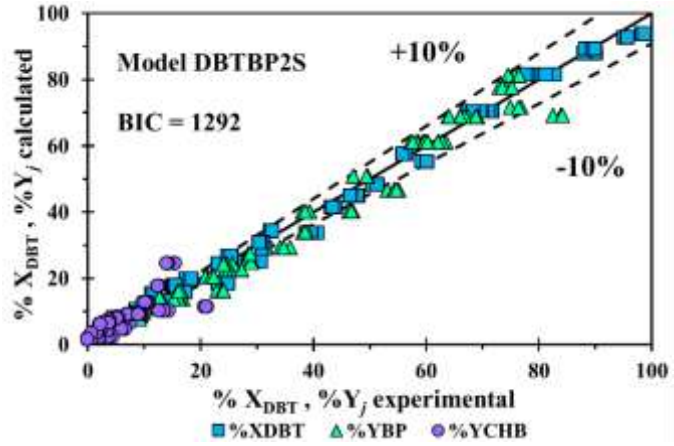

Figure 15. Parity diagrams for comparing experimental with calculated conversion of DBT ($\%X_{DBT}$) and the yields of BP ($\%Y_{BP}$) and CHB ($\%Y_{CHB}$), for the three kinetic models the HDS of DBT: a) DBT1S, b) DBT2S, and c) DBTBP2S. *p*=5 MPa, T=260-300°C, liquid-flow rate of 30 $mL \cdot h^{-1}$ and H_2/liquid feed ratio of 500.

Considering the best fitting of the DBTBP2S model, the values calculated for its parameters are presented in Table 13 together with 95% probability confidence intervals and the corresponding *t*-values. In general, all parameters were found to be statistically significant. Furthermore, the values of adsorption enthalpies and adsorption entropies on both σ and π sites satisfied Boudart et al. (Boudart & Djega-Mariadassou, 2014) criteria, vide Eqs (2.31)-(2.33). Therefore, values of $-\Delta H_{i,\sigma}^{0}$ and $-\Delta H_{i,\pi}^{0}$ were indeed positive as well as $-\Delta S_{i,\sigma}^{0}$ and $-\Delta S_{i,\tau}^{0}$. The latter were also lower than the corresponding standard entropy of the gas phase species, i.e. they were below than 316, 384, and 205 J (mol K)$^{-1}$ for DBT, BP, and H_2S, respectively. The second criterion for the adsorption entropy (Eq. 2.33) was also satisfied for values derived from the DBTBP2S model in all cases except for H_2S adsorption on π sites ($-\Delta S_{H_2S,\tau}^{0}$), probably due to poor adsorption of this compound on these sites. On the other hand, the activation energies obtained from the model were within the range proposed by Santacesaria (Santacesaria, 1997), that is from 21 to about 210 kJ mol^{-1}. It is worth noting that activation energies lower than 21 kJ mol^{-1} suggest the presence of external diffusion limitations, whereas values larger than 210 kJ mol^{-1} are related to the existence of thermal gradients during the experimentation. To this end, activation energies obtained herein are well adjusted to intrinsic kinetic measurements.

Table 13**.**

Kinetic parameters values and corresponding 95% probability confidence intervals for the kinetic model DBTBP2S used to describe the HDS of DBT.

Parameter	Estimated value	Lower limit	Upper limit	*t*-value
$A_{DBT,\sigma}$ mmol (g h)$^{-1}$	0.533	0.531	0.536	458.6
$A_{DBT,\pi}$ mmol (g h)$^{-1}$	0.179	0.177	0.180	299.7
$A_{BP,\pi}$ mmol (g h)$^{-1}$	0.012	0.012	0.013	104.4
$E_{a\ DBT,\sigma}$ kJ mol^{-1}	47.1	46.6	47.6	201.8
$E_{a\ DBT,\pi}$ kJ mol^{-1}	131.9	130.4	133.3	182.1
$E_{a\ BP,\pi}$ kJ mol^{-1}	162.4	159.7	165.2	115.5
$-\Delta S^0_{DBT,\sigma}$ J (mol K)$^{-1}$	69.6	69.5	69.7	1259.0
$-\Delta S^0_{BP,\sigma}$ J (mol K)$^{-1}$	89.5	88.3	90.7	141.8
$-\Delta S^0_{CHB,\sigma}$ J (mol K)$^{-1}$	65.7	65.2	66.1	269.3
$-\Delta S^0_{H2S,\sigma}$ J (mol K)$^{-1}$	126.1	119.6	132.5	38.6
$-\Delta S^0_{DBT,\pi}$ J (mol K)$^{-1}$	105.8	105.2	106.3	363.6
$-\Delta S^0_{BP,\pi}$ J (mol K)$^{-1}$	41.2	41.7	42.0	519.2
$-\Delta S^0_{CHB,\pi}$ J (mol K)$^{-1}$	41.0	40.8	41.2	475.8
$-\Delta S^0_{H2S,\pi}$ J (mol K)$^{-1}$	113.9	112.4	115.4	148.8
$-\Delta H^0_{DBT,\sigma}$ kJ mol^{-1}	33.8	33.3	34.3	132.7
$-\Delta H^0_{BP,\sigma}$ kJ mol^{-1}	34.8	34.2	35.4	114.0
$-\Delta H^0_{CHB,\sigma}$ kJ mol^{-1}	18.2	17.9	18.5	117.4
$-\Delta H^0_{H2S,\sigma}$ kJ mol^{-1}	203.1	198.3	207.8	84.6
$-\Delta H^0_{DBT,\pi}$ kJ mol^{-1}	58.7	58.2	59.2	236.8
$-\Delta H^0_{BP,\pi}$ kJ mol^{-1}	42.0	41.4	42.6	143.4
$-\Delta H^0_{CHB,\pi}$ kJ mol^{-1}	2.6	2.5	2.6	147.7
$-\Delta H^0_{H2S,\pi}$ kJ mol^{-1}	1.4	1.4	1.5	63.1

Note: F-value = 29274. Ftab = 2.79, ttab = 1.963 at 1-α = 0.95 and 922 degrees of freedom.

2.3.2.1 Simultaneous HDS of DBT and hydrogenation of aromatics. For the kinetic models DBTNP, DBTFL, and DBTPHE both reactions are modeled simultaneous, i.e. the hydrodesulfurization of dibenzothiophene and the hydrogenation of respective aromatic compound. Considering that DBTBP2S was the model that better fitted the experimental results for the hydrodesulfurization of dibenzothiophene, it was chosen as a basis for further kinetic analysis of the hydrodesulfurization of dibenzothiophene in the presence of the aromatic compounds. Figure 16 presents the parity plot for the reactions carried out in the presence of naphthalene. The DBTNP kinetic model was found to predict the subtle effect of naphthalene on the hydrodesulfurization of dibenzothiophene under the studied reaction conditions. Furthermore, the model was capable of fitting experimental observations for the conversion of DBT and for the production of BP, CHB, NP, and TTL with an error margin below 10%.

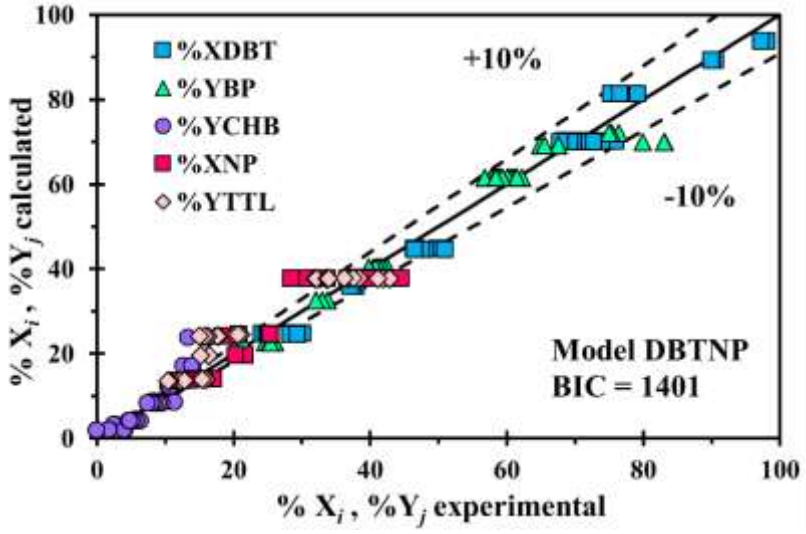

Figure 16. Parity diagram for comparing experimental with the calculated conversion of DBT ($\%X_{DBT}$) and NP ($\%X_{NP}$), and the yields of their reaction products ($\%Y_{BP}$, $\%Y_{CHB}$, $\%Y_{TTL}$). The simulated values were calculated from the model DBTNP that describe the simultaneous HDS of DBT and hydrogenation of NP. *p*=5 MPa, T=260-300°C, liquid-flow rate of 30 $mL \cdot h^{-1}$ and H_2/liquid feed ratio of 500.

Likewise, the models DBTFL and DBTPHE fitted adequately the experimental observation of the conversion of dibenzothiophene and product yields, and also the conversion of fluorene and phenanthrene, and their respective product yields, as shown in the parity plots showed in Figures 17 and 18, respectively.

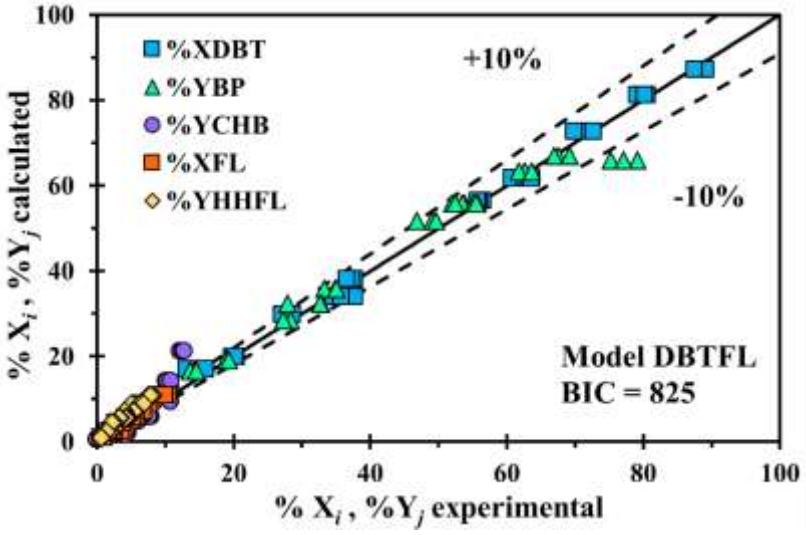

*Figure 17***.** Parity diagram for comparing experimental with the calculated conversion of DBT ($\%X_{DBT}$) and FL ($\%X_{FL}$), and the yields of their reaction products ($\%Y_{BP}$, $\%Y_{CHB}$, $\%Y_{HHFL}$). The simulated values were calculated from the model DBTFL that describe the simultaneous HDS of DBT and hydrogenation of FL. *p*=5 MPa, T=260-300°C, liquid-flow rate of 30 $mL \cdot h^{-1}$ and H_2/liquid feed ratio of 500.

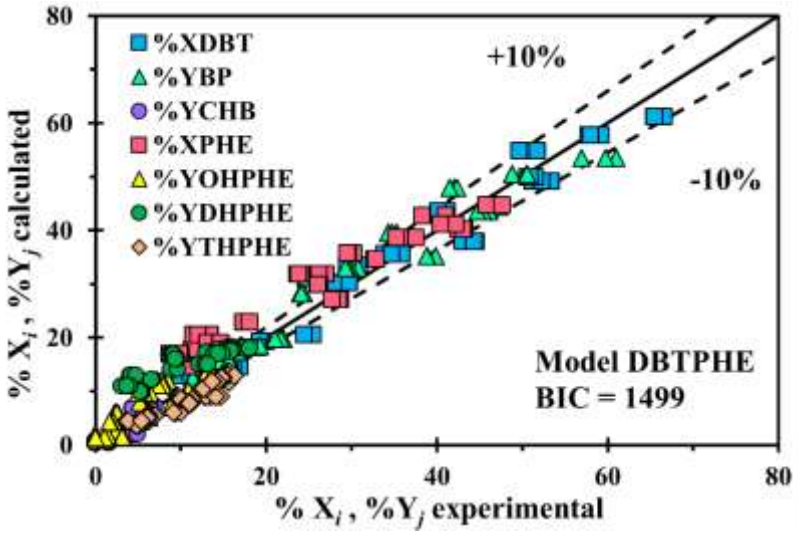

Figure 18. Parity diagram for comparing experimental with the calculated conversion of DBT ($\%X_{DBT}$) and PHE ($\%X_{PHE}$), and the yields of their reaction products ($\%Y_{BP}$, $\%Y_{CHB}$, $\%Y_{OHPHE}$, $\%Y_{DHPHE}$, $\%Y_{THPHE}$). The simulated values were calculated from the model DBTPHE that describe the simultaneous HDS of DBT and hydrogenation of PHE. *p*=5 MPa, T=260-300°C, liquid-flow rate of 30 $mL \cdot h^{-1}$ and H_2/liquid feed ratio of 500.

In general, the developed kinetic models also fitted the results for the hydrogenation of the studied aromatics. The BIC for the global significance of the regressions amounted to 1401, 825, and to 1499 for DBTNP, DBTFL, and DBTPHE, respectively, thus evidencing a suitable statistical significance of these regressions. Values for the parameters of dibenzothiophene and its reaction products corresponding to the reactions under the presence of naphthalene, phenanthrene, and fluorine are presented in Table 13. Tables 14 to 16 present the kinetic parameters related to the studied aromatic compounds and its reaction products. The DBTNP and DBTFL models led to statistically significant regressions, vide Table 14 and Table 15, respectively, since all parameters presented narrow confidence intervals and *t*-values larger than the tabulated *t*-values. The parameters estimated for the DBTPHE model, their corresponding 95% confidence intervals, and the calculated *t*-values are shown in Table 16. The thermodynamic consistency of these parameters

was also verified except for those related to the production and adsorption of OHPHE. This behavior is typically considered to stem from a relatively weak chemisorption of the molecule in comparison to other compounds (Raghuveer et al., 2016). Adsorption equilibrium constants and rates coefficients at 280°C for the reactions of hydrodesulfurization of dibenzothiophene, hydrogenation of naphthalene, fluorene, and phenanthrene are presented in Appendix B (Section S2.6).

Table 14**.**

Kinetic parameters values and corresponding 95% probability confidence intervals for the kinetic model DBTNP used to describe the HDS of DBT and hydrogenation of NP.

Parameter	Estimated value	Lower limit	Upper limit	*t*-value
$A_{NP^F,\sigma}$, mmol (g h)$^{-1}$	0.0067	0.0065	0.0069	70.6
$A_{NP^F,\pi,}$, mmol (g h)$^{-1}$	0.0749	0.0743	0.0755	23.9
$A_{NP^R,\sigma}$, mmol (g h)$^{-1}$	0.1000	0.0972	0.1028	70.5
$A_{NP^R,\pi}$, mmol (g h)$^{-1}$	0.0094	0.0090	0.0098	44.1
$E_{a\ NP^F,\sigma}$, kJ mol^{-1}	66.6	65.8	67.3	178.3
$E_{a\ NP^F,\pi,}$,kJ mol^{-1}	50.7	50.1	51.3	161.2
$E_{a\ NP^R,\sigma}$, kJ mol^{-1}	97.8	93.9	101.6	49.8
$E_{a\ NP^R,\pi}$, kJ mol^{-1}	107.8	105.2	110.5	79.6
$-\Delta S^0_{NP,\sigma}$, J (mol K)$^{-1}$	126.1	125.0	127.3	210.6
$-\Delta S^0_{TTL,\sigma}$, J (mol K)$^{-1}$	108.8	106.6	111.0	96.8
$-\Delta S^0_{NP,\pi}$, J (mol K)$^{-1}$	120.4	119.8	121.1	379.5
$-\Delta S^0_{TTL,\pi}$, J (mol K)$^{-1}$	73.0	72.5	73.5	305.5
$-\Delta H^0_{NP,\sigma}$, kJ mol^{-1}	31.6	31.0	32.2	100.4
$-\Delta H^0_{TTL,\sigma}$, kJ mol^{-1}	28.5	27.4	29.5	51.8
$-\Delta H^0_{NP,\pi}$, kJ mol^{-1}	60.5	59.8	61.3	155.6
$-\Delta H^0_{TTL,\pi}$, kJ mol^{-1}	31.5	30.7	32.3	79.1

Note: F-value = 8848. Ftab = 2.79, ttab = 1.964 at 1-α = 0.95 and 560 degrees of freedom

Table 15**.**

Kinetic parameters values and corresponding 95% probability confidence intervals for the kinetic model DBTFL used to describe the HDS of DBT and hydrogenation of FL.

Parameter	Estimated value	Lower limit	Upper limit	*t*-value
$A_{FL,\pi}$ mmol (g h)$^{-1}$	0.0792	0.0773	0.0787	232.7
$E_{a\ FL,\pi}$ kJ mol^{-1}	76.5	77.3	78.7	179.8
$-\Delta S^0_{FL,\sigma}$ J (mol K)$^{-1}$	94.8	94.2	95.3	340.7
$-\Delta S^0_{HHFL,\sigma}$ J (mol K)$^{-1}$	65.7	65.2	66.2	272.2
$-\Delta S^0_{FL,\pi}$ J (mol K)$^{-1}$	68.7	68.4	69.1	350.9
$-\Delta S^0_{HHFL,\pi}$ J (mol K)$^{-1}$	42.0	41.3	42.7	126.0
$-\Delta H^0_{FL,\sigma}$ kJ mol^{-1}	89.7	86.5	93.0	53.7
$-\Delta H^0_{HHFL,\sigma}$ kJ mol^{-1}	11.5	11.3	11.7	114.1
$-\Delta H^0_{FL,\pi}$ kJ mol^{-1}	71.5	69.2	73.8	60.3
$-\Delta H^0_{HHFL,\pi}$ kJ mol^{-1}	69.4	66.7	72.2	49.8

Note: F-value = 42985. Ftab = 2.85, ttab = 1.966 at 1-α = 0.95 and 422 degrees of freedom.

Table 16**.**

Kinetic parameters values and corresponding 95% probability confidence intervals for the kinetic model DBTPHE used to describe the HDS of DBT and hydrogenation of PHE.

Parameter	Estimated value	Lower limit	Upper limit	*t*-value
$A_{PHE\text{-}THPHE,\pi}$,mmol (g h)$^{-1}$	0.9309	0.9004	0.9613	60.0
$A_{PHE\text{-}DHPHE,\pi}$,mmol (g h)$^{-1}$	1.7619	1.7280	1.7957	102.1
$A_{DHPHE,\pi}$,mmol (g h)$^{-1}$	3.8704	3.7774	3.9635	81.7
$A_{THPHE,\pi}$,mmol (g h)$^{-1}$	2.3959	2.1125	2.6793	16.6
$E_{a\ PHE\text{-}THPHE,\pi}$,kJ mol^{-1}	40.1	38.5	41.6	51.0

Parameter	Estimated value	Lower limit	Upper limit	*t*-value
$E_{a\ PHE\text{-}DHPHE,\pi}$,,kJ mol^{-1}	30.0	29.1	30.9	69.0
$E_{a\ DHPHE,\pi}$,,kJ mol^{-1}	59.8	56.9	62.7	40.5
$E_{a\ THPHE,\pi}$,,kJ mol^{-1}	40.0	37.8	42.2	35.8
$-\Delta S^0_{PHE,\sigma}$, J $(mol\ K)^{-1}$	104.8	95.7	114.0	22.5
$-\Delta S^0_{DHPHE,\sigma}$, J $(mol\ K)^{-1}$	66.7	63.4	70.0	39.6
$-\Delta S^0_{THPHE,\sigma}$, J $(mol\ K)^{-1}$	70.5	52.1	88.9	7.5
$-\Delta S^0_{PHE,\pi}$, J $(mol\ K)^{-1}$	89.2	87.8	90.6	125.5
$-\Delta S^0_{DHPHE,\pi}$, J $(mol\ K)^{-1}$	63.4	61.5	65.3	65.2
$-\Delta S^0_{THPHE,\pi}$, J $(mol\ K)^{-1}$	60.1	59.1	61.0	123.3
$-\Delta H^0_{PHE,\sigma}$, kJ mol^{-1}	78.2	59.3	97.1	8.1
$-\Delta H^0_{DHPHE,\sigma}$, kJ mol^{-1}	23.8	21.4	26.1	19.7
$-\Delta H^0_{,\sigma}$, kJ mol^{-1}	13.6	5.8	21.3	3.4
$-\Delta H^0_{PHE,\pi}$, kJ mol^{-1}	78.0	76.1	79.9	81.2
$-\Delta H^0_{DHPHE,\pi}$, kJ mol^{-1}	61.0	59.0	63.1	58.3
$-\Delta H^0_{THPHE,\pi}$, kJ mol^{-1}	73.3	68.9	77.6	32.8

Note: = 9971. Ftab = 2.79, ttab = 1.963 at $1-\alpha = 0.95$ and 792 degrees of freedom.

2.4 Discussion

2.4.1 Kinetics of the hydrodesulfurization of dibenzothiophene

2.4.1.1 Comparison of the kinetic model presented herein with previous works. Though the hydrodesulfurization of dibenzothiophene has been thoroughly studied in the past (Houalla et al., 1978; Kilanowski et al., 1978), the majority of kinetic studies have oversimplified modeling using mainly pseudo-first-order rate equations (Bataille et al., 2000; Egorova & Prins, 2004b; Kagami,

Vogelaar, Langeveld, & Moulijn, 2005; H. Wang & Prins, 2009; Y. Wang et al., 2004). This approach is capable to fit well experimental observations. However, pseudo-first-order rate equations do not take into consideration elementary steps for the reaction mechanism and do not provide a description of the adsorption-desorption steps for the different species on the catalyst (Alsolami, Berger, Makkee, & Moulijn, 2013; de Oliveira, Hudebine, Guillaume, & Verstraete, 2016). In order to understand the catalytic surface reactions for the hydrodesulfurization of dibenzothiophene, some mechanisms have been evaluated using Langmuir-Hinshelwood-Hougen-Watson (LHHW) model as shown in Table 17. Singhal et al. (Singhal et al., 1981) and Vrinat (Vrinat, 1983) modeled the hydrodesulfurization of dibenzothiophene considering that the DDS and HYD pathways take place on the same catalytic site. Meanwhile, Broderick et al. (Broderick & Gates, 1981) and Vanrysselberghe et al. (Vanrysselberghe & Froment, 1996) assumed that the sites involved in hydrogenation and desulfurization are different. All of them, using one or two sites for the adsorption of dibenzothiophene and its products on the catalyst gave a good fit to the experimental data. Nevertheless, most of these kinetic models lack of a proper statistical and phenomenological analysis of the model itself and of the estimated kinetic parameters. Kinetic parameters should be not only capable to represent adequately the occurred physicochemical phenomena but also to exhibit statistical significance and thermodynamic consistency (Froment et al., 2011).

Table 17**.**

Kinetic expressions for dibenzothiophene hydrodesulfurization based on Langmuir-Hinshelwood-Hougen-Watson approach.

Catalysts	Catalytic Sites			Rate Expression	Activation Energy (kJ mol^{-1})	Reference
	DDS Route	HID Route	H_2			
CoMo/γ-Al_2O_3	X	X	X	$r_{DBT} = \frac{kK_{DBT}P_{DBT}}{1 + K_{DBT}P_{DBT} + K_{PROD}P_{PROD}} \cdot \frac{K_{H_2}P_{H_2}}{1 + K_{H_2}P_{H_2}}$ $r_{BP} = \frac{kK_{BP}P_{BP}}{1 + K_{BP}P_{BP} + K_{CHB}P_{CHB}} \cdot \frac{K_{H_2}P_{H_2}}{1 + K_{H_2}P_{H_2}}$	163.3 210.6	Singhal et al.[14]
CoMo/γ-Al_2O_3	X		X	$r_{DBT} = \frac{kK_{DBT}P_{DBT}}{1 + K_{DBT}P_{DBT} + K_{H_2S}P_{H_2S}} \cdot \frac{K_{H_2}P_{H_2}}{1 + K_{H_2}P_{H_2}}$	96.3	Vrinat[18]
CoMo/γ-Al_2O_3	X	X	X	$r_{DBT_\sigma} = \frac{k_{DBT,\sigma}K_{H,\sigma}K_{DBT,\sigma}C_{H_2}C_{DBT}}{\left(1 + \left(K_{H,\sigma}C_{H_2}\right)^{0.5} + K_{DBT,\sigma}C_{DBT} + K_{BP,\sigma}C_{BP} + K_{H_2S,\sigma}C_{H_2S}\right)^3}$ $r_{DBT_\pi} = \frac{k_{DBT,\pi}K_{H,\pi}K_{DBT,\pi}C_{H_2}C_{DBT}}{\left(1 + \left(K_{H,\pi}C_{H_2}\right)^{0.5} + K_{DBT,\pi}C_{DBT} + K_{BP,\pi}C_{BP}\right)^3}$ $r_{BP_\pi} = \frac{k_{BP,\pi}K_{H,\pi}K_{BP,\pi}C_{H_2}C_{BP}}{\left(1 + \left(K_{H,\pi}C_{H_2}\right)^{0.5} + K_{DBT,\pi}C_{DBT} + K_{BP,\pi}C_{BP}\right)^3}$	122 186 255.7	Vanrysselberghe et al.[27]
CoMo/γ-Al_2O_3	X	X	X	$r_{DBT_\sigma} = \frac{k_{DBT,\sigma}K_{DBT,\sigma}C_{DBT}}{\left(1 + K_{DBT,\sigma}C_{DBT} + K_{H_2S,\sigma}C_{H_2S}\right)^2} \cdot \frac{K_{H_2}C_{H_2}}{1 + K_{H_2}C_{H_2}}$ $r_{DBT_\pi} = \frac{k_{DBT,\pi}K_{DBT,\pi}K_{H_2}C_{DBT}C_{H_2}}{1 + K_{DBT,\pi}C_{DBT}}$	125.6 117.2	Broderick et al.[26]

2.4.1.2 Nature of the active sites. As already discussed in the results section, among the three kinetic models developed in this work, only those considering two active sites: one for hydrogenolysis and the other for hydrogenation, were able to properly describe experimental results. Few kinetic models for the hydrodesulfurization of dibenzothiophene have been developed assuming two different sites for the adsorption of DBT and its products (Broderick & Gates, 1981; Edvinsson & Irandoust, 1993; Farag, 2006; Vanrysselberghe & Froment, 1996). The development of this type of kinetic models does not seek to give information on the chemical structure of the active sites but characterizes reaction rates relating them to both a macroscopic reaction mechanism and macroscopic process variables such as concentration, pressure, and temperature. Nevertheless, several theoretical studies and DFT calculations have been carried out in recent years aiming to elucidate the atomic structure and nature of the active sites of hydrotreatment catalysts (Grønborg, Šarić, Moses, Rossmeisl, & Lauritsen, 2016; Lauritsen & Besenbacher, 2015; Lauritsen et al., 2004; Rangarajan & Mavrikakis, 2015; Tuxen et al., 2012). Most authors accept that coordinately unsaturated sites (CUS) (sulfur vacancy sites) at the edges and corners of molybdenum sulfide (MoS_2) play an important role for the DDS route. In this respect, the MoS_2 particles expose two types of edges: Mo-edge and S-edge. Under typical sulfidation conditions, nickel atoms might replace the molybdenum atoms from the Mo-edge to form the so-called NiMoS phase hence promoting the formation of CUS at the edges and corners due to the reduction of the sulfur binding energy (Ding, Jiang, Zhou, Wei, & Zhou, 2017; Rangarajan & Mavrikakis, 2017). The desulfurization of DBTs via DDS would preferably take place on vacancies at corner sites via perpendicular adsorption through the sulfur atom (Chen, Long, Li, Nie, & Li, 2017; Cristol et al., 2004; Rangarajan & Mavrikakis, 2017; Tuxen et al., 2012). On the other hand, the nature of the sites for the HYD pathway remains yet unclarified. Topsøe and coworkers (Besenbacher et al.,

2008; Lauritsen et al., 2004; Moses et al., 2007; Tuxen et al., 2012), based on scanning tunneling microscopy (STM) images of the top of MoS_2 and CoMoS slabs, proposed that the so-called *brim sites* are involved in hydrogenation reactions. *Brim sites* are modeled as bridge sites presenting a metallic character and located at the cluster top and perimeter sites along the cluster edges. They are supposed not to be sterically hindered as the adsorption of aromatic molecules does not require the formation of sulfur vacancies (Kibsgaard et al., 2010; Rangarajan & Mavrikakis, 2016). As expected, on *brim sites* the adsorption of H_2S is negligibly weak, explaining the low inhibition effect of H_2S on HYD pathway (Rangarajan & Mavrikakis, 2016). Moreover, it is often theorized that aromatics adsorb flat on hydrogenation sites. Therefore, π-flat adsorption of dibenzothiophene and of other aromatic structure is feasible on *brim sites*.

As mentioned earlier, this work is not aimed at determining the nature of the active sites. Nevertheless, based on literature, and as a matter of speculation, the developed models hint that σ and π sites might well correspond to CUS and brim sites, respectively. Considering the above arguments, the results obtained in this work can be interpreted considering that dibenzothiophene would preferably be adsorbed on corner CUS sites of a mixed NiMoS phase. Experimental evidence shows that in these sites (Kabe, Qian, & Ishihara, 1997), the sulfur atom from dibenzothiophene might replace the sulfur atom from the CUS hence leading to direct hydrogenolysis for producing biphenyl. Furthermore, and provided the strongest kinetic viability of the model including the subsequent hydrogenation of biphenyl to cyclohexylbenzene, the former product should re-adsorb on *brim sites*. On the other hand, the HYD route might be accounted to proceed via the adsorption of dibenzothiophene in a π-flat bonding between the benzene ring and the *brim site*, where partially hydrogenated intermediates are to be produced. These intermediates would desorb to react on CUS sites to further C-S-C bond scission. This proposition is summarized

in Figure 19. It is interesting to remark that the mechanism postulated herein resembles previous considerations for the reactivity of dibenzothiophene over noble metal based catalysts (Baldovino-Medrano, Eloy, et al., 2009; Baldovino-Medrano et al., 2008; Baldovino-Medrano, Giraldo, & Centeno, 2009).

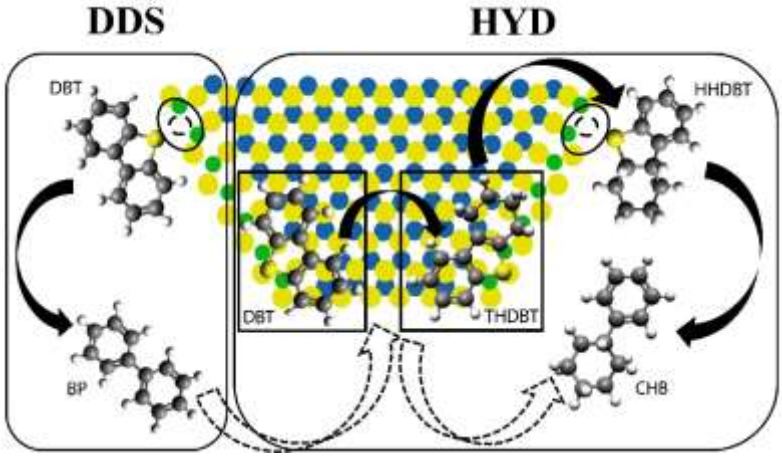

*Figure 19***.** Illustration of the adsorption of DBT on the two routes of HDS on NiMoS/γ-Al_2O_3.The rectangular box represents brim regions, and the oval marks the CUS-like sites. Color scheme: green, nickel; blue, molybdenum; yellow, sulfur.

2.4.1.3 Considerations about the reaction mechanism. Given the scarcity of literature reports dealing with kinetic studies over NiMo catalysts, it was necessary to qualitatively compare the present results with reports for CoMo catalysts (Broderick & Gates, 1981; Vanrysselberghe & Froment, 1996) and with theoretical studies performed via molecular simulation (Kibsgaard et al., 2010; Lauritsen & Besenbacher, 2015; Rangarajan & Mavrikakis, 2015, 2016; Tuxen et al., 2012). According to Table 13, activation energies for dibenzothiophene on σ and π sites and of its DDS product over π sites followed the trend: $Ea_{BP,\pi} > Ea_{DBT,\pi} \gg Ea_{DBT,\sigma}$. This trend is in good agreement with literature reports, vide Table 17. As an exception, Broderick et al. (Broderick &

Gates, 1981) found that $Ea_{DBT,\sigma} > Ea_{DBT,\pi}$. However, their report may be criticized because they raised the denominator of their rate expression for hydrogenolysis to the square without providing a justification. Furthermore, these authors did not check their results for thermodynamic consistency. The order found for activation energies coincides with the high selectivity of NiMo sulfides to the DDS route. In addition, the highest value found for $Ea_{BP,\pi}$ also agrees with the experimental evidence on the low rate of the hydrogenation of biphenyl to cyclohexylbenzene. Theoretical studies have determined that this reaction is hindered by the fact that the two phenyl rings of biphenyl are not coplanar making difficult its adsorption on π sites (Egorova & Prins, 2004c).

On the other hand, calculated entropy values (Table 13) suggest that the mobility of dibenzothiophene on σ sites is greater than on π sites. Conversely, biphenyl, cyclohexylbenzene, and H_2S might present a higher mobility on π sites. Rangarajan et al. (Rangarajan & Mavrikakis, 2016), using density functional theory for evaluating the adsorption of different hydrocarbons on a CoMoS formulation, reported an apparent opposite result to the obtained herein, i.e. DBT and its alkyl-substituted aromatics presented a larger entropy when adsorbed on *brim sites* than on CUS. Nevertheless, the authors did not probe the adsorption of dibenzothiophene on a CUS located in corner sites. In fact, in a later work, these authors (Rangarajan & Mavrikakis, 2015) considered the adsorption of dibenzothiophene on these corner type sites, suggesting that the C-S bond scission is rather more feasible to occur on these sites. Tuxen et al. (Tuxen et al., 2012) carried out a similar study but using scanning tunneling microscopy to investigate the atomic-scale adsorption of DBT and 4,6-DMDBT on MoS_2 and CoMoS nanoclusters. These authors, based on chemisorption calculations, elucidated also the preference of DBT to adsorb on corner type-sites. According to Ding et al. (Ding et al., 2017), the Co atom on a corner exhibits a square planar

coordinated structure with four sulfur atoms, which allow for the high mobility of dibenzothiophene and the high hydrogenolysis activity. Given the values of entropy calculated herein, the same kind of explanation could apply to Ni promoted sulfides.

Concerning the calculated values for adsorption enthalpies, Yang et al. (Hong Yang, Fairbridge, & Ring, 2003) [86] observed that a flat π-bonding on sites related to HYD route leads to larger values of this thermodynamic parameter as compared to the perpendicular adsorption of on σ sites. The authors related this observation to the type of interactions established between the sulfur atom (η1S), thiophene (η5), and the aromatic rings (η6) of dibenzothiophene with the corresponding active sites of the catalyst. It is worth stressing that these theoretical analyses are in agreement with our calculated values, which indicate that adsorption enthalpy of dibenzothiophene is a bit larger on π hydrogenation sites than on σ hydrogenolysis sites. To this respect, the adsorption enthalpy for dibenzothiophene on π and σ sites reported in the literature agrees with values estimated herein (Broderick & Gates, 1981; Edvinsson & Irandoust, 1993; Vanrysselberghe & Froment, 1996). For biphenyl, unlike as for cyclohexylbenzene, it was found that this product adsorbs more strongly on π sites; $-\Delta H^0_{BP,\pi} = 42$ kJ mol^{-1}. Literature reports for adsorption enthalpies of biphenyl over hydrodesulfurization catalysts range from 38 to 50 kJ mol^{-1} (Edvinsson & Irandoust, 1993; Vanrysselberghe & Froment, 1996). For cyclohexylbenzene, the relatively low values of adsorption enthalpy on π sites point to a high mobility under the conditions of the reaction atmosphere. Unfortunately, values derived from the present study could not be compared to theoretical or experimental data from literature, since they were not found in the literature survey.

Finally, in regards to H_2S, values calculated for its adsorption entropy and enthalpy on σ sites, 126 J (mol K)$^{-1}$ and 203 kJ mol^{-1}, respectively, were in a good agreement with literature (Raghuveer et al., 2016; Romero et al., 2008; Vanrysselberghe & Froment, 1996). Furthermore, it

has been postulated that this compound selectively inhibits σ sites (Bataille et al., 2000; Egorova & Prins, 2004b; Kabe et al., 2001; Lamure-Meille, Schulz, Lemaire, & Vrinat, 1995; Lauritsen & Besenbacher, 2015). In contrast, a low value of enthalpy; 1.24 kJ mol^{-1}, was found for the adsorption H_2S on π sites suggesting a weak adsorption on *brim sites*. In this sense, Lauritsen et al. (Lauritsen & Besenbacher, 2015); using high-resolution STM studies on hydrotreating HDS model systems, claimed that H_2S does not compete for adsorption on *brim sites*. Additionally, other reports (Bataille et al., 2000; Egorova & Prins, 2004b; Kabe et al., 2001) have presented evidence of an increment of the selectivity to partially hydrogenated intermediates of DBT and 4,6 DMDBT with the partial pressure of H_2S. This agrees with the mechanism proposed for the hydrodesulfurization of dibenzothiophene in Table 8. On the HYD pathway the molecules are first hydrogenated on π sites and then moved to σ sites to the C-S bond scission. Therefore, H_2S inhibits both the DDS pathway and the final desulfurization step in the HYD pathway, generating an increase in the concentration of the partially hydrogenated intermediates of DBTs. Thermodynamic calculations performed from the kinetic modeling of this contribution are deemed relevant to developing a better understanding of the mechanism of hydrodesulfurization.

2.4.2 Kinetics of the hydrodesulfurization of dibenzothiophene and hydrogenation of aromatics

2.4.2.1 Simultaneous hydrodesulfurization of dibenzothiophene and hydrogenation of naphthalene

2.4.2.1.1 Reactivity of dibenzothiophene and naphthalene. Results showed that the presence of naphthalene did not modify the reactivity of dibenzothiophene over the tested sulfided NiMo/γ-

Al_2O_3 catalyst. However, the conversion of naphthalene significantly dropped under the presence of dibenzothiophene. From the different models evaluated for the simultaneous hydrodesulfurization of dibenzothiophene and hydrogenation of naphthalene, the one assuming that the hydrogenation of naphthalene can be carried out on both σ and π sites showed the best fitting of the experimental data. In this regard, the fact that the DDS/HYD selectivity was not affected suggests that naphthalene does not have a preferential adsorption site. Considering the latter, the values of the Arrhenius and van't Hoff parameters for the selected kinetic model were fixed for dibenzothiophene and its reaction products, vide Table 13, whereas the corresponding values for naphthalene and tetralin were estimated from the model, vide Table 8. In this instance, the calculated values for entropy indicate that naphthalene and tetralin might present more mobility on π sites than on σ sites. Conversely, entropy values for tetralin suggest a larger mobility of this compound as compared to naphthalene at both types of active sites. Such a result is reasonable considering their difference in aromaticity. The resonance energy of the aromatic ring of tetralin is greater than that of the naphthalene ring since the latter is first hydrogenated and has lower aromaticity than the former (Rautanen et al., 2002; Weitkamp, 1968). On the other hand, the adsorption enthalpy of naphthalene and tetralin on π sites was found larger than on σ sites. This might be related to the fact that the π-flat adsorption of naphthalene and tetralin on π sites involves multipoint interactions so adsorption would be stronger than on σ sites where η6 is theorized to occur (Rautanen et al., 2002). Though under the reaction conditions of this work, no significant impact of naphthalene on the hydrodesulfurization of dibenzothiophene was remarked, other authors have reported otherwise. Egorova et al. (Egorova & Prins, 2004a) investigated the inhibition effect of naphthalene on the hydrodesulfurization of DBT and 4,6 DMDBT and found that naphthalene may inhibit the hydrodesulfurization of DBT and 4,6 DMDBT under conditions

in which both the DDS and the HYD pathways were affected to the same extent. Consequently, these authors proposed that the hydrogenation of naphthalene occurred on both DDS and HYD sites. Conversely, Egorova et al. (Egorova & Prins, 2004a) also reported that the hydrogenation of naphthalene was inhibited by the presence of both organo-sulfur compounds.

2.4.2.1.2 Considerations about the reaction mechanism DBTNP. Some studies have elucidated how hydrogenation of small molecules such as naphthalene may take place on more than one type of catalytic sites. Gutiérrez et al. (Gutiérrez et al., 2014) proposed that the size of the molecules should dictate their accessibility to hydrogenolysis CUS sites. They speculated that the hydrogenation of *o*-propylaniline, a molecule with a single aromatic ring, occurs on both CUS and *brim sites* in view of their weak effect on the selectivities of hydrodenitrogenation and hydrodesulfurization reactions. Moreover, other authors have associated CUS sites not only with hydrogenolysis but also with hydrogenation reactions (Rana, Navarro, & Leglise, 2004; Romero et al., 2008). Kinetic studies published for the hydrogenation of naphthalene in the absence and presence of other compounds assumed that naphthalene is only adsorbed and hydrogenated on one type of active sites (Girgis & Gates, 1991; Monteiro-Gezork, Natividad, & Winterbottom, 2008; Romero et al., 2008; Sapre & Gates, 1981; Antonymuthu Stanislaus & Cooper, 1994). Cortés et al. (Romero et al., 2008) developed a LHHW kinetic model for the hydrogenation of naphthalene over a NiMo/γ-Al_2O_3 assuming that the chemisorption of naphthalene and tetralin only occurred on CUS sites. Since there is a lack of information related to kinetic parameters on *brim sites*, a proper comparison of our results with those from literature is not carried out. However, our results are in agreement with those reported elsewhere (Monteiro-Gezork et al., 2008; Rautanen et al., 2002; Romero et al., 2008).

2.4.2.2 Simultaneous hydrodesulfurization of dibenzothiophene and hydrogenation of fluorene

2.4.2.2.1 Reactivity of dibenzothiophene and fluorine. The presence of fluorene affected the conversion of dibenzothiophene and mainly inhibited the HYD pathway during the hydrodesulfurization reaction. There are few reports on this effect in open literature. Koltai et al. (Koltai et al., 2002) reported that among the aromatic compounds: anthracene, phenanthrene, and fluorene, the latter had the strongest inhibiting effect on the transformation of 4,6 DMDBT. The authors ascribed this trend to the structural similarity between 4,6 DMDBT and fluorene. Unlike DBT, 4,6 DMDBT principally reacts via the HYD route. They argued that both molecules adsorbed in the same manner over the catalytic active sites, remarking a preference for hydrogenation sites. On the other hand, the very low conversion of fluorene compared with the other aromatic compounds was also reported by Koltai et al. (Koltai et al., 2002).

2.4.2.2.2 Considerations about the reaction mechanism DBTFL. The kinetic model proposed in this work effectively accounted for the effect of fluorene on reactivity of dibenzothiophene. Furthermore, results from the model justify the assumption that fluorene and its partially hydrogenated product: hexahydrofluorene, adsorb on both π and σ sites but that fluorene hydrogenation can only be carried out on π sites. On the other hand, the activation energy for the hydrogenation of fluorene amounted to 77 kJ mol^{-1}; a value similar to the one reported by Lapinas et al. (Lapinas et al., 1991) using a NiW/Al_2O_3. The chemisorption entropies indicate that fluorene has higher mobility on π sites than on σ sites. The low conversion observed for fluorene is related to the strong adsorption of this molecule on σ sites since it cannot be hydrogenated therein.

Besides, HHFL presents a higher chemisorption enthalpy on π sites than on σ sites, indicating that HHFL produced on π sites mainly contributes to the inhibition of hydrodesulfurization of dibenzothiophene on these sites.

2.4.2.3 Simultaneous hydrodesulfurization of dibenzothiophene and hydrogenation of phenanthrene

2.4.2.3.1 Reactivity of dibenzothiophene and phenanthrene. Phenanthrene had the strongest inhibition effect on dibenzothiophene hydrodesulfurization. In addition, this molecule affected both the DDS and the HYD pathways to the same extent. As in the case of the other aromatics, phenanthrene conversion was also inhibited by dibenzothiophene. The hydrogenation of phenanthrene has been studied by several authors and different reactions networks have been proposed (Ishihara et al., 2003; Korre et al., 1995; Schachtl, Zhong, et al., 2015; Huibin Yang et al., 2014). The product distribution for the hydrogenation of phenanthrene in the absence of dibenzothiophene obtained herein was similar to that reported in literature (Schachtl, Zhong, et al., 2015; Huibin Yang et al., 2014). Particularly, a high production of aromatics with two hydrogenated aromatic rings were detected, namely, 1,8-OHPHE and 1,10-OHPHE. Schachtl et al. (Schachtl, Zhong, et al., 2015) reported similar results for Ni promoted MoS_2/ γ-Al_2O_3 catalysts. Authors found that Ni favored the adsorption of phenanthrene leading to its deep hydrogenation and producing mainly 1,8-OHPHE and 1,10-OHPHE. On the other hand, the addition of dibenzothiophene to the reaction feed both decreased conversion and shifted selectivity to less OHPHE and more DHPHE and THPHE. Such an increase, particularly in the selectivity to THPHE, agrees with suggestions made by Schachtl et al. (Schachtl, Zhong, et al., 2015) who

postulated that the hydrogenation of the two aromatic rings of phenanthrene essentially occurred via the THPHE intermediate.

2.4.2.3.2 Considerations about the reaction mechanism DBTPHE. The kinetic model that best fitted the experimental values for the hydrodesulfurization of dibenzothiophene and for the hydrogenation of phenanthrene assumed that both phenanthrene and its reaction products adsorb on both σ and π sites, but only react on π sites. The adsorption entropies of phenanthrene and its reaction products (Table 16) elucidated that aromatic molecules have a higher mobility on π sites than on σ sites. At π sites, the molecule mobility increased as the molecule became hydrogenated: PHE ($-\Delta S^0_{PHE,\pi}$ = 89.2 J (mol K)$^{-1}$) < DHPHE ($-\Delta S^0_{DHPHE,\pi}$ = 63.4 J (mol K)$^{-1}$) < THPHE ($-\Delta S^0_{THPHE,\pi}$ = 60.1 J (mol K)$^{-1}$). On the other hand, the chemisorption enthalpy of phenanthrene is similar on σ sites (78.2 kJ mol^{-1}) and π sites (78.0 kJ mol^{-1}). This result is in agreement with the large inhibition effect of this molecule during the hydrodesulfurization of dibenzothiophene. However, the selectivity to HYD and DDS pathways were affected in the same extend. According to results though, phenanthrene would only be hydrogenated on π sites, probably because the π sites are clearly less sterically hindered (Lauritsen & Besenbacher, 2015). Regarding the enthalpies for the primary products on π sites, THPHE showed a higher value than DHPHE. However, on σ sites results were in contraposition since the chemisorption enthalpy for DHPHE was higher than that found for THPHE. Concerning σ sites, the geometrical configuration of the aromatic rings of phenanthrene dictate their accessibility. DHPHE and THPHE present their aromatic ring in different positions. According to Beltramone et al. (Beltramone et al., 2008), the central ring of the THPHE presents a steric constraint that limits its adsorption. This might be related to the larger adsorption enthalpy of DHPHE than that of THPHE on σ sites. Finally, it is worth mentioning that

the chemisorption entropy and enthalpy of OHPHE was not found to be statistically significant, so a discussion on this parameter is not possible herein. Such an outcome might be related to the lumping procedure carried out; i.e. 1,8-OHPHE and 1,10-OHPHE were lumped as OHPHE.

2.5 Conclusions

A kinetic study of the hydrodesulfurization of dibenzothiophene was undertaken over NiMo/γ-Al_2O_3 catalysts, in the absence and in the presence of aromatic compounds with different chemical structures: naphthalene, phenanthrene, and fluorene. Among three proposed models for the hydrodesulfurization of dibenzothiophene in the absence of the aromatics, the one considering two different types of active sites; one for hydrogenation and another for C-S-C bond scission, and considering the subsequent hydrogenation of biphenyl to cyclohexylbenzene was found to best fit observations. The developed model presented both physicochemical and statistical significance. With respect to the nature of the HYD and DDS mechanisms, σ and π sites proposed in this work for carrying out the hydrogenolysis and hydrogenation reactions, might be interpreted to correspond CUS and *brim sites*, respectively. Under such a consideration, the DDS pathway would mainly take place on CUS sites. Meanwhile, for the HYD pathway, the molecules would be first hydrogenated on *brim sites* and then move to a CUS site for the hydrogenolysis of C-S-C bond. On the other hand, the weak chemisorption of H_2S on π sites agreed with the hypothesis that the adsorption of H_2S does not occur on the *brim sites*, but only on the CUS sites hence mainly inhibiting the hydrogenolysis reaction.

The inhibition effect of the polyaromatic compounds on the hydrodesulfurization of dibenzothiophene was found to be related to the size of the molecules. Phenanthrene was the

molecule that most affected the conversion of dibenzothiophene and naphthalene was the one that affected it the least. However, regardless of size, the model predicted that both molecules did not have a preference for being adsorbed on a specific site hence inhibiting both the DDS and HYD pathways to the same extent. Fluorene was found to mostly inhibit the HYD pathway. Such a trend was found to correlate to its structure and geometry. The similarity between dibenzothiophene and fluorene and the results from kinetic modelling suggest that the two molecules would be adsorbed in the same manner on the π hydrogenation sites.

Finally, regarding the hydrogenation of the tested aromatics, the model predicted that these compounds are adsorbed on both σ and π sites. However, it was postulated that the size of the molecules dictates their accessibility to σ sites to be hydrogenated. In general, the kinetic models that best represented the experimental observations of the simultaneous hydrodesulfurization of dibenzothiophene and hydrogenation of aromatics considered that naphthalene is hydrogenated on both σ and π sites, whereas fluorene and phenanthrene are hydrogenated only on π sites.

3. Effect of Nitrogen-Containing Compounds on the Hydrodesulfurization of Dibenzothiophene

The content of nitrogen in crude oils is usually less than 1 wt % (Prado, Rao, & de Klerk, 2017). At this low concentration, the nitrogen-containing compounds affect hydrotreating (Dong, Jeong, & Massoth, 1997; Nguyen et al., 2019). Several reviews (Koltai et al., 2002; Liu, Zhang, Zheng, & Chen, 2008; Sumbogo Murti, Yang, Choi, Korai, & Mochida, 2003; Tao et al., 2017) show that

there are more than one hundred articles studying the effect of nitrogen compounds over hydrotreating and more specifically over hydrodesulfurization, hence reflecting the need to rationalize this effect. About 70% of the studies have been carried out with real feeds, e.g. atmospheric gas oil (AGA), light cycle oil (LCO), and straight run gas oil (SRGO), and have shown that hydrodesulfurization is inhibited by organic nitrogen compounds (García-Gutiérrez, Laredo, Fuentes, García-Gutiérrez, & Jiménez-Cruz, 2014; Rana, Al-Barood, Brouresli, Al-Hendi, & Mustafa, 2018; Yang et al., 2004). Nevertheless, it is difficult to correlate the physical and chemical properties of the N-containing compounds with the inhibitory effects on hydrodesulfurization due to the wide variety of nitrogen and sulfur compounds present in the feedstocks and to their mutual interactions.

Generally, organic nitrogen compounds are plainly classified as basic (six-membered heterocycles) and non-basic compounds (five-membered heterocycles). In the six-membered pyridinic rings, e.g. pyridine, quinoline, and acridine, the nitrogen atom has an unshared electron pair that does not make part of the aromatic system. Therefore, these molecules behave as Lewis bases. Conversely, the lone electron pair of the nitrogen atom in five-membered pyrrolic rings, e.g. pyrrol, carbazol, and indole, completes sextet of electrons of the aromatic system and it is not available for interacting with acids (Ho, 1988; Moreau & Geneste, 1990; Valencia, Klimova, & García-Cruz, 2012). Therefore, in contradiction with common assumptions, this type of molecules is more acidic than basic and their planarity makes them behave more like phenols (Baltazzi & Krimen, 1963).

Some studies (Dorneles de Mello, de Almeida Braggio, da Costa Magalhães, Zotin, & Pereira da Silva, 2017; Farag, Kishida, & Al-Megren, 2014; Han et al., 2017; Zepeda et al., 2016) have used model feeds in order to elucidate the influence of the type and concentration of the nitrogen

compounds on hydrodesulfurization. These studies report contradictory trends; e.g. most of researchers (Farag et al., 2014; Han et al., 2017; Prins, 2001; Rabarihoela-Rakotovao, Diehl, & Brunet, 2009; Stanislaus, Marafi, & Rana, 2010) report that nitrogen compounds are the strongest inhibitors of hydrodesulfurization while a few others (Egorova & Prins, 2004c; LaVopa & Satterfield, 1988b; Nagai, 1985) reported that hydrodesulfurization is promoted by basic nitrogen compounds under certain reaction conditions. On the other hand, most of the reports presented in the literature (Beltramone, Crossley, Resasco, Alvarez, & Choudhary, 2008; García-Martínez, Castillo-Araiza, De los Reyes Heredia, Trejo, & Montesinos, 2012; Kwak, Lee, Bae, & Moon, 2001; Wei et al., 2015) show evidence indicating that the basic nitrogen compounds are stronger inhibitors for hydrodesulfurization than the so-called non-basic nitrogen compounds while other researchers (Ho, 2003; Laredo, Altamirano, & De los Reyes, 2003; Laredo S, De los Reyes H, Luis Cano D, & Jesús Castillo M, 2001; Xiang, Chai, Liu, & Liu, 2008) have presented evidence showing that the latter exert either stronger or similar inhibition effects over hydrodesulfurization. The inhibition effect of the basic nitrogen compounds is often explained arguing that they adsorb on the catalytic surface through the nitrogen heteroatom hence blocking catalytic sites either by accepting the proton of a Brønsted site or by donating its unpaired electrons to a Lewis site (Rangarajan & Mavrikakis, 2015, 2017; Salazar, Schmidt, & Lauritsen, 2019). Concerning the effect of the non-basic nitrogen compounds, a clear explanation of their effects on hydrodesulfurization has not been achieved. Laredo et al. (Laredo S et al., 2001) reported that indole exerted a stronger inhibition on the hydrodesulfurization of dibenzothiophene as compared to basic quinoline. To explain this trend, these authors argued that indole was hydrogenated rapidly to a basic reaction intermediate; possibly polymerized on the catalyst surface, exerting a stronger inhibition effect than quinoline. Nevertheless, a further report by the same research group (Laredo

et al., 2003) ruled out such explanation and ascribed inhibition by indole to strong initial adsorption and slow kinetics of desorption.

In the previous chapter, the hydrodesulfurization of dibenzothiophene has been analyzed in terms of the selectivity to its two reaction routes: namely, direct desulfurization (DDS) and hydrogenation mediated desulfurization (HYD). The effect of N-containing molecules on these routes has been analyzed (Egorova & Prins, 2004a, 2004b; Ho & Qiao, 2010), and most of the authors agree that while the HYD pathway is strongly suppressed, the DDS pathway is less affected, regardless of the basicity of the nitrogen compounds. However, to the best of our knowledge, three studies found that the DDS pathway was actually promoted by the presence of the nitrogen compounds. Such an effect was marked by increases on the hydrodesulfurization of dibenzothiophene up to 43% (Egorova & Prins, 2004c; LaVopa & Satterfield, 1988b; Nagai, 1985). These studies have some experimental conditions in common: (i) the reactions were carried out in a continuous flow reactor; (ii) the catalysts were promoted by nickel; namely, sulfided NiMo/γ-Al_2O_3 and NiW/γ-Al_2O_3; (iii) dibenzothiophene was used as a model sulfur containing molecule; and, (iv) the tested nitrogen molecules were basic. Though the above cited authors postulated some hypothesis to explain the promotion effect, the reasons behind promotion remain unclear. Furthermore, whether the acid-base properties of the nitrogen molecule plays a role on such an effect has not been studied yet.

Although nitrogen compounds are conventionally classified as basic or non-basic, this classification seems vague because it does not permit to analyze the correlation between the basicity of the N-containing compounds and their effect on the HDS; on the contrary, such a classification generates contradiction. Aiming to improve on this, some authors (LaVopa & Satterfield, 1988a; Nagai, Sato, & Aiba, 1986) used the concept of proton affinity, the negative of

the enthalpy change in the reaction between the molecule and proton in gas phase (Hunter & Lias, 1998), to explain the effect of nitrogen compounds on hydrodesulfurization. LaVopa et al. (LaVopa & Satterfield, 1988a) and Nagai et al. (Nagai et al., 1986) found a linear correlation between the proton affinity of different nitrogen compounds and their adsorption equilibrium constants related to the surface Brønsted acid sites of HDT catalysts (S-H groups) (LaVopa & Satterfield, 1988a; Nagai et al., 1986; Salazar et al., 2019). However, it is not clear if the adsorption equilibrium constants on other catalytic sites like coordinately unsaturated sites (CUS) have the same linear correlation with proton affinity. It is important to remember that it is agreed that CUS are where desulfurization takes place.

Kinetic studies and modelling taking into account the mutual effect of nitrogen molecules and sulfur molecules in hydrotreatment are rather scarce (García-Martínez et al., 2012; Ho & Nguyen, 2004; Ho & Qiao, 2010) since most of the studies (Dorneles de Mello et al., 2017; Laredo et al., 2003; Laredo S et al., 2001; Rabarihoela-Rakotovao et al., 2009) concern themselves with modeling the effect of the nitrogen compounds on hydrodesulfurization. Oversimplified pseudo-first-order models and simplified Langmuir−Hinshelwood−Hougen−Watson (LHHW) equations assuming one catalytic site have been used for this purpose (Dorneles de Mello et al., 2017; Koltai et al., 2002; Laredo S et al., 2001; LaVopa & Satterfield, 1988a) whereas rigorous approaches accounting for the physicochemical and statistical consistency of the parameters of the model have not been considered so far.

Considering the discussion made above, this chapter studies the simultaneous hydrotreating of dibenzothiophene and quinoline and indole. The latter were chosen as nitrogen compound representative of diesel fractions and have proton affinity of 953.2 kJ mol^{-1} and 933.4 kJ mol^{-1}, respectively (Hunter & Lias, 1998). The mutual effect of dibenzothiophene and both nitrogen

compounds on their reactivities is analyzed. The kinetic model found to better represent the hydrodesulfurization and hydrogenation of aromatics in Chapter 2 was applied to analyze the kinetics of the simultaneous hydrodesulfurization of dibenzothiophene and hydrotreating of the selected nitrogen compounds. We recall that this model considers the existence of two different types of active sites; one for hydrogenation, the π-site, and another for C−S−C bond scission, the σ-site.

3.1 Catalytic Tests

The catalytic tests were carried out in the same fixed-bed continuous flow reactor (Catatest II) presented in previous chapters. The reactor was packed with the same NiMo/γ-Al_2O_3 commercial catalyst (Procatalyse) described in Chapter 2. Tests were performed independently using fresh catalyst at every run and were conducted until the catalytic conversion and selectivity did not change more than ±2% with time on stream. The feed stream contained the following compounds individually or in blends: dibenzothiophene (DBT) (Sigma-Aldrich, 98%), as a model sulfur compound in ultra-deep hydrodesulfurization; quinoline (Q) (Merck, 97%) and indole (IND) (Sigma-Aldrich, ≥99%), as models of heterocyclic nitrogen compounds with high and low proton affinity, respectively. Hexadecane (Sigma-Aldrich, ≥ 99%) was used as an internal standard for chromatography and cyclohexane (Sigma-Aldrich, 99.8%) as a solvent.

Two sets of experiments were carried out to elucidate the simultaneous effects of dibenzothiophene and nitrogen compounds on hydrodesulfurization (HDS) and hydrodenitrogenation (HDN). In the first set, HDS of dibenzothiophene (1.7 wt % - 3.6 wt %) and HDN of quinoline (0.24 wt%) and indole (0.22 wt%) were performed individually. The second set

of experiments was conducted to evaluate simultaneously the HDS of dibenzothiophene and HDN of quinoline or indole. The concentrations of quinoline and indole were between 0.2 wt % and 0.4 wt % and the concentration of dibenzothiophene was adjusted to keep a sulfur/nitrogen molar ratio of 5. The reaction temperatures were between 260°C and 300°C. The identification and quantification of the liquid products were made by gas chromatography and mass spectroscopy as described in Chapter 2. The catalytic results were expressed in terms of conversion (%X_i), and products yield (%Y_j). Additionally, we defined a parameter named impact factor (%λ) to show the degree of promotion or inhibition by the nitrogen compounds on the conversion of dibenzothiophene and product yields. The formula developed for this purpose is the following:

$$\%\lambda = \frac{\%i_j^N - \%i_j}{\%i_j} \times 100\% \qquad (3.1)$$

Where, $\%i_j$ and $\%i_j^N$ are the conversion of dibenzothiophene or the yield of product *j* in the absence and in the presence of the nitrogen compound, respectively. If the nitrogen compounds promotes the conversion of dibenzothiophene or the yield of *j*, the %λ is positive, but if they produced an inhibition effect the %λ is negative.

3.2 Kinetic Modeling

Kinetic models for the simultaneous hydrodesulfurization of dibenzothiophene and hydrodenitrogenation of quinoline and indole were based on the LHHW formalism adopted in Chapter 2. The mechanism for the hydrodesulfurization of dibenzothiophene in the presence of quinoline and indole was based on the same considerations as those made for the best kinetic model developed on Chapter 2 (DBTBP2S) for the simultaneous HDS of dibenzothiophene and

hydrogenation of aromatics. On the other hand, for modeling the reactions of the nitrogen compounds in the presence of dibenzothiophene, different kinetic models were proposed assuming that quinoline, indole and their reaction products are adsorbed and react on π, σ, or on both type of sites. Kinetic parameters were estimated by minimizing a weighted objective function following the methodology presented in the previous chapter. The F-test for the global significance of the regression as well as the individual t-test and the confidence limits for the estimates were computed. In addition, the physicochemical consistency of the parameters were tested according to the criteria proposed by Boudart as presented in Chapter 2.

3.3 Results

The individual reactions of the hydrodesulfurization of dibenzothiophene and hydrodenitrogenation of quinoline and indole are presented first (Sections 3.4.1-3.4.3). Then, the results of the conversion, product yields, and impact factor of the hydrodesulfurization of dibenzothiophene in the presence of nitrogen compounds (Section 3.4.4), and the hydrodenitrogenation of quinoline and indole in the presence of dibenzothiophene (Section 3.4.5) are presented. Finally, Sections 3.4.6.1 and 3.4.6.2 present the statistical significance and thermodynamic consistence of the kinetic models for the hydrodesulfurization of dibenzothiophene simultaneous to the hydrodenitrogenation of quinoline and indole, respectively.

3.3.1 Hydrodesulfurization of Dibenzothiophene. The hydrodesulfurization of dibenzothiophene was discussed in Chapter 2, but it is important to analyze the reaction under the conditions employed for the present catalytic tests. Figure 20 shows the conversion of

dibenzothiophene and the yields of biphenyl (BP), cyclohexylbenzene (CHB), and tetra-hydro-dibenzothiophene (THDBT) as a function of space-time velocity of dibenzothiophene ($W_{cat}F_{DBT_0}^{-1}$). The conversion of dibenzothiophene increased with space-time velocity. Biphenyl was the main product even at the lowest space-time velocity, demonstrating that hydrodesulfurization of dibenzothiophene proceeded predominantly via the DDS route. Tetra-hydro-dibenzothiophene was observed at very low concentrations and decreased with space-time velocity, at $W_{cat}F_{DBT_0}^{-1}$ > 88 only traces were detected.

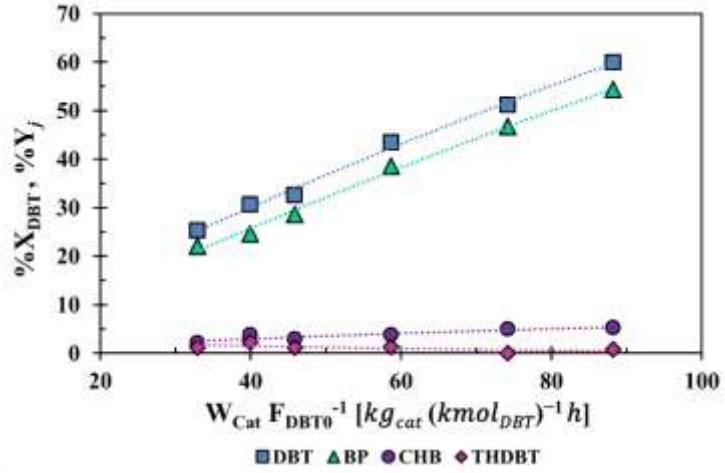

*Figure 20***.** Conversion of DBT and yields of BP, CHB, and THDBT at different $W_{cat}F_{DBT_0}^{-1}$. Conditions: p = 5 MPa, T = 300°C, liquid-flow rate of 30 mL·h^{-1} and H_2/liquid feed ratio of 500.

3.3.2 Hydrodenitrogenation of Quinoline. Figure 21 presents the reaction network proposed for the hydrotreating of quinoline as based on the observed distribution of products. The values of conversion and yield of products recorded during the reactions in the absence and in the presence of dibenzothiophene are placed below each compound. In the absence of dibenzothiophene, the conversion of quinoline was 95% and its main products were: 1,2,3,4-tetrahydroquinoline (14THQ) and decahydroquinoline (DHQ) with yields of ca. 73% and 16%, respectively. The yield

of orthopopylaniline (OPA) was ca. 3%, whereas the yield of denitrogenated products, i.e. propylbenzene (PB), propylcyclohexene (PCHE), and propylcyclohexane (PCH) were nearly 1% for each one. 5,6,7,8-tetrahydroquinoline (58THQ) and propyl-cyclohexylamine (PCHA) were only observed as traces. A similar result was reported by Jian and Prins (Jian & Prins, 1998) over a sulfided NiMo/γ-Al_2O_3 catalyst tested at 320°C in the absence of H_2S.

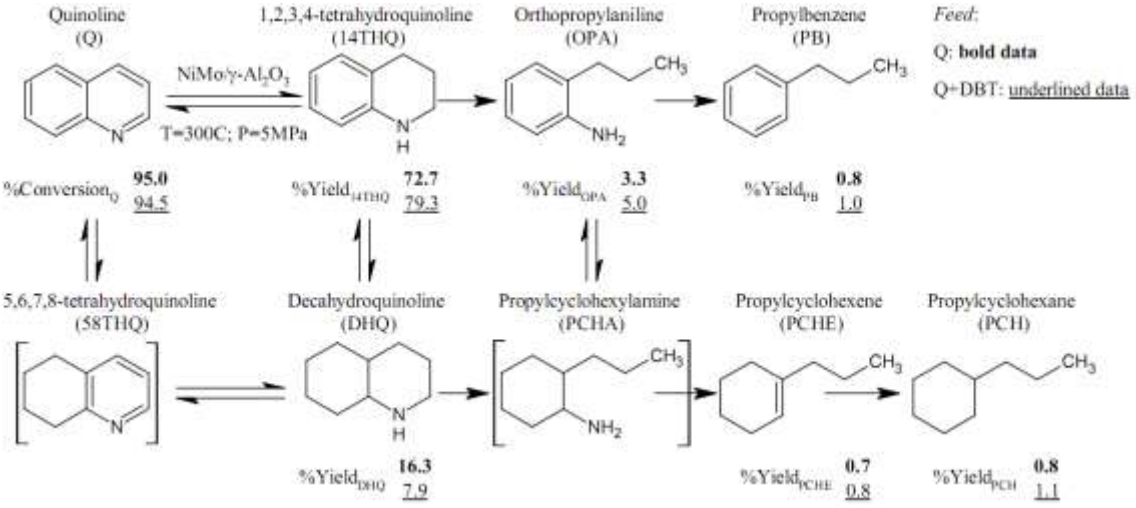

*Figure 21***.** Reaction network of the HDN of quinoline. Conversion of quinoline and yields of products in the absence (bold data) and in the presence of DBT (underlined data). Conditions: Q=0.24 wt %, DBT= 1.7 wt %, *p*=5 MPa, T=300°C, liquid-flow rate of 30 $mL \cdot h^{-1}$ and H_2/liquid feed ratio of 500.

The above reaction network is consistent with previous proposals made in the literature (Dorneles de Mello et al., 2017; García-Martínez et al., 2012; Jian & Prins, 1998; Nguyen, Tayakout-Fayolle, Pirngruber, Chainet, & Geantet, 2015; Prins, 2001). These works have shown that the hydrogenation and dehydrogenation steps of the network are reversible and in thermodynamic equilibrium (Nguyen et al., 2015; Prins, 2001). According to the scheme, quinoline can be hydrogenated via two pathways. The first one is the hydrogenation of the aromatic

ring to produce 5,6,7,8-tetrahydroquinoline, and the second one is the hydrogenation of the nitrogen-contained ring to obtain 1,2,3,4-tetrahydroquinoline. It has been reported that the hydrogenation of the N-containing ring is very rapid and more favorable than the hydrogenation of the benzenic ring, this is because the nitrogen atom decreases the resonance energy of the ring and makes it more reactive (García-Martínez et al., 2012; Nguyen et al., 2015). For that reason, the hydrogenation of quinoline to 1,2,3,4-tetrahydroquinoline is much faster than that of quinoline to 5,6,7,8-tetrahydroquinoline. Likewise, the hydrogenation of 5,6,7,8-tetrahydroquinoline to decahydroquinoline is more favorable than that of 1,2,3,4-tetrahydroquinoline to decahydroquinoline. The low concentration of 5,6,7,8-tetrahydroquinoline obtained in our work is in line with this interpretation. 1,2,3,4-tetrahydroquinoline can be transformed either by hydrogenation to form decahydroquinoline or by ring-opening (C_{sp3}-N cleavage) to obtain orthopopylaniline. Then, orthopopylaniline can be converted via two pathways, by direct denitrogenation through the cleavage of the C_{sp2}-N bond to form propylbenzene or by hydrogenation to form propyl-cyclohexylamine. Decahydroquinoline can be converted also to propyl-cyclohexylamine to then break the C-N bond to form propylcyclohexene and propylcyclohexane. Although propyl-cyclohexylamine is formed via two routes, the hydrogenation of orthopopylaniline and the ring-opening of decahydroquinoline, scarce concentration of propyl-cyclohexylamine was observed in the products. However, this result is in agreement with other authors that reported the high apparent rate constants for the transformation of propyl-cyclohexylamine (Jian & Prins, 1998; Nguyen et al., 2015).

3.3.3 Hydrodenitrogenation of Indole. Figure 22 illustrates the reaction network for the hydrotreating of indole as based on the evidence collected in our work. The conversion of indole

and yield of products for the reactions in the absence and in the presence of dibenzothiophene are presented below each molecule. In the absence of dibenzothiophene, the conversion of indole was ca. 37%. Indoline (HIN) was the main product with a yield of ca.17%, while the yield of the other N-containing intermediates products, namely, orthoethylaniline (OEA) and ethylcyclohexylamine (OECHA), were ca. 1% and 3%, respectively. Meantime, the yields of denitrogenated products, i.e. ethylbenzene (EB), ethylcyclohexene (ECHE), and ethylcyclohexane (ECH) were ca. 2%, 5% and 7, respectively. Octahydroindoline (OHI) was only observed as traces. According to Xiang et al. (Xiang et al., 2008) octahydroindoline is rapidly transformed to ortho-ethylcyclohexylamine.

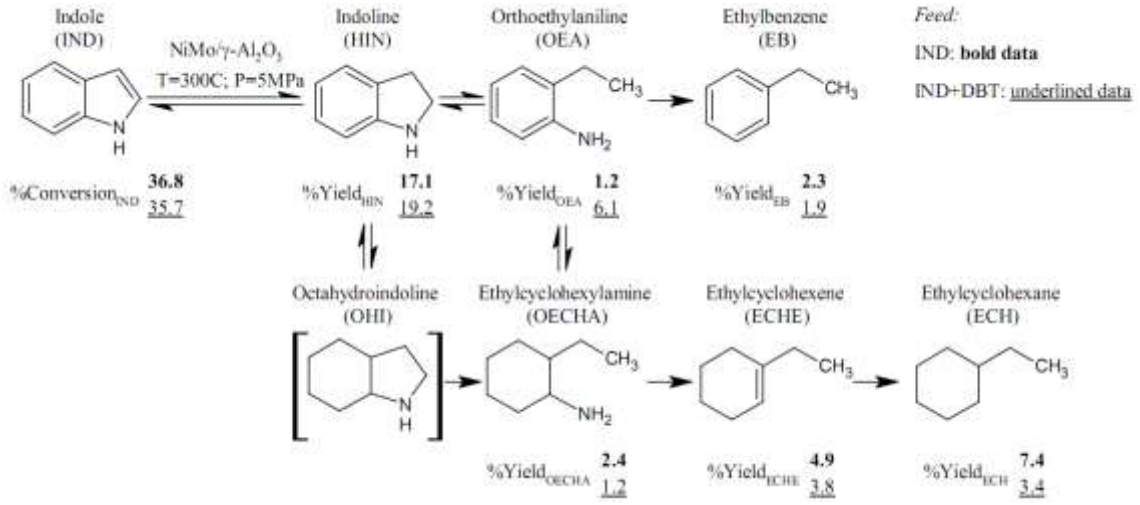

*Figure 22***.** Reaction network of the HDN of indole. Conversion of indole and products yields in the absence (bold data) and in the presence of DBT (underlined data). Conditions: IND=0.22 wt%, DBT=1.7 wt %, *p*=5 MPa, T=300°C, liquid-flow rate of 30 mL·h^{-1} and H_2/liquid feed ratio of 500.

The reaction network proposed in Figure 22 is in agreement with the literature (Bunch, Zhang, Karakas, & Ozkan, 2000; Nguyen, Pirngruber, Chainet, Tayakout-Fayolle, & Geantet, 2017; Prins, 2001; Xiang et al., 2008) and follows the same chemical logic than the one proposed for the hydrotreating of quinoline (vide supra Figure 21). In particular, Nguyen et al. (Nguyen et al., 2017)

mentioned that under hydrotreating conditions indole reaches equilibrium with indoline. Indoline can react via two different paths, through the hydrogenation of the benzenic ring to form octahydroindoline, or via ring-opening (C_{sp3}-N cleavage) to form orthoethylaniline (OEA). Thereafter, orthoethylaniline can also react via two pathways, by the direct C-N bond breaking to obtain ethylbenzene (EB), and by the previous hydrogenation of the aromatic ring to form o-ethylcyclohexylamine (OECHA) and subsequently by C−N cleavage to ethylcyclohexene (ECHE) and ethylcyclohexane (ECH).

3.3.4 Hydrodesulfurization of Dibenzothiophene in the Presence of Nitrogen Compounds. The influence of quinoline and indole on the hydrodesulfurization of dibenzothiophene is presented in terms of the impact factor (%λ) in Figure 23. Under our reaction conditions, both nitrogen compounds promoted the conversion of dibenzothiophene, and, in turn, the promotion effect was influenced by temperature and space-time velocity. The promotion effect was favored at lower temperatures; e.g., at 40 $W_{cat}F_{DBT_0}^{-1}$, in the presence of quinoline, the conversion of dibenzothiophene increased 0.4% at 300°C while it increased 69.1% at 260°C. The same trend was observed with indole but with higher impact factors. For example, at 260°C the conversion of dibenzothiophene increased 129.4% while at 300°C it increased 63.4%. The influence of temperature on the promotion effect was stronger at low space-time velocities, but, when the space-time velocity increased, the effect was similar at the tested temperatures. On the other hand, the impact factor for hydrodesulfurization in the presence of quinoline produced a volcano-type plot when represented as a function of space-time velocity (Figure 23a) whereas a roughly linear monotonous drop of the impact factor was observed in the presence of indole as a function of space-time velocity (Figure 23 b).

a)

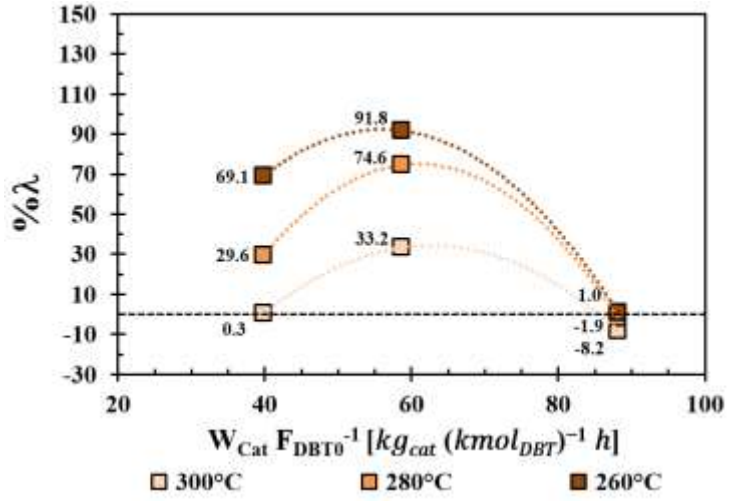

b)

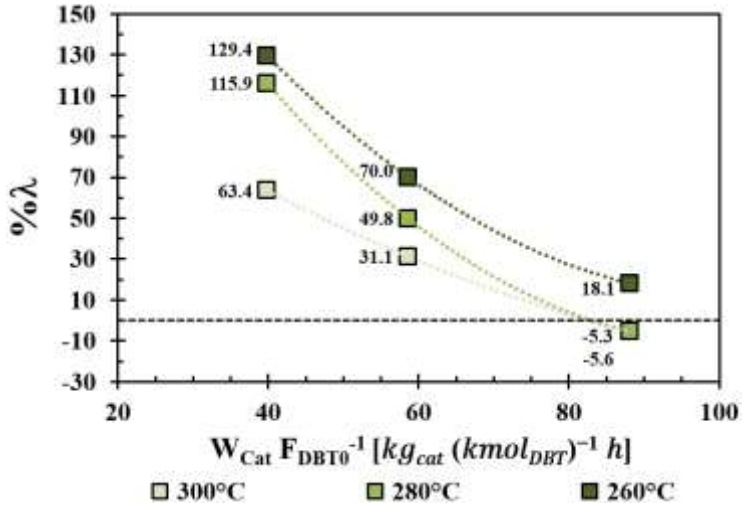

*Figure 23***.** Impact factors on the HDS of DBT of: a) Quinoline, and b) Indole. The reactions were carried out at a fixed molar ratio sulfur/nitrogen of 5, *p*=5 MPa, liquid-flow rate of 30 mL·h^{-1} and H_2/liquid feed ratio of 500.

The effect of quinoline and indole over the products yields of the hydrodesulfurization of dibenzothiophene are presented in Table 18. The yield of biphenyl, the product of the DDS route, was promoted by quinoline and indole, whereas the yield to the products of the HYD pathway decreased regardless of the particular reaction conditions. The influence of the temperature and

space-time velocity on the yield of biphenyl was the same as the one observed for the total conversion of dibenzothiophene described above. At high space-time velocities (88 $W_{cat}F_{DBT_0}^{-1}$), i.e. at larger residence time of the molecules in the reactor, the yield to the DDS route remained constant while the yield to the HYD pathway decreased. Therefore, the decrease in the conversion of dibenzothiophene found under such conditions was ascribed to quinoline and indole inhibiting the HYD pathway. When the residence time of the reactants in the reactor increased, the DDS pathway was promoted by both quinoline and indole while the HYD pathway was inhibited. Thus, the promotion effect exerted by both nitrogen compounds on the hydrodesulfurization of dibenzothiophene is correlated to an enhancement of the reactivity of the sulfur molecule via direct desulfurization.

Table 18**.**

Conversion and yield of the products of the HDS of DBT under different feeds. Reaction conditions: T=300°C, p=5 MPa, and fixed molar ratio sulfur/nitrogen of 5.

$W_{Catal.}F_{DBT_0}^{-1}$	**Feed**	$\%X_{DBT}$	$\%Y_{BP}$	$\%Y_{THDBT}$	$\%Y_{CHB}$
40	DBT	30.6	24.6	2.2	3.8
	DBT+Q	30.7 ≈	29.9 ↑	0.3 ↓↓	0.5 ↓↓
	DBT+IND	50.1 ↑↑	48.6 ↑↑	0.5 ↓	1.0 ↓
59	DBT	43.5	38.5	1.3	3.8
	DBT+Q	57.9 ↑↑	56.9 ↑↑	0.4 ↓↓	0.9 ↓↓
	DBT+IND	57.0 ↑↑	55.6 ↑↑	0.5 ↓↓	1.2 ↓↓
	DBT+NP[a]	*63.6* ↑↑	*55.0* ↑↑	*0.8* ↓↓	*6.7* ↑↑
88	DBT	59.9	54.3	0.8	5.3
	DBT+Q	55.0 ↓	54.7 ≈	0.4 ↓	1.1 ↓↓
	DBT+IND	56.5 ↓	54.8 ≈	0.6 ↓	1.6 ↓↓

[a] Reaction of DBT in the presence of naphthalene (NP) at molar ratio DBT/NP of 5

3.3.5 Hydrodenitrogenation of Quinoline and Indole in the Presence of Dibenzothiophene. The influence of dibenzothiophene on the product distribution of the HDN of quinoline is shown in Figure 21. The conversion of quinoline was not affected by the presence of dibenzothiophene. Nevertheless, the products distribution changed. Particularly, the yield of 1,2,3,4-tetrahydroquinoline increased from 72.7% to 79.3%, whereas the yield of decahydroquinoline decreased from 16.3% to 7.9%. This indicated that the hydrogenation of the N-containing ring of quinoline was not affected by the presence of dibenzothiophene, but the hydrogenation of the benzene ring of 1,2,3,4-tetrahydroquinoline to form decahydroquinoline was affected and decreased. In this sense, the yield of 1,2,3,4-tetrahydroquinoline increased because its hydrogenation to decahydroquinoline diminished. On the other hand, the yield of orthopopylaniline increased with the presence of dibenzothiophene from 3.3% to 5.0%, it is also possibly due to the inhibition of the hydrogenation of the aromatic ring of orthopopylaniline to form propyl-cyclohexylamine, or that the ring-opening of 1,2,3,4-tetrahydroquinoline to form orthopopylaniline was favored, as well as, the C-N bond breaking to form propylbenzene, propylcyclohexene, and propylcyclohexane.

On the other hand, Table 20 presents the conversion of quinoline and product yields in the presence of dibenzothiophene at different $W_{cat}F_{DBT_0}^{-1}$. The high conversion of quinoline was kept at the different studied space-time velocities. Quinoline is mainly transformed on 1,2,3,4-tetrahydroquinoline; however, as mentioned before, the hydrogenation of 1,2,3,4-tetrahydroquinoline to decahydroquinoline is affected by the presence of dibenzothiophene. When the space-time velocity increases, fewer sulfur molecules are on the surface, so more 1,2,3,4-tetrahydroquinoline can be transformed to decahydroquinoline. For this, as space-time increased the yield of 1,2,3,4-tetrahydroquinoline decreased, and the yield of decahydroquinoline increased.

The C-N bond cleavage to obtain propylbenzene, propylcyclohexene, and propylcyclohexane were favored with the increment of the space-time velocity.

Table 19**.**

Conversion of quinoline and product yields in the presence of DBT at different $W_{cat}F_{DBT_0}^{-1}$*. Conditions: T=300°C, p=5 MPa, and fixed molar ratio sulfur/nitrogen of 5.*

$W_{Catal.}F_{DBT_0}^{-1}$	$\%X_Q$	$\%Y_{14THQ}$	$\%Y_{DHQ}$	$\%Y_{OPA}$	$\%Y_{PB}$	$\%Y_{PCHE}$	$\%Y_{PCH}$
40	95.9	88.1 ↑	2.8 ↓	2.8	0.0 ↓	0.6 ↓	0.0 ↓
59	95.6	80.1 ↑	6.0 ↓	6.3	0.9 ↓	0.7 ↓	1.1 ↓
88	94.5	79.3 ↑	7.9 ↓	5.0	1.0 ↓	0.8 ↓	1.1 ↓

Figure 22 displays the effect of the presence of dibenzothiophene on the conversion of indole and the yields of the reaction products. The conversion of indole was not affected considerably by dibenzothiophene, changed slightly from 36.8% to 35.7%. Nevertheless, the yields of products varied with the presence of dibenzothiophene. The yields of indoline and orthoethylaniline increased from 17.1% to 19.2, and from 1.2% to 6.1%, respectively; whereas, the yields of ethylcyclohexylamine, ethylcyclohexene, and ethylcyclohexane diminished with the presence of dibenzothiophene. This behavior is similar to that observed in hydronitrogenation of quinoline; it is possible that the hydrogenation of indoline to octahydroindoline, and orthoethylaniline to ethylcyclohexylamine were inhibited by dibenzothiophene, therefore the yields of indoline and orthoethylaniline increased while the yields of ethylcyclohexylamine and subsequent by-products diminished.

On the other hand, Table 20 presents the conversion of indole and the product yields on the simultaneous reactions with dibenzothiophene at different $W_{cat}F_{DBT_0}^{-1}$. The conversion of indole and the yields of the denitrogenated products, i.e. ethylcyclohexene, ethylcyclohexane, and

ethylbenzene increased with the space-time velocity. Nevertheless, indoline, orthoethylaniline, and ethylcyclohexylamine did not change significantly at the different space-time velocities.

Table 20**.**

Conversion of indole and product yields in the presence of DBT at different $W_{cat}F_{DBT_0}^{-1}$.

Conditions: T=300°C, p=5 MPa, and fixed molar ratio sulfur/nitrogen of 5.

$W_{Catal}F_{DBT_0}^{-1}$	$\%X_{IND}$	$\%Y_{HIN}$	$\%Y_{OEA}$	$\%Y_{OECHA}$	$\%Y_{ECHE}$	$\%Y_{ECH}$	$\%Y_{EB}$
40	31.4	19.5	5.8	1.1	2.8	2.0	1.2
59	33.4	20.3	6.5	1.2	3.4	2.7	1.4
88	35.7	19.2	6.1	1.2	3.8	3.4	1.9

3.3.6 Kinetic Modeling. The kinetic models that led to the best results of simultaneous reactions of HDS of dibenzothiophene and HDN of quinoline and HDN of indole were named DBTQ and DBTIND, respectively. Only these models are presented for the sake of brevity, the reader may refer to Section S3.1 of the Appendix C for data concerning other models tested in this work.

3.3.6.1 Hydrodesulfurization of Dibenzothiophene Simultaneous to the Hydrodenitrogenation of Quinoline. The following assumptions were made for the kinetic model of the hydrodenitrogenation of quinoline in the presence of dibenzothiophene: (i) the concentration of hydrogen is constant during the reaction due to its large partial pressure. In consequence, the concentration of both H_2 and sites β were lumped into the kinetic constant of the corresponding reaction rate; (ii) quinoline adsorbs and reacts on both π and σ sites; (iii) the ring-opening from 1,2,3,4-tetrahydroquinoline to orthopopylaniline only occurs on σ sites; (iv) the hydrogenation of 1,2,3,4-tetrahydroquinoline to decahydroquinoline only takes place on π sites; (v) a simplification

of the reaction network was made and only the hydrogenation of quinoline to 1,2,3,4-tetrahydroquinoline, and the subsequent ring-opening to orthopopylaniline were considered; and, finally (vi) 1,2,3,4-tetrahydroquinoline, the main reaction product, was the only compound taken into account in the competitive adsorption on π and σ sites.

Table 21 presents the mechanism postulated for the hydrogenation of quinoline. This mechanism can be described as follows: the dissociation of H_2 was considered to occur only on β sites (step A). Quinoline is adsorbed on σ sites (step B) and π sites (step G), and also is hydrogenated to 1,2,3,4-tetrahydroquinoline on both sites (steps C and H). The direct hydrogenolysis of 1,2,3,4-tetrahydroquinoline to form orthopopylaniline occurs on σ sites (step E), while the hydrogenation of 1,2,3,4-tetrahydroquinoline to decahydroquinoline takes place on π sites (step J). Finally, desorption of the products is represented by steps D, F, I, and K.

Table 21.

Reaction Mechanism and Catalytic Cycles for the Kinetic Model DBTQ to Describe the Hydrogenation of Quinoline.

step	mechanism	v_1	v_2	v_3	v_4
A	$H_2 + 2\beta \rightleftarrows 2H\beta$	2	1	2	3
B	$Q + \sigma \rightleftarrows Q\sigma$	1	0	0	0
C	$Q\sigma + 4H\beta \rightarrow 14THQ\sigma + 4\beta$	1	0	0	0
D	$14THQ\sigma \rightarrow 14THQ + \sigma$	1	0	0	0
E	$14THQ\sigma + 2H\beta \rightarrow OPA\sigma + 2\beta$	0	1	0	0
F	$OPA\sigma \rightarrow OPA + \sigma$	0	1	0	0
G	$Q + \pi \rightleftarrows Q\pi$	0	0	1	0
H	$Q\pi + 4H\beta \rightarrow 14THQ\pi + 4\beta$	0	0	1	0
I	$14THQ\pi \rightarrow 14THQ + \pi$	0	0	1	0
J	$14THQ\pi + 6H\beta \rightarrow DHQ\sigma + 2\beta$	0	0	0	1
K	$DHQ\pi \rightarrow DHQ + \pi$	0	0	0	1
	Global Reactions				
1	$Q + 2H_2 \rightarrow 14THQ$	1	0	1	0
2	$14THQ + H_2 \rightarrow OPA$	0	1	0	0
3	$14THQ + 3H_2 \rightarrow DHQ$	0	0	0	1

The rate expressions for the simultaneous hydrodesulfurization of dibenzothiophene and hydrogenation of quinoline were described by the following equations:

$$r_{DBTQ,\sigma} = -k_{DBT,\sigma}K_{DBT,\sigma}P_{DBT}\theta_{DBTQ,\sigma} \quad (3.2)$$

$$r_{DBTQ,\pi} = -k_{DBT,\pi}K_{DBT,\pi}P_{DBT}\theta_{DBTQ,\pi} \quad (3.3)$$

$$r_{BPQ,\pi} = -k_{BP,\pi}K_{BP,\pi}P_{BP}\theta_{DBTQ,\pi} \quad (3.4)$$

$$r_{Q,\sigma} = -k_{Q,\sigma}K_{Q,\sigma}P_{Q}\theta_{DBTQ,\sigma} \quad (3.5)$$

$$r_{Q,\pi} = -k_{Q,\pi}K_{Q,\pi}P_{Q}\theta_{DBTQ,\pi} \quad (3.6)$$

$$r_{14THQ-OPA,\sigma} = -k_{14THQ-OPA,\sigma}K_{14THQ,\sigma}P_{14THQ}\theta_{DBTQ,\sigma} \quad (3.7)$$

$$r_{14THQ-DHQ,\pi} = -k_{14THQ-DHQ,\pi} K_{14THQ,\pi} P_{14THQ} \theta_{DBTQ,\pi} \quad (3.8)$$

where:

$$\theta_{DBTQ,\sigma} = \frac{1}{1 + K_{DBT,\sigma}P_{DBT} + K_{BP,\sigma}P_{BP} + K_{CHB,\sigma}P_{CHB} + K_{H_2S,\sigma}P_{H_2S} + K_{Q,\sigma}P_Q + K_{14THQ,\sigma}P_{14THQ}} \quad (3.9)$$

$$\theta_{DBTQ,\pi} = \frac{1}{1 + K_{DBT,\pi}P_{DBT} + K_{BP,\pi}P_{BP} + K_{CHB,\pi}P_{CHB} + K_{H_2S,\pi}P_{H_2S} + K_{Q,\pi}P_Q + K_{14THQ,\pi}P_{14THQ}} \quad (3.10)$$

From the calculations derived from the above expressions, the parameters calculated for the kinetic model are presented in Table 22 together with the corresponding 95% confidence intervals and the corresponding t-values. Calculations led to conclude that the adsorption entropies of quinoline and 1,2,3,4-tetrahydroquinoline are higher on π sites than on σ sites. Such a trend suggests that these molecules present more mobility on hydrogenation sites than on hydrogenolysis sites. This behavior agrees with the adsorption entropies of the polyaromatic structures reported in Chapter 2; where, naphthalene, fluorene, phenanthrene, and their reactions products were also assumed to have a higher mobility on π sites. Besides, the adsorption enthalpy of quinoline and 1,2,3,4-tetrahydroquinoline was greater on π sites than on σ sites, and quinoline was adsorbed stronger than 1,2,3,4-tetrahydroquinoline on both sites. These trends agree with a correlation between the gas phase proton affinities and chemisorption strength. The proton affinity of quinoline is 953.2 kJ mol^{-1} (Hunter & Lias, 1998) while for 1,2,3,4-tetrahydroquinoline is 941.4 kJ mol^{-1} (LaVopa & Satterfield, 1988a). The activation energies of the hydrogenation of quinoline to 1,2,3,4-tetrahydroquinoline are lower on σ sites than on π sites. Likewise, the activation energy for the hydrogenolysis of 1,2,3,4-tetrahydroquinoline to orthopopylaniline on σ sites (69.8 kJ mol^{-1}) was lower than the activation energy for the hydrogenation of 1,2,3,4-tetrahydroquinoline to

decahydroquinoline (90.2 kJ mol^{-1}). This suggested that the perpendicular adsorption of quinoline and 1,2,3,4-tetrahydroquinoline through the lone pair of electrons of the nitrogen atom on σ sites may favor both the hydrogenation of the nitrogen-containing ring (Q→14THQ) and the direct hydrogenolysis (14THQ→OPA).

Table 22**.**

Values of the Kinetic Parameters and Corresponding 95% Probability Confidence Intervals for the Model DBTQ Used to Describe the HDS of DBT and Hydrogenation of Quinoline[a].

Parameter	Estimated value	Lower limit	Upper limit	*t*-value
$A_{Q\text{-}14THQ,\sigma}$ (mmol (g h)$^{-1}$)	1.814	1.761	1.866	67.8
$A_{Q\text{-}14THQ,\pi}$ (mmol (g h)$^{-1}$)	1.173	1.135	1.212	59.7
$A_{14THQ\text{-}OPA,\sigma}$ (mmol (g h)$^{-1}$)	0.007	0.006	0.009	9.5
$A_{14THQ\text{-}DHQ,\pi}$ (mmol (g h)$^{-1}$)	0.021	0.016	0.026	8.0
$E_{a\ Q\text{-}14THQ,\sigma}$ (kJ mol^{-1})	35.3	32.8	37.8	27.5
$E_{a\ Q\text{-}14THQE,\pi}$ (kJ mol^{-1})	51.7	49.4	54.0	44.3
$E_{a\ 14THQ\text{-}OPA,\sigma}$ (kJ mol^{-1})	69.8	63.3	76.4	20.9
$E_{a\ 14THQ\text{-}DHQ,\pi}$ (kJ mol^{-1})	90.2	80.1	100.3	17.6
$-\Delta S^0_{Q,\sigma}$ (J (mol K)$^{-1}$)	91.1	87.8	94.4	53.6
$-\Delta S^0_{14THQ,\sigma}$ (J (mol K)$^{-1}$)	104.3	94.5	114.2	20.9
$-\Delta S^0_{Q,\pi}$ (J (mol K)$^{-1}$)	86.3	83.5	89.1	61.3
$-\Delta S^0_{14THQ,\pi}$ (J (mol K)$^{-1}$)	66.3	64.0	68.6	57.3
$-\Delta H^0_{Q,\sigma}$ (kJ mol^{-1})	78.4	74.6	82.2	40.5
$-\Delta H^0_{14THQ,\sigma}$ (kJ mol^{-1})	60.2	38.9	81.5	5.6
$-\Delta H^0_{Q,\pi}$ (kJ mol^{-1})	140.6	133.9	147.3	41.1
$-\Delta H^0_{14THQ,\pi}$ (kJ mol^{-1})	66.9	63.6	70.1	40.6

[a]Note: F-value = 909. Ftab = 2.79, ttab = 1.965 at 1-α = 0.95 and 452 degrees of freedom

Concerning the statistical fitting of the reaction data by the model, Figure 24 presents a parity plot for the simultaneous hydrodesulfurization of dibenzothiophene and quinoline hydrotreating. The model was able to predict satisfactorily some of the experimental observations, but most of the data were predicted with errors larger than 10 %. Therefore, although the model was found to predict reasonable thermodynamic parameters, its power for predicting the catalytic data was not adequate hence evidencing the shortcomings of its assumptions.

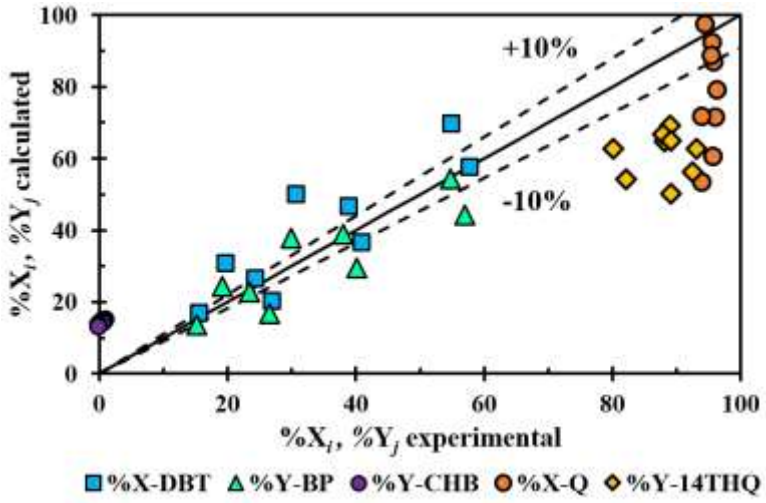

*Figure 24***.** Parity diagram for comparing experimental with the calculated conversion of DBT and Q, and the yields of their reaction products. The simulated values were calculated from the model DBTQ that describe the simultaneous HDS of DBT and hydrogenation of quinoline. Conditions: p = 5 MPa, T = 260−300 °C, and space-time velocity= 40-88 $W_{cat}F_{DBT_0}^{-1}$.

3.3.6.2 Hydrodesulfurization of Dibenzothiophene Simultaneous to the Hydrodenitrogenation of Indole. For the kinetic model of HDN of indole in the presence of dibenzothiophene, the following assumptions were made: i) indole is adsorbed and reacts on both π and σ sites; (ii) the ring-opening from indoline to orthoethylaniline only occurs on σ sites; (iii) a simplification of the reaction network was made, and only the hydrogenation of indole to indoline, and the subsequent ring-opening to orthoethylaniline were assumed; and, finally (iv) indoline and

orthoethylaniline, the main reaction products, were the only reaction products taken into account in the competitive adsorption on π and σ sites.

The corresponding reaction mechanism to describe the hydrogenation of indole is shown in Table 23. The dissociation of H_2 occurs over β sites (step A). Indole is adsorbed on σ sites (step B) and π sites (step G), and also is hydrogenated to indoline on both sites (steps C and H). The C(sp^3)-N bond rupture of indoline to form orthoethylaniline occurs on σ sites (step E). Finally, desorption of the products is represented by steps D, F, and I.

Table 23.

Reaction Mechanism and Catalytic Cycles for the Kinetic Model DBTIND to Describe the Hydrogenation of Indole

step	mechanism	v_1	v_2	v_3
A	$H_2 + 2\beta \rightleftarrows 2H\beta$	1	1	1
B	$IND + \sigma \rightleftarrows IND\sigma$	1	0	0
C	$IND\sigma + 2H\beta \rightarrow HIN\sigma + 2\beta$	1	0	0
D	$HIN\sigma \rightarrow HIN + \sigma$	1	0	0
E	$HIN\sigma + 2H\beta \rightarrow OEA\sigma + 2\beta$	0	1	0
F	$OEA\sigma \rightarrow OEA + \sigma$	0	1	0
G	$IND + \pi \rightleftarrows IND\pi$	0	0	1
H	$IND\pi + 2H\beta \rightarrow HIN\pi + 4\beta$	0	0	1
I	$HIN\pi \rightarrow HIN + \pi$	0	0	1
	Global Reactions			
1	$IND + H_2 \rightarrow HIN$	1	0	1
2	$HIN + H_2 \rightarrow OEA$	0	1	0

The rate expressions for the simultaneous HDS of dibenzothiophene and hydrogenation of indole were described by the following equations:

$$r_{DBTIND,\sigma} = -k_{DBT,\sigma} K_{DBT,\sigma} P_{DBT} \theta_{DBTIND,\sigma} \qquad (3.11)$$

$$r_{DBTIND,\pi} = -k_{DBT,\pi}K_{DBT,\pi}P_{DBT}\theta_{DBTIND,\pi} \quad (3.12)$$

$$r_{BPIND,\pi} = -k_{BP,\pi}K_{BP,\pi}P_{BP}\theta_{DBTIND,\pi} \quad (3.13)$$

$$r_{IND,\sigma} = -k_{IND,\sigma}K_{IND,\sigma}P_{IND}\theta_{DBTIND,\sigma} \quad (3.14)$$

$$r_{IND,\pi} = -k_{IND,\pi}K_{IND,\pi}P_{IND}\theta_{DBTIND,\pi} \quad (3.15)$$

$$r_{HIN-OEA,\sigma} = -k_{HIN-OEA,\sigma}K_{HIN,\sigma}P_{HIN}\theta_{DBTIND,\sigma} \quad (3.16)$$

where:

$$\theta_{DBTIND,\sigma} = \frac{1}{1 + K_{DBT,\sigma}P_{DBT} + K_{BP,\sigma}P_{BP} + K_{CHB,\sigma}P_{CHB} + K_{H_2S,\sigma}P_{H_2S} + K_{IND,\sigma}P_{IND} + K_{HIN,\sigma}P_{HIN} + K_{OEA,\sigma}P_{OEA}} \quad (3.17)$$

$$\theta_{DBTIND,\pi} = \frac{1}{1 + K_{DBT,\pi}P_{DBT} + K_{BP,\pi}P_{BP} + K_{CHB,\pi}P_{CHB} + K_{H_2S,\pi}P_{H_2S} + K_{IND,\pi}P_{IND} + K_{HIN,\pi}P_{HIN} + K_{OEA,\pi}P_{OEA}} \quad (3.18)$$

The parameters estimated for the DBTIND model, their corresponding 95% confidence intervals, and the calculated t-values are shown in Table 24. The calculated values for entropy of quinoline, 1,2,3,4-tetrahydroquinoline, indole, and indoline show the same trend that found for the polyaromatic molecules studied in Chapter 2, i.e. naphthalene, fluorene, and phenanthrene; which implies that also these molecules would have a higher mobility on π sites than on σ sites. The adsorption enthalpy of indoline is much higher than that of indole and orthoethylaniline on both sites. This might be associated to the differences on the acid-base nature of the molecules, since quinoline has a higher proton affinity (957.1 kJ mol^{-1}) (Hunter & Lias, 1998) than indole (933.4 kJ mol^{-1}) (Hunter & Lias, 1998) and orthoethylaniline (861.1 kJ mol^{-1}) (Laredo et al., 2003). Besides, the adsorption enthalpy of indole and orthoethylaniline was significantly higher on π sites than on σ sites. The hydrogenation of indole to indoline had a lower activation energy on π sites

than on σ sites. This trend was contrary to the one determined for the hydrogenation of quinoline to 1,2,3,4-tetrahydroquinoline which was found to be favored on σ sites

.

Table 24**.**

Values of the Kinetic Parameters and Corresponding 95% Probability Confidence Intervals for the Model DBTIND Used to Describe the HDS of DBT and HDN of IND[a]

Parameter	Estimated value	Lower limit	Upper limit	*t*-value
$A_{IND\text{-}HIN,\sigma}$ (mmol (g h)$^{-1}$)	0.004	0.004	0.005	26.7
$A_{IND\text{-}HIN,\pi}$ (mmol (g h)$^{-1}$)	0.056	0.055	0.058	66.8
$A_{HIN\text{-}OEA,\sigma}$ (mmol (g h)$^{-1}$)	0.032	0.009	0.054	2.8
$E_{a\ IND\text{-}HIN,\sigma}$ (kJ mol^{-1})	60.31	57.5	63.1	42.9
$E_{a\ IND\text{-}HIN,\pi}$ (kJ mol^{-1})	20.0	18.8	21.2	33.1
$E_{a\ HIN\text{-}OEA,\sigma}$ (kJ mol^{-1})	20.0	12.4	27.6	5.2
$-\Delta S^0_{IND,\sigma}$ (J (mol K)$^{-1}$)	100.7	97.9	103.5	71.4
$-\Delta S^0_{HIN,\sigma}$ (J (mol K)$^{-1}$)	196.8	143.6	249.9	7.3
$-\Delta S^0_{OEA,\sigma}$ (J (mol K)$^{-1}$)	42.0	35.8	48.2	13.3
$-\Delta S^0_{IND,\pi}$ (J (mol K)$^{-1}$)	75.8	74.9	76.7	168.7
$-\Delta S^0_{HIN,\pi}$ (J (mol K)$^{-1}$)	52.2	51.1	53.3	91.8
$-\Delta S^0_{OEA,\pi}$ (J (mol K)$^{-1}$)	42.0	22.9	61.1	4.3
$-\Delta H^0_{IND,\sigma}$ (kJ mol^{-1})	0.10	0.09	0.11	22.0
$-\Delta H^0_{HIN,\sigma}$ (kJ mol^{-1})	200	97.3	497.3	1.3
$-\Delta H^0_{OEA,\sigma}$ (kJ mol^{-1})	0.10	0.06	0.14	5.1
$-\Delta H^0_{IND,\pi}$ (kJ mol^{-1})	60.7	59.8	61.6	130.1
$-\Delta H^0_{HIN,\pi}$ (kJ mol^{-1})	200	196.3	203.7	106.8
$-\Delta H^0_{OEA,\pi}$ (kJ mol^{-1})	56.1	30.6	81.7	4.3

[a]Note: F-value = 1602.6 Ftab = 2.79, ttab = 1.964 at 1-α = 0.95 and 528 degrees of freedom

Figures 25 shows the parity diagram for the simultaneous hydrodesulfurization of dibenzothiophene and hydrogenation of indole. The model was capable of fitting satisfactorily most of experimental observations for the conversion of dibenzothiophene and for the production

of orthoethylaniline. However, most of the data of the other compounds were predicted with an error higher than 10%.

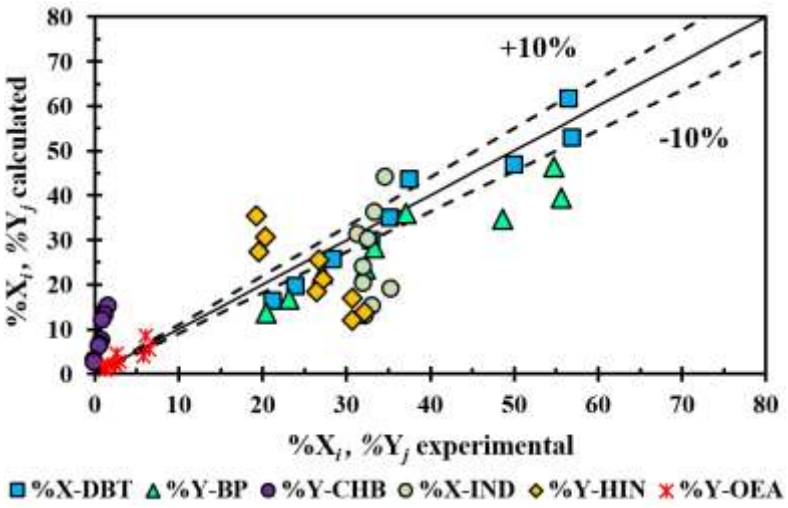

Figure 25. Parity diagram for comparing experimental with the calculated conversion of DBT and IND, and the yields of their reaction products. The simulated values were calculated from the model DBTIND that describe the simultaneous HDS of DBT and hydrogenation of indole. Conditions: p = 5 MPa, T = 260−300 °C, and space-time velocity= 40-88 $W_{cat}F_{DBT_0}^{-1}$.

3.4 Discussion

3.4.1 Effect of quinoline and indole on the hydrodesulfurization of dibenzothiophene

3.4.1.1 Inhibition effect of nitrogen compounds on the Hydrodesulfurization of Dibenzothiophene. The evidenced collected in this work showed that the presence of quinoline and indoline promoted the reactivity of dibenzothiophene over a sulfided NiMo/γ-Al_2O_3 catalyst under the following reaction conditions: p = 5 MPa, T = 260−300 °C, and space-time velocity = 40-88 $W_{cat}F_{DBT_0}^{-1}$, H_2/liquid feed ratio of 500, and molar ratio sulfur/nitrogen of 5. In general, the

DDS reaction pathway was promoted by the presence of both nitrogen compounds, while the HYD reaction pathway was inhibited. The observed catalytic trends, the adsorption enthalpies of both N-containing compounds on π sites, and their proton affinities correlated to a level where a physically meaningful explanation can be argued. The nitrogen compounds adsorb strongly enough on π sites as to inhibit the hydrogenation mediated route of desulfurization of dibenzothiophene. As discussed in Chapter 2, π sites in our work can be rationalized in terms of the proven existence of the so-called *brim sites* (Lauritsen et al., 2004; Rangarajan & Mavrikakis, 2016; Tuxen et al., 2012) possessing a metallic character and hydrogenating character. On these sites, which are found to be located on the top along the periphery of the sulfided catalytic clusters, molecules are theorized to adsorb in a flat-lying configuration before reacting with neighboring S-H sites acting as Brønsted acid sites located at the edge of the sulfided clusters (Salazar et al., 2019; Temel et al., 2010). The adsorption of nitrogen compounds and the competition with organosulfur compounds on the different kind of active sites has been analyzed via density functional theory calculations (Rangarajan & Mavrikakis, 2015; Salazar et al., 2019). Authors seem to agree that nitrogen compounds likely bind more strongly than organosulfur compounds on *brim sites*. Furthermore, LaVopa et al. (LaVopa & Satterfield, 1988a) and Nagai et al. (Nagai et al., 1986) found a lineal correlation between the proton affinity of different nitrogen compounds and the adsorption equilibrium constants on Brønsted sites. Such a correlation can be observed in Figure 26 that was built from the results found in literature. Therefore, we conclude that the inhibition effect of the nitrogen compounds on hydrodesulfurization is explained by their strong adsorption on hydrogenation sites (π sites) and favored by an increase in the basic character of the molecules when expressed as proton affinity. Therefore, our contribution in this sense, was to disregard the conventionally assumed division between basic and non-basic nitrogen molecules.

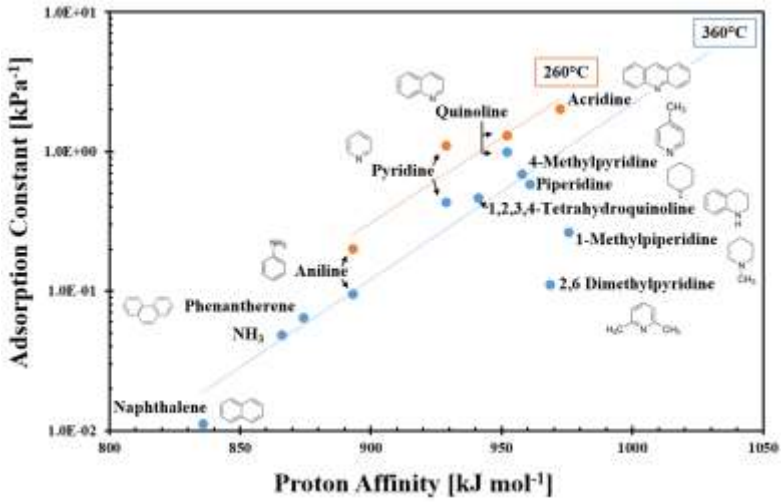

Figure 26. Adsorption equilibrium constants correlate with proton affinity. Data obtained by LaVopa et al. (LaVopa & Satterfield, 1988a) at 360ºC (blue marks) and by Nagai et al.(Nagai et al., 1986) at 260ºC (orange marks), both studied used NiMo/γ-Al_2O_3 catalyst.

3.4.1.2 Promotion effect of the DDS pathway and overall conversion of Dibenzothiophene.

The catalytic promotion was specifically for the direct desulfurization pathway of hydrodesulfurization which raises two big why and how questions. Why the presence of nitrogen compounds promotes direct desulfurization? How does the basic character and concentration of the nitrogen compounds influence this promotion? To try to answer these questions, we will analyze the effects of temperature and of space-time velocity on the recorded promotion.

With both nitrogen compounds, quinoline and indole, the promotion of the HDS was favored by decreasing temperature as in agreement with reports by LaVopa et al. (LaVopa & Satterfield, 1988b) who analyzed this phenomenon for quinoline. A correlation of such a trend with adsorption appears to be evident since adsorption is almost always exothermic and thus their equilibrium constants decrease with temperature. Therefore, the evidence suggests that the promotion effect of nitrogen compounds on hydrodesulfurization must be related to a higher surface coverage of these molecules. This interpretation is further supported by the fact that a decrease in space-time velocity

also enhanced the promotion. A particular difference between both nitrogen molecules, in this sense, was that for quinoline the promotion followed volcano-type plot, while the same was not observed for indole. It is useful to remind that quinoline and indole have a different acid-base character. In the introductory section of the Chapter, quinoline was defined as a Lewis base whereas indole was defined as an acidic molecule (Baltazzi & Krimen, 1963).

The scarce reports about the promotion of HDS by nitrogen compounds have been made exclusively with basic molecules, e.g. acridine, quinoline, pyridine, and piperidine; but the reasons for such promotion are not clear yet. Nagai (Nagai, 1985) speculated that the nitrogen compounds may rearrange the surface structure of the Ni-MoS_2 phase hence making it to become more active without providing any further arguments. LaVopa et al. (LaVopa & Satterfield, 1988b), from an analysis of the effect of temperature on promotion, argued for a possible destabilization in the adsorption of the reaction products of hydrodesulfurization by the presence of quinoline, thus enhancing the reaction rate of HDS. The destabilization and the decrease of the binding energy of the molecules due to the presence of other compounds have been reported (Rangarajan & Mavrikakis, 2015, 2017). However, in this case, LaVopa and Satterfield (LaVopa & Satterfield, 1988b) assumed that quinoline affects exclusively the adsorption of the reaction products, i.e. biphenyl and cyclohexylbenzene, and not the adsorption of dibenzothiophene, which is unlikely because dibenzothiophene is also adsorbed on the same sites than biphenyl, cyclohexylbenzene, and quinoline. On the other hand, Egorova et al. (Egorova & Prins, 2004c) found that 2-methylpyridine (MPy) inhibited the HDS of dibenzothiophene at the range of concentrations (1 kPa DBT and 0.1, 0.5, 1, 2, and 6 kPa 2-MPy) that they studied, while 2-methylpiperidine (2-MPiper) also inhibited the conversion of dibenzothiophene at high concentrations (2 and 6 kPa 2-MPiper), but promoted it at low concentrations (0.1, 0.5, and 1 kPa 2-MPiper). The authors

proposed three possible explanations for the enhancement of DDS pathway. The first one was based on the assumption that hydrogenation and hydrogenolysis reactions occur on the same kind of active sites, but hydrogenation reactions require multiple vacancies (CUS) sites; this was justified by considering that the adsorption of 2-methylpyridine occurs via a π-type mode, whereas 2-methylpiperidine could be adsorbed via σ-bonding through the nitrogen atom on a single vacancy. In this way, when 2-methylpiperidine is adsorbed on the hydrogenation sites, it inhibits the HYD route by impeding the flat adsorption of dibenzothiophene, but, in turn, it transforms the multi vacancies on single vacancies that are not available to the hydrogenation but to the hydrogenolysis, thus increasing the conversion through the DDS route. Nonetheless, Tuxen et al. (Tuxen et al., 2012) found by scanning tunneling microscopy (STM) analyses that multiple vacancies are extremely rare and that their formation is not energetically favored. Moreover, most theoretical studies agree that the most stable mode of adsorption of dibenzothiophene and nitrogen-containing compounds is the perpendicular σ-mode over the plane of vacancies at CUS sites (Rangarajan & Mavrikakis, 2015; Salazar et al., 2019). The second explanation proposed by Egorova and Prins (Egorova & Prins, 2004c) was an acid-base interaction between dibenzothiophene and 2-methylpiperidine. However, they discarded this explanation arguing that the lone pair of 2-methylpiperidine is bonded to the catalyst surface, thus becoming unavailable for an interaction with dibenzothiophene. In this sense, Rabarihoela-Rakotovao et al. (Rabarihoela-Rakotovao, Brunet, Berhault, Perot, & Diehl, 2004) proposed that nitrogen-containing compounds could act as co-catalytic centers for C-S bond cleavage based on the hypothesis that desulfurization takes place via an elimination reaction involving a basic site, probably a sulfur anion (-S^{2-}-), and a Lewis acid site as a coordinatively unsaturated molybdenum ion. They suggested that, due to their basic character, nitrogen compounds in the gas phase could react with an adsorbed organosulfur

complex by a Rideal-Eley reaction mechanism without further validating such a mechanism. The third explanation proposed by Egorova and Prins (Egorova & Prins, 2004c) was that the adsorption of the nitrogen compound may led to an increase of the electron density on the active metal atoms hence generating an increase in the number of the CUS sites on the Ni-MoS surface or to an enhancement of the intrinsic reaction rate of these sites. Nevertheless, the authors did not elaborate further such an explanation. In general, despite their effort, there has been no validation of their explanations.

To try to understand the mechanism behind the promotion of the direct desulfurization route by nitrogen compounds, it is necessary to elucidate over which catalytic centers the promotion phenomenon occurs. It is commonly agreed that the direct desulfurization route takes place on CUS sites located at the edges and corners of the molybdenum sulfide (MoS_2) phase (Lauritsen & Besenbacher, 2015; Rangarajan & Mavrikakis, 2016, 2017). According to atom-resolved microscopy and theoretical studies, the nanocrystals of MoS_2 or Co/Ni-promoted MoS_2 terminate by two different edge types called Mo-edge and S-edge. However, Šarić et al. (Šarić, Rossmeisl, & Moses, 2017, 2018) determined that the formation of vacancies under typical reaction conditions occurs mostly at the Mo-edge and corners, because their formation at the S-edge is energetically unfavorable. On the other hand, it is well established that, as promoters of the MoS_2 phase, Co or Ni (and even platinum (Pinzón, Centeno, & Giraldo, 2006)) specifically enhance the catalytic rate of the direct desulfurization pathway (Bataille et al., 2000; Gutiérrez et al., 2014). For Co and Ni, such promotion has been associated to their ability to donate electrons to Mo which in turn decreases the strength of the Mo-S bonds hence increasing the rate of formation of surface sulfur vacancies (Gutiérrez et al., 2012; Schachtl, Kondratieva, Gutiérrez, & Lercher, 2015). On the other hand, several authors (Gutiérrez et al., 2014; Rangarajan & Mavrikakis, 2015; Sun, Nelson, &

Adjaye, 2004) have determined that Ni replaces, partially or completely, molybdenum atoms mostly located at the Mo-edge.

Considering the above, we propose two non-mutually excluding hypotheses about the promotion effect of nitrogen compounds on hydrodesulfurization. The first hypothesis is that nitrogen compounds promote hydrodesulfurization via direct desulfurization because their adsorption lowers the strength of the neighboring metal-sulfur bond (S-H group binding energy) hence easing the formation of more sulfur vacancies (CUS). The second hypothesis is that the hydrogenation-dehydrogenation equilibrium established in the first step of the hydrotreating reaction sequence for the nitrogen organic compounds, vide Figure 21 and 22, supplies additional surface hydrogen for the C-S bond scission reaction than the one produced after activating the H_2 of the gas feed of the reactor.

The first hypothesis is supported by studies (Moses et al., 2014; Permyakov, Solkan, & Kogan, 2015; Sharifvaghefi, Yang, & Zheng, 2018) reporting a correlation between the SH group binding energy and the activity in hydrodesulfurization reactions. Indeed, Moses et al.(Moses et al., 2014) proposed the SH binding energy as a descriptor for the rate of hydrodesulfurization. From our results, it was evidenced that the promotion effect of nitrogen compounds over hydrodesulfurization was favored by their larger surface coverage of the catalytic sites. According to DFT calculations, the most stable adsorption structure for nitrogen compounds is achieved over hydrogenation sites, but they can also adsorb on the same sulfur vacancies where dibenzothiophene reacts (Rangarajan & Mavrikakis, 2017; Salazar et al., 2019). Therefore, organonitrogen and organosulfur compounds compete for the same active sites and can interact with the same surface neighbors. In this sense, due to the propensity of the nitrogen heteroatom to donate electrons, it is probable that these compounds can modify the strength of the SH group of the adjacent metal

hence generating more vacancies available for C-S scission reactions. Therefore, we rationalize the observed catalytic trends in Table 18 considering that when surface coverage of the organonitrogen compounds increased, the fast saturation of *brim sites* led them to a stronger competition for coordinatively unsaturated sites near surface SH groups whose bond strength was modulated by their interaction with the adsorbed complex from the organonitrogen compound. This effect is modulated by the nature of the organonitrogen molecule. If the latter is a Lewis base, e.g. quinoline, a volcano type behavior is observed for the promotion. Moses et al. (Moses et al., 2014) found a trend between the HDS activity and the surface properties of transition metal-sulfides, and they mentioned that an intermediate strength of the SH binding would be at optimum range for the HDS activity according to the Sabatier principle. To the left of the maximum the HS binding energy becomes weaker and on the right side increases the strength of HS binding. But, if the organonitrogen molecule is acidic, e.g. indole, other kind of interaction could be established between the adsorbed surface complex of the organonitrogen compound and the neighboring SH groups from the catalytic surface. This is interaction has a straightforward effect on the promotion because the latter linearly depended on the surface coverage. According to Rangarajan et al.(Rangarajan & Mavrikakis, 2017) quinoline is adsorbed on the CUS sites trough the nitrogen atom, while the adsorption of indole is preferentially via the carbon adjacent to the nitrogen atom that belongs only to the heteroaromatic ring. The difference in the adsorption structures and the strength of the adsorption of both compounds affect the degree of influence on the SH binding energy, and, therefore, the promotion of the DDS pathway.

The second hypothesis arose when considering recent experimental evidence on the role of surface hydrogen provided by dehydrogenation reactions under HDS atmospheres. Particularly, the group of Iglesia (Li, Yu, & Iglesia, 2002; Yu, Li, & Iglesia, 1999) has provided evidence

suggesting that surface produced via the dehydrogenation of alkanes is more effective for the hydrodesulfurization of thiophene than hydrogen activated from the molecular H_2 fed to the reactor. Inspired by this finding, we took a second look at one of the results from the simultaneous reactions of hydrodesulfurization of dibenzothiophene and hydrogenation of naphthalene, Chapter 2, where the conversion of dibenzothiophene increased slightly from 70.8% to 72.2% (vide Table 12, Chapter 2) hence suggesting a promotion of hydrodesulfurization by naphthalene. Therefore, we decided to make a new catalytic test to verify such promotion using a molar dibenzothiophene to naphthalene ratio equal to 5. The result of the test was included in Table 18 and confirmed that besides the organonitrogen compounds also naphthalene can promote the hydrodesulfurization of dibenzothiophene by enhancing the direct desulfurization route. The hydrogenation of the organosulfur compounds and naphthalene are reversible reactions shifting from hydrogenation to dehydrogenation of the aromatic structures. This being the case, surface hydrogen can be supplied by these reactions as when alkanes are dehydrogenated.

As mentioned earlier, the two hypotheses proposed to explain the promotion of hydrodesulfurization by organonitrogen are not mutually excluding. Both the adsorption of the aromatic and nitrogen compounds and the release of hydrogen by dehydrogentaion may modify the binding energy of the surface SH groups and promote the formation of more CUS. In the case of the surface hydrogen supplied by dehydrogenation, this activated species could react with an SH group to form H_2S hence leaving behind a new sulfur vacancy available for desulfurization. Additional evidence supporting the above hypotheses can be derived from the results of the kinetic modelling of the reactions and the fact that they failed to reproduce the experimental observations. Therefore, it is clear that some of the assumptions employed in formulating the models cannot be applied when analyzing the simultaneous hydrotreating of organosulfur and organonitrogen

compounds. One may first argue that the mismatch between the experimental data and the predictions of the model can be overcome by either including a larger number of parameters or by further parameters optimization. However, we found that the former is not the case in Chapter 2 whereas the second was already performed and reported herein. This leaves us with the possibility that the fundamental assumptions of the Langmuir-Hinshelwood formalism do not allow modelling the promotion effects found herein. The more critical assumptions of the model are that all catalytic sites are equivalent and their number is fixed, and that there is no interaction between neighboring adsorbed molecules or between adsorbed molecules with other active sites. For further kinetic studies it would be interesting to analyze other formalisms different from LHHW that could describe the promotion phenomenon.

Finally, it is interesting to discuss the effect of dibenzothiophene over the hydrotreating of the organonitrogen compounds. According to the results, the conversion of quinoline and indole were not affected by the presence of dibenzothiophene. However, the product distribution changed in the simultaneous reaction. We noticed that the distribution of reaction products was affected by the presence of dibenzothiophene in the following manner. For indole, the hydrogenation of indoline to octahydroindoline, and orthoethylaniline to ethylcyclohexylamine decreased, whereas, for quinoline, the hydrogenation of 1,2,3,4-tetrahydroquinoline to decahydroquinoline, and orthopopylaniline to propylcyclohexylamine also decreased. Regardless of the acid-base nature of the organonitrogen compound, these four reactions have in common that the benzene ring of the structure is free of steric hindrance. Gutiérrez et al. (Gutiérrez et al., 2014) proposed that small molecules like orthopopylaniline can access CUS sites and be hydrogenated therein. Therefore, according to this author, due to their size and the absence of steric hindrance, these compounds could be hydrogenated on both CUS sites and brim sites. In this sense, in the reactions in the

absence of dibenzothiophene, the nitrogen compounds, i.e. indoline, orthoethylaniline, 1,2,3,4-tetrahydroquinoline, and orthopopylaniline, may access both catalytic sites to be hydrogenated. However, as dibenzothiophene preferably adsorbs on CUS sites, a competition for these sites arises. Since sulfur vacancies can behave like Lewis acid sites, nitrogen compounds would be expected to adsorb more strongly than sulfur compounds. However, Rangarajan and Mavrikakis (Rangarajan & Mavrikakis, 2017) found that due to the larger atomic radius of sulfur atoms in comparison to nitrogen atoms, dibenzothiophene interacts with both metal atoms of the site, while nitrogen compounds bind with only one. They concluded that this additional metal-sulfur bond leads the higher adsorption strength of sulfur compounds. For that reason, the hydrogenation of the nitrogen compounds that take place on CUS sites was inhibited by the presence of dibenzothiophene.

3.5 Conclusions

The hydrodesulfurization of dibenzothiophene was studied over a NiMo/γ-Al_2O_3 catalyst in the presence of two nitrogen compounds with different basicity, i.e. quinoline and indole. Both nitrogen compounds suppressed the HYD pathway. Quinoline with a higher proton affinity than indole inhibited more strongly the hydrogenation sites which are related to Brønsted acid sites (S-H groups). Therefore, the inhibition of this sites was according to the basicity of the N-containing compounds. On the other hand, the DDS pathway was promoted by the presence of quinoline and indole. This promotion had only been reported by the presence of nitrogen compounds of basic nature, e.g. acridine, pyridine, and quinoline, but not by weakly basic molecules like indole. The promotion of the direct desulfurization was favored at low temperatures and low space-time

velocities, indicating that the influences of the nitrogen compounds are correlated to the adsorption of this molecules and their collateral effects on the catalytic surface, either by the modification of the strength of the adsorption of SH groups arousing the creation of more sulfur vacancies, or by the availability to have on surface hydrogen via dehydrogenation reactions which are more effective hydrogen source for the direct desulfurization than the hydrogen fed in the reaction. The kinetic models based on Langmuir-Hinshelwood formalism for the simultaneous HDS of dibenzothiophene and HDN of quinoline and indole were not capable of fitting experimental observations. This indicated that is necessary to develop kinetic models based on other formalism that can describe the promotion effect that can describe the promotion effect possibly due to the creation of more sulfur vacancies during the reaction.

4. General Conclusions

In the first chapter, the reactivity and influence of different olefins on the hydrodesulfurization of 2-methylthiophene was studied. All type of olefins, i.e. cyclic, linear, and branched, inhibited the conversion of 2-methylthiophene. However, the grade of inhibition was related to the structure of the molecules. Planar olefins inhibited more the conversion of 2-methylthiophene than non-planar olefins. Meanwhile, the inhibition of the direct desulfurization of 2-methylthiophene was influenced by the steric hindrance of the olefins. Branched olefins, inhibited less the desulfurization sites than non-branched olefins. Results suggest that 2-methylthiophene may react on two different sites, the first one which is accessible to π-flat adsorption of the molecules, and

the other one which is a restricted site for the adsorption of branched olefins. These sites may well correspond to brim and CUS sites, respectively.

Aiming to build robust kinetic models of the hydrotreatment process with chemical sense at the molecular level from a bottom to top approach, the Chapter 2 analyzed the kinetics of simultaneous hydrodesulfurization and hydrogenation model reactions from a Langmuir−Hinshelwood-Hougen-Watson perspective applying fundamental concepts for kinetic modelling. It allows the determination of the thermodynamic parameters related to catalytic elementary steps. The chapter started by analyzing the kinetics of the hydrodesulfurization of dibenzothiophene when one or two surface sites were considered for performing the chemical steps necessary for the removal of sulfur from the molecule. Based on the physicochemical consistency of the thermodynamic parameters of the postulated models and on the statistical significance of the model fitting of the experimental data, it was determined that two catalytic surface sites: one where hydrogenation reactions occur (π) and another where the C-S-C scission step takes place (σ), lead to a suitable kinetic model for describing the surface catalytic process for the hydrodesulfurization of dibenzothiophene. Such finding was in agreement with molecular level studies claiming the existence of the so-called CUS and brim active sites. Making use of the resulting model for hydrodesulfurization, the second part of the Chapter 2 analyzes the kinetics of simultaneous hydrodesulfurization-hydrogenation reactions comprising dibenzothiophene and selected compounds; namely, naphthalene, fluorene, and phenanthrene, with different degrees of aromaticity. The following key findings were found from an analysis of the model: (i) the tested aromatic structures and their reaction products adsorb on both catalytic sites; (ii) the aromatic structures with higher aromaticity; i.e. fluorene and phenanthrene, only react on π sites. In contrast, naphthalene is able to react on both kind of sites; (iii) except for DBT, the mobility of the tested

aromatics over π sites is higher than on σ sites; (iv) the structural similarity between the aromatic molecules enhances competition for occupying π sites which in the case of fluorene traduces into inhibiting the hydrodesulfurization of dibenzothiophene.

Chapter 3 evaluates the effect of the N-containing compounds on the hydrodesulfurization of dibenzothiophene. Quinoline and indole were selected as model nitrogen compounds because of their proton affinity, 953.2 kJ mol^{-1} and 933.4 kJ mol^{-1}, respectively. Both N-containing compounds inhibited the hydrogenation pathway of the hydrodesulfurization of dibenzothiophene. The inhibition was related to the basicity of the compounds, quinoline with higher proton affinity suppressed more strongly the hydrogenation pathway than indole. On the other hand, the direct desulfurization pathway was promoted by the presence of quinoline and indole. This promotion was favored at low temperatures and low space-time velocities. The increment of the direct desulfurization correlated to the adsorption of quinoline and indole on the catalytic surface. The binding energy of the SH groups might be modified by the presence of the N-containing compounds or by the release of hydrogen from denitrogenating reactions of quinoline and indole, which could react with an SH group to form H_2S, promoting the formation of more sulfur vacancies available for C-S scission reactions. Finally, kinetic models for the simultaneous reaction of the hydrodesulfurization of dibenzothiophene and hydrodenitrogenation of quinoline and indole were developed following the Langmuir−Hinshelwood-Hougen-Watson formalism adopted in Chapter 2. The kinetic parameters estimated were physically reasonable and thermodynamically consistent, but the model fitted several experimental points with an error larger than ca. 10%. Kinetic models cannot describe correctly the promotion effect of the nitrogen compounds. This promotion effect was associated to the creation of more sulfur vacancies, however, Langmuir−Hinshelwood approach neglected the interaction between neighboring adsorbed molecules or between adsorbed

molecules with other active sites. For further kinetic studies it would be interesting to analyze other kinetic formalisms that could describe the promotion phenomenon.

References

Agency European Environment. (n.d.). Air Pollution. Retrieved December 16, 2018, from https://www.eea.europa.eu/themes/air/intro

Al-Barood, A., & Stanislaus, A. (2007). Ultra-Deep Desulfurization of Coker and Straight-Run Gas Oils: Effect of Lowering Feedstock 95% Boiling Point. Fuel Processing Technology, 88(3), 309–315. https://doi.org/10.1016/J.FUPROC.2006.10.008

Alkandari, M., Mujtaba, I. M., & Arellando-Garciaa, H. (2017). Model Based Analysis of a Petroleum Refinery Plant with Hydrotreating as a Pre-treatment Unit. Computer Aided Chemical Engineering, 40, 835–840. https://doi.org/10.1016/B978-0-444-63965-3.50141-0

Alsolami, B. H., Berger, R. J., Makkee, M., & Moulijn, J. A. (2013). Catalyst Performance Testing in Multiphase Systems: Implications of Using Small Catalyst Particles in Hydrodesulfurization. Industrial & Engineering Chemistry Research, 52(26), 9069–9085. https://doi.org/10.1021/ie4010749

Anabtawi, J. A., Alam, K., Ali, M. A., Ali, S. A., & Siddiqui, M. A. B. (1995). Performance Evaluation of HDS Catalysts by Distribution of Sulfur Compounds in Naphtha. Fuel, 74(9), 1254–1260. https://doi.org/10.1016/0016-2361(95)00076-H

Babich, I. ., & Moulijn, J. . (2003). Science and Technology of Novel Processes for Deep Desulfurization of Oil Refinery Streams: A Review. Fuel, 82(6), 607–631. https://doi.org/10.1016/S0016-2361(02)00324-1

Badawi, M., Vivier, L., & Duprez, D. (2010). Kinetic Study of Olefin Hydrogenation on Hydrotreating Catalysts. Journal of Molecular Catalysis A: Chemical, 320(1–2), 34–39. https://doi.org/10.1016/J.MOLCATA.2009.12.012

Badawi, M., Vivier, L., Pérot, G., & Duprez, D. (2008). Promoting Effect of Cobalt and Nickel on the Activity of Hydrotreating Catalysts in Hydrogenation and Isomerization of Olefins. Journal of Molecular Catalysis A: Chemical, 293(1–2), 53–58. https://doi.org/10.1016/J.MOLCATA.2008.07.006

Baldovino-Medrano, V. G., Eloy, P., Gaigneaux, E. M., Giraldo, S. A., & Centeno, A. (2009). Development of the HYD Route of Hydrodesulfurization of Dibenzothiophenes over Pd–Pt/γ-Al_2O_3 Catalysts. Journal of Catalysis, 267(2), 129–139. https://doi.org/10.1016/J.JCAT.2009.08.004

Baldovino-Medrano, V. G., Giraldo, S. A., & Centeno, A. (2008). The Functionalities of Pt/γ-Al_2O_3 Catalysts in Simultaneous HDS and HDA Reactions. Fuel, 87(10–11), 1917–1926. https://doi.org/10.1016/J.FUEL.2007.12.008

Baldovino-Medrano, V. G., Giraldo, S. A., & Centeno, A. (2009). Reactivity of Dibenzothiophene Type Molecules over Pd Catalysts. Journal of Molecular Catalysis A: Chemical, 301(1–2), 127–133. https://doi.org/10.1016/J.MOLCATA.2008.11.021

Baltazzi, E., & Krimen, L. I. (1963). Recent Advances in the Chemistry of Pyrrole. Chemical Reviews, 63(5), 511–556. https://doi.org/10.1021/cr60225a004

Bandyopadhyay, R., & Upadhyayula, S. (2018). Thermodynamic Analysis of Diesel Hydrotreating Reactions. Fuel, 214, 314–321. https://doi.org/10.1016/J.FUEL.2017.10.015

Bataille, F., Lemberton, J.-L., Michaud, P., Pérot, G., Vrinat, M., Lemaire, M., Kasztelan, S. (2000). Alkyldibenzothiophenes Hydrodesulfurization-Promoter Effect, Reactivity, and Reaction Mechanism. Journal of Catalysis, 191(2), 409–422. https://doi.org/10.1006/JCAT.1999.2790

Beltramone, A. R., Crossley, S., Resasco, D. E., Alvarez, W. E., & Choudhary, T. V. (2008). Inhibition of the Hydrogenation and Hydrodesulfurization Reactions by Nitrogen Compounds over NiMo/Al_2O_3. Catalysis Letters, 123(3–4), 181–185. https://doi.org/10.1007/s10562-008-9468-7

Beltramone, A. R., Resasco, D. E., Alvarez, W. E., & Choudhary, T. V. (2008). Simultaneous Hydrogenation of Multiring Aromatic Compounds over NiMo Catalyst. Industrial & Engineering Chemistry Research, 47(19), 7161–7166. https://doi.org/10.1021/ie8004258

Besenbacher, F., Brorson, M., Clausen, B. S., Helveg, S., Hinnemann, B., Kibsgaard, J., … Topsøe, H. (2008). Recent STM, DFT and HAADF-STEM Studies of Sulfide-Based Hydrotreating Catalysts: Insight Into Mechanistic, Structural and Particle Size Effects. Catalysis Today, 130(1), 86–96. https://doi.org/10.1016/J.CATTOD.2007.08.009

Bhaskar, M., Valavarasu, G., Sairam, B., Balaraman, K. S., & Balu, K. (2004). Three-Phase Reactor Model to Simulate the Performance of Pilot-Plant and Industrial Trickle-Bed Reactors Sustaining Hydrotreating Reactions. Industrial & Engineering Chemistry Research. https://doi.org/10.1021/IE049642B

Boggs, P. T., Donaldson, J. R., Byrd, R. h., & Schnabel, R. B. (1989). Algorithm 676 ODRPACK: Software for Weighted Orthogonal Distance Regression. ACM Transactions on Mathematical Software, 15(4), 348–364. https://doi.org/10.1145/76909.76913

Boudart, M., & Djega-Mariadassou, G. (2014). Kinetics of Heterogeneous Catalytic Reactions. Princeton Univ Press.

Broderick, D. H., & Gates, B. C. (1981). Hydrogenolysis and Hydrogenation of Dibenzothiophene Catalyzed by Sulfided CoO-MoO_3/γ-Al_2O_3: The Reaction Kinetics. AIChE Journal, 27(4), 663–673. https://doi.org/10.1002/aic.690270419

Brown, P. N., Byrne, G. D., & Hindmarsh, A. C. (1989). VODE: A Variable-Coefficient ODE Solver. SIAM Journal on Scientific and Statistical Computing, 10(5), 1038–1051. https://doi.org/10.1137/0910062

Brunet, S., Mey, D., Pérot, G., Bouchy, C., & Diehl, F. (2005). On the Hydrodesulfurization of FCC Gasoline: A Review. Applied Catalysis A: General, 278(2), 143–172. https://doi.org/10.1016/J.APCATA.2004.10.012

Bunch, A., Zhang, L., Karakas, G., & Ozkan, U. S. (2000). Reaction Network of Indole Hydrodenitrogenation over $NiMoS/\gamma$-Al_2O_3 Catalysts. Applied Catalysis A: General, 190(1–2), 51–60. https://doi.org/10.1016/S0926-860X(99)00270-7

Campbell, P., Zhang, Y., Yan, F., Lu, Z., & Streets, D. (2018). Impacts of Transportation Sector Emissions on Future U.S. air Quality in a Changing Climate. Part I: Projected Emissions, Simulation Design, and Model Evaluation. Environmental Pollution, 238, 903–917. https://doi.org/10.1016/J.ENVPOL.2018.04.020

Carrillo, J. A., & Corredor, L. M. (2013). Upgrading of Heavy Crude Oils: Castilla. Fuel Processing Technology, 109, 156–162. https://doi.org/10.1016/J.FUPROC.2012.09.059

Castillo-Araiza, C. O., Chávez, G., Dutta, A., de los Reyes, J. A., Nuñez, S., & García-Martínez, J. C. (2015). Role of Pt–Pd/γ-Al_2O_3 on the HDS of 4,6-DMBT: Kinetic Modeling & Contribution Analysis. Fuel Processing Technology, 132, 164–172. https://doi.org/10.1016/J.FUPROC.2014.12.028

Celis-Cornejo, C.-M., Granados-Zarta, G.-A., Bravo-Villarreal, C.-E., Pérez-Martínez, D. de J., & Giraldo-Duarte, S.-A. (2013). Kinetic Parameters Determination of FCC Gasoline Hydrotreating Using Genetic Algorithms. CT&F - Ciencia, Tecnología y Futuro, 5, 79–93.

Chandak, N., Al Hamadi, A., Yousef, M., Mohamed, A., Inamura, K., & Berthod, M. (2014). A Pilot Reactor Study to Determine Operational Factors of the Commercial Hydrodesulphurization (HDS) Catalyst to Produce Ultra-Low Sulphur Diesel (ULSD). Fuel, 138, 37–44. https://doi.org/10.1016/J.FUEL.2014.07.050

Che-Galicia, G., Ruiz-Martínez, R. S., López-Isunza, F., & Castillo-Araiza, C. O. (2015). Modeling of Oxidative Dehydrogenation of Ethane to Ethylene on a MoVTeNbO/TiO_2 Catalyst in an Industrial-Scale Packed Bed Catalytic Reactor. Chemical Engineering Journal, 280, 682–694. https://doi.org/10.1016/J.CEJ.2015.05.128

Chen, W., Long, X., Li, M., Nie, H., & Li, D. (2017). Influence of Active Phase Structure of CoMo/Al_2O_3 Catalyst on the Selectivity of Hydrodesulfurization and Hydrodearomatization. Catalysis Today, 292, 97–109. https://doi.org/10.1016/J.CATTOD.2016.09.029

Chevron Corporation. (n.d.). Diesel Fuel Technical Review. Retrieved December 12, 2019, from https://www.chevron.com/-/media/chevron/operations/documents/diesel-fuel-tech-review.pdf

Choi, J.-S., Maugé, F., Pichon, C., Olivier-Fourcade, J., Jumas, J.-C., Petit-Clair, C., & Uzio, D. (2004). Alumina-Supported Cobalt–Molybdenum Sulfide Modified by tin via Surface Organometallic Chemistry: Application to the Simultaneous Hydrodesulfurization of Thiophenic Compounds and the Hydrogenation of Olefins. Applied Catalysis A: General, 267(1–2), 203–216. https://doi.org/10.1016/J.APCATA.2004.03.005

Choi, K.-H., Kunisada, N., Korai, Y., Mochida, I., & Nakano, K. (2003). Facile Ultra-Deep Desulfurization of Gas Oil Through Two-Stage or -Layer Catalyst Bed. Catalysis Today, 86(1–4), 277–286. https://doi.org/10.1016/S0920-5861(03)00413-9

Clews, R. J. (2016). Fundamentals of the Petroleum Industry. Project Finance for the International Petroleum Industry, 83–99. https://doi.org/10.1016/B978-0-12-800158-5.00005-0

Colvile, R. ., Hutchinson, E. ., Mindell, J. ., & Warren, R. . (2001). The Transport Sector as a Source of Air Pollution. Atmospheric Environment, 35(9), 1537–1565. https://doi.org/10.1016/S1352-2310(00)00551-3

Correa Pabón, R. E., & Souza Filho, C. R. de. (2019). Crude Oil Spectral Signatures and Empirical Models to Derive API Gravity. Fuel, 237, 1119–1131. https://doi.org/10.1016/J.FUEL.2018.09.098

Cristol, S., Paul, J.-F., Payen, E., Bougeard, D., Hutschka, F., & Clémendot, S. (2004). DBT Derivatives Adsorption over Molybdenum Sulfide Catalysts: A Theoretical Study. Journal of Catalysis, 224(1), 138–147. https://doi.org/10.1016/J.JCAT.2004.02.008

Daudin, A., Brunet, S., Perot, G., Raybaud, P., & Bouchy, C. (2007). Transformation of a Model FCC Gasoline Olefin Over Transition Monometallic Sulfide Catalysts. Journal of Catalysis, 248(1), 111–119. https://doi.org/10.1016/J.JCAT.2007.03.009

De Oliveira, L. P., Hudebine, D., Guillaume, D., & Verstraete, J. J. (2016). A Review of Kinetic Modeling Methodologies for Complex Processes. Oil & Gas Science and Technology – Revue d'IFP Energies Nouvelles, 71(3), 45. https://doi.org/10.2516/ogst/2016011

Demirbas, A., Alidrisi, H., & Balubaid, M. A. (2015). API Gravity, Sulfur Content, and Desulfurization of Crude Oil. Petroleum Science and Technology, 33(1), 93–101. https://doi.org/10.1080/10916466.2014.950383

Demirbas, A., Bafail, A., & Nizami, A.-S. (2016). Heavy Oil Upgrading: Unlocking the Future Fuel Supply. Petroleum Science and Technology, 34(4), 303–308. https://doi.org/10.1080/10916466.2015.1136949

DieselNet. (n.d.). Fuels: Brazil: Automotive Diesel Fuel. Retrieved December 16, 2018, from https://www.dieselnet.com/standards/br/fuel_automotive.php#anp_2009

Ding, S., Jiang, S., Zhou, Y., Wei, Q., & Zhou, W. (2017). Catalytic Characteristics of Active Corner Sites in CoMoS Nanostructure Hydrodesulfurization – A Mechanism Study Based on DFT Calculations. Journal of Catalysis, 345, 24–38. https://doi.org/10.1016/J.JCAT.2016.11.011

Dong, D., Jeong, S., & Massoth, F. E. (1997). Effect of Nitrogen Compounds on Deactivation of Hydrotreating Catalysts by Coke. Catalysis Today, 37(3), 267–275. https://doi.org/10.1016/S0920-5861(97)00022-9

Dorneles de Mello, M., de Almeida Braggio, F., da Costa Magalhães, B., Zotin, J. L., & Pereira da Silva, M. A. (2017). Effects of Phosphorus Content on Simultaneous Ultradeep HDS and HDN Reactions over NiMoP/Alumina Catalysts. Industrial & Engineering Chemistry Research, 56(37), 10287–10299. https://doi.org/10.1021/acs.iecr.7b02718

Dos Santos, N., Dulot, H., Marchal, N., & Vrinat, M. (2009). New Insight on Competitive Reactions During Deep HDS of FCC Gasoline. Applied Catalysis A: General, 352(1–2), 114–123. https://doi.org/10.1016/J.APCATA.2008.09.035

Duayne Whitehurst, D., Isoda, T., & Mochida, I. (1998). Present State of the Art and Future Challenges in the Hydrodesulfurization of Polyaromatic Sulfur Compounds. Advances in Catalysis, 42, 345–471. https://doi.org/10.1016/S0360-0564(08)60631-8

Edvinsson, R., & Irandoust, S. (1993). Hydrodesulfurization of Dibenzothiophene in a Monolithic Catalyst Reactor. Industrial & Engineering Chemistry Research, 32(2), 391–395. https://doi.org/10.1021/ie00014a016

Egorova, M., & Prins, R. (2004a). Competitive Hydrodesulfurization of 4,6-Dimethyldibenzothiophene, Hydrodenitrogenation of 2-Methylpyridine, and Hydrogenation of Naphthalene over Sulfided NiMo/γ-Al_2O_3. Journal of Catalysis, 224(2), 278–287. https://doi.org/10.1016/J.JCAT.2004.03.005

Egorova, M., & Prins, R. (2004b). Hydrodesulfurization of Dibenzothiophene and 4,6-Dimethyldibenzothiophene over Sulfided NiMo/γ-Al_2O_3, CoMo/γ-Al_2O_3, and Mo/γ-Al_2O_3 Catalysts. Journal of Catalysis, 225(2), 417–427. https://doi.org/10.1016/J.JCAT.2004.05.002

Egorova, M., & Prins, R. (2004b). Mutual Influence of the HDS of Dibenzothiophene and HDN of 2-Methylpyridine. Journal of Catalysis, 221(1), 11–19. https://doi.org/10.1016/S0021-9517(03)00264-1

Egorova, M., & Prins, R. (2004b). Promotion Effect of 2-Methylpiperidine on the Direct Desulfurization of Dibenzothiophene over NiMo/γ-Al_2O_3. Catalysis Letters, 92(3/4), 87–91. https://doi.org/10.1023/B:CATL.0000014344.37981.9c

Egorova, M., & Prins, R. (2004c). Mutual Influence of the HDS of Dibenzothiophene and HDN of 2-Methylpyridine. Journal of Catalysis, 221(1), 11–19. https://doi.org/10.1016/S0021-9517(03)00264-1

Egorova, M., & Prins, R. (2004c). Promotion Effect of 2-Methylpiperidine on the Direct Desulfurization of Dibenzothiophene over NiMo/γ-Al_2O_3. Catalysis Letters, 92(3/4), 87–91. https://doi.org/10.1023/B:CATL.0000014344.37981.9c

ENI (Ente Nazionale Idrocarburi). (2018). World Oil Review 2018 - Volume 1.

European Commission. (n.d.). Emissions in the automotive sector. Retrieved December 4, 2018, from https://ec.europa.eu/growth/sectors/automotive/environment-protection/emissions_en

Fan, Y. Van, Perry, S., Klemeš, J. J., & Lee, C. T. (2018). A Review on Air Emissions Assessment: Transportation. Journal of Cleaner Production, 194, 673–684. https://doi.org/10.1016/J.JCLEPRO.2018.05.151

Farag, H. (2006). Kinetic Analysis of the Hydrodesulfurization of Dibenzothiophene: Approach Solution to the Reaction Network. Energy & Fuels, 20(5), 1815–1821. https://doi.org/10.1021/ef060225g

Farag, H., Kishida, M., & Al-Megren, H. (2014). Competitive Hydrodesulfurization of Dibenzothiophene and Hydrodenitrogenation of Quinoline over Unsupported MoS2 Catalyst. Applied Catalysis A: General, 469, 173–182. https://doi.org/10.1016/J.APCATA.2013.09.003

Farag, H., Sakanishi, K., Mochida, I., & Whitehurst, D. D. (1998). Kinetic Analyses and Inhibition by Naphthalene and H_2S in Hydrodesulfurization of 4,6-Dimethyldibenzothiophene (4,6-

DMDBT) over CoMo-Based Carbon Catalyst. Energy & Fuels, 13(2), 449–453. https://doi.org/10.1021/EF980141A

Froment, G. F., De Wilde, J., & Bischoff, K. B. (2011). Chemical Reactor Analysis and Design. Wiley.

García-Gutiérrez, J. L., Laredo, G. C., Fuentes, G. A., García-Gutiérrez, P., & Jiménez-Cruz, F. (2014). Effect of Nitrogen Compounds in the Hydrodesulfurization of Straight-Run Gas Oil Using a CoMoP/γ-Al_2O_3 Catalyst. Fuel, 138, 98–103. https://doi.org/10.1016/J.FUEL.2014.08.008

García-Martínez, J. C., Castillo-Araiza, C. O., De los Reyes Heredia, J. A., Trejo, E., & Montesinos, A. (2012). Kinetics of HDS and of the Inhibitory Effect of Quinoline on HDS of 4,6-DMDBT over a Ni–Mo–P/Al_2O_3 Catalyst: Part I. Chemical Engineering Journal, 210, 53–62. https://doi.org/10.1016/J.CEJ.2012.08.048

Gilbert, W. R. (2014). Formation of Thiophenic Species in FCC Gasoline from H2S Generating Sulfur Sources in FCC Conditions. Fuel, 121, 65–71. https://doi.org/10.1016/J.FUEL.2013.12.033

Girgis, M. J., & Gates, B. C. (1991). Reactivities, Reaction Networks, and Kinetics in High-Pressure Catalytic Hydroprocessing. Industrial & Engineering Chemistry Research, 30(9), 2021–2058. https://doi.org/10.1021/ie00057a001

Grønborg, S. S., Šarić, M., Moses, P. G., Rossmeisl, J., & Lauritsen, J. V. (2016). Atomic Scale Analysis of Sterical Effects in the Adsorption of 4,6-Dimethyldibenzothiophene on a CoMoS Hydrotreating Catalyst. Journal of Catalysis, 344, 121–128. https://doi.org/10.1016/J.JCAT.2016.09.004

Gutiérrez, O. Y., Hrabar, A., Hein, J., Yu, Y., Han, J., & Lercher, J. A. (2012). Ring Opening of 1,2,3,4-Tetrahydroquinoline and Decahydroquinoline on MoS2/γ-Al_2O_3 and Ni–MoS_2/γ-Al_2O_3. Journal of Catalysis, 295, 155–168. https://doi.org/10.1016/J.JCAT.2012.08.003

Gutiérrez, O. Y., Singh, S., Schachtl, E., Kim, J., Kondratieva, E., Hein, J., & Lercher, J. A. (2014). Effects of the Support on the Performance and Promotion of (Ni)MoS_2 Catalysts for Simultaneous Hydrodenitrogenation and Hydrodesulfurization. ACS Catalysis, 4(5), 1487–1499. https://doi.org/10.1021/cs500034d

Han, W., Nie, H., Long, X., Li, M., Yang, Q., & Li, D. (2017). Effects of the Support Brønsted Acidity on the Hydrodesulfurization and Hydrodenitrogention Activity of Sulfided $NiMo/Al_2O_3$ Catalysts. Catalysis Today, 292, 58–66. https://doi.org/10.1016/J.CATTOD.2016.11.049

Hatanaka, S., Yamada, M., & Sadakane, O. (1997a). Hydrodesulfurization of Catalytic Cracked Gasoline. 1. Inhibiting Effects of Olefins on HDS of Alkyl(benzo)thiophenes Contained in Catalytic Cracked Gasoline. Industrial & Engineering Chemistry Research, 36(5), 1519–1523. https://doi.org/10.1021/IE9603777

Hatanaka, S., Yamada, M., & Sadakane, O. (1997b). Hydrodesulfurization of Catalytic Cracked Gasoline. 2. The Difference between HDS Active Site and Olefin Hydrogenation Active Site. Industrial & Engineering Chemistry Research, 36(12), 5110–5117. https://doi.org/10.1021/IE9703494

Ho, T. C. (1988). Hydrodenitrogenation Catalysis. Catalysis Reviews, 30(1), 117–160. https://doi.org/10.1080/01614948808078617

Ho, T. C. (2003). Inhibiting Effects in Hydrodesulfurization of 4,6-Diethyldibenzothiophene. Journal of Catalysis, 219(2), 442–451. https://doi.org/10.1016/S0021-9517(03)00215-X

Ho, T. C., & Nguyen, D. (2004). Poisoning Effect of Ethylcarbazole on Hydrodesulfurization of 4,6-Diethyldibenzothiophene. Journal of Catalysis, 222(2), 450–460. https://doi.org/10.1016/J.JCAT.2003.12.010

Ho, T. C., & Qiao, L. (2010). Competitive Adsorption of Nitrogen Species in HDS: Kinetic Characterization of Hydrogenation and Hydrogenolysis Sites. Journal of Catalysis, 269(2), 291–301. https://doi.org/10.1016/J.JCAT.2009.11.012

Ho, T. C., & Sobel, J. E. (1991). Kinetics of Dibenzothiophene Hydrodesulfurization. Journal of Catalysis, 128(2), 581–584. https://doi.org/10.1016/0021-9517(91)90316-V

Houalla, M., Nag, N. K., Sapre, A. V., Broderick, D. H., & Gates, B. C. (1978). Hydrodesulfurization of Dibenzothiophene Catalyzed by Sulfided $CoO\text{-}MoO_3\gamma\text{-}Al_2O_3$: The Reaction Network. AIChE Journal, 24(6), 1015–1021. https://doi.org/10.1002/aic.690240611

Hunter, E. P. L., & Lias, S. G. (1998). Evaluated Gas Phase Basicities and Proton Affinities of Molecules: An Update. Journal of Physical and Chemical Reference Data, 27(3), 413–656. https://doi.org/10.1063/1.556018

Ishihara, A., Lee, J., Dumeignil, F., Takashi, M., Qian, E. W., & Kabe, T. (2003). Elucidation of Retarding Effects of Sulfur and Nitrogen Compounds on Aromatic Compounds Hydrogenation. Energy & Fuels, 17(5), 1338–1345. https://doi.org/10.1021/EF020283B

Itatani, H., & Bailar, J. C. (1972). Selective Transition Metal Catalysts Complexed with Triphenyl Phosphine. Industrial & Engineering Chemistry Product Research and Development, 11(2), 146–155. https://doi.org/10.1021/i360042a005

Jae Lee, W., & Froment, G. F. (2008). Ethylbenzene Dehydrogenation into Styrene: Kinetic Modeling and Reactor Simulation. Industrial & Engineering Chemistry Research, 47(23), 9183–9194. https://doi.org/10.1021/ie071098u

Jian, M., & Prins, R. (1998). Mechanism of the Hydrodenitrogenation of Quinoline over NiMo(P)/Al_2O_3 Catalysts. Journal of Catalysis, 179(1), 18–27. https://doi.org/10.1006/JCAT.1998.2181

Jiménez, F., Kafarov, V., & Nuñez, M. (2007). Modeling of Industrial Reactor for Hydrotreating of Vacuum Gas Oils: Simultaneous Hydrodesulfurization, Hydrodenitrogenation and Hydrodearomatization Reactions. Chemical Engineering Journal, 134(1–3), 200–208. https://doi.org/10.1016/J.CEJ.2007.03.080

Kabe, T., Aoyama, Y., Wang, D., Ishihara, A., Qian, W., Hosoya, M., & Zhang, Q. (2001). Effects of H2S on Hydrodesulfurization of Dibenzothiophene and 4,6-Dimethyldibenzothiophene on Alumina-Supported NiMo and NiW Catalysts. Applied Catalysis A: General, 209(1–2), 237–247. https://doi.org/10.1016/S0926-860X(00)00770-5

Kabe, T., Qian, W., & Ishihara, A. (1997). Elucidation of Hydrodesulfurization Mechanism Using 35S radioisotope Pulse Tracer Methods. Catalysis Today, 39(1–2), 3–12. https://doi.org/10.1016/S0920-5861(97)00083-7

Kagami, N., Vogelaar, B. M., Langeveld, A. D. van, & Moulijn, J. A. (2005). Reaction Pathways on NiMo/Al_2O_3 Catalysts for Hydrodesulfurization of Diesel Fuel. Applied Catalysis A: General, 293, 11–23. https://doi.org/10.1016/J.APCATA.2005.05.042

Kass, R. E., & Raftery, A. E. (1995). Bayes Factors. Journal of the American Statistical Association, 90(430), 773–795. https://doi.org/10.1080/01621459.1995.10476572

Kaufmann, T. ., Kaldor, A., Stuntz, G. ., Kerby, M. ., & Ansell, L . (2000). Catalysis Science and Technology for Cleaner Transportation Fuels. Catalysis Today, 62(1), 77–90. https://doi.org/10.1016/S0920-5861(00)00410-7

Kibsgaard, J., Tuxen, A., Knudsen, K. G., Brorson, M., Topsøe, H., Lægsgaard, E., … Besenbacher, F. (2010). Comparative Atomic-Scale Analysis of Promotional Effects by Late 3d-Transition Metals in MoS_2 Hydrotreating Catalysts. Journal of Catalysis, 272(2), 195–203. https://doi.org/10.1016/J.JCAT.2010.03.018

Kilanowski, D. R., Teeuwen, H., de Beer, V. H. J., Gates, B. C., Schuit, G. C. A., & Kwart, H. (1978). Hydrodesulfurization of Thiophene, Benzothiophene, Dibenzothiophene, and Related Compounds Catalyzed by Sulfided CoO-MoO_3/γ-Al_2O_3: Low-Pressure Reactivity Studies. Journal of Catalysis, 55(2), 129–137. https://doi.org/10.1016/0021-9517(78)90199-9

Koltai, T., Macaud, M., Guevara, A., Schulz, E., Lemaire, M., Bacaud, R., & Vrinat, M. (2002). Comparative Inhibiting Effect of Polycondensed Aromatics and Nitrogen Compounds on the Hydrodesulfurization of Alkyldibenzothiophenes. Applied Catalysis A: General, 231(1–2), 253–261. https://doi.org/10.1016/S0926-860X(02)00063-7

Korre, S. C., Klein, M. T., & Quann, R. J. (1995). Polynuclear Aromatic Hydrocarbons Hydrogenation. 1. Experimental Reaction Pathways and Kinetics. Industrial & Engineering Chemistry Research, 34(1), 101–117. https://doi.org/10.1021/ie00040a008

Kwak, C., Lee, J. J., Bae, J. S., & Moon, S. H. (2001). Poisoning Effect of Nitrogen Compounds on the Performance of $CoMoS/Al_2O_3$ Catalyst in the Hydrodesulfurization of Dibenzothiophene, 4-Methyldibenzothiophene, and 4,6-Dimethyldibenzothiophene. Applied Catalysis B: Environmental, 35(1), 59–68. https://doi.org/10.1016/S0926-3373(01)00233-8

Lamic, A. F., Daudin, A., Brunet, S., Legens, C., Bouchy, C., & Devers, E. (2008). Effect of H_2S Partial Pressure on the Transformation of a Model FCC Gasoline Olefin over Unsupported Molybdenum Sulfide-Based Catalysts. Applied Catalysis A: General, 344(1–2), 198–204. https://doi.org/10.1016/J.APCATA.2008.04.023

Lamure-Meille, V., Schulz, E., Lemaire, M., & Vrinat, M. (1995). Effect of Experimental Parameters on the Relative Reactivity of Dibenzothiophene and 4-Methyldibenzothiophene. Applied Catalysis A: General, 131(1), 143–157. https://doi.org/10.1016/0926-860X(95)00118-2

Lapinas, A. T., Klein, M. T., Gates, B. C., Macris, A., & Lyons, J. E. (1991). Catalytic Hydrogenation and Hydrocracking of Fluorene: Reaction Pathways, Kinetics, and Mechanisms. Industrial & Engineering Chemistry Research, 30(1), 42–50. https://doi.org/10.1021/ie00049a007

Laredo S, G. C., De los Reyes H, J. A., Luis Cano D, J., & Jesús Castillo M, J. (2001). Inhibition Effects of Nitrogen Compounds on the Hydrodesulfurization of Dibenzothiophene. Applied Catalysis A: General, 207(1–2), 103–112. https://doi.org/10.1016/S0926-860X(00)00620-7

Laredo, G. C., Altamirano, E., & De los Reyes, J. A. (2003). Inhibition Effects of Nitrogen Compounds on the Hydrodesulfurization of Dibenzothiophene: Part 2. Applied Catalysis A: General, 243(2), 207–214. https://doi.org/10.1016/S0926-860X(02)00321-6

Laredo, G. C., Leyva, S., Alvarez, R., Mares, M. T., Castillo, J., & Cano, J. L. (2002). Nitrogen Compounds Characterization in Atmospheric Gas Oil and Light Cycle Oil from a Blend of Mexican Crudes. Fuel, 81(10), 1341–1350. https://doi.org/10.1016/S0016-2361(02)00047-9

Lauritsen, J. V., & Besenbacher, F. (2015). Atom-Resolved Scanning Tunneling Microscopy Investigations of Molecular Adsorption on MoS_2 and CoMoS Hydrodesulfurization Catalysts. Journal of Catalysis, 328, 49–58. https://doi.org/10.1016/J.JCAT.2014.12.034

Lauritsen, J. V., Nyberg, M., Nørskov, J. K., Clausen, B. S., Topsøe, H., Lægsgaard, E., & Besenbacher, F. (2004). Hydrodesulfurization Reaction Pathways on MoS_2 Nanoclusters Revealed by Scanning Tunneling Microscopy. Journal of Catalysis, 224(1), 94–106. https://doi.org/10.1016/J.JCAT.2004.02.009

LaVopa, V., & Satterfield, C. N. (1988a). Poisoning of Thiophene Hydrodesulfurization by Nitrogen Compounds. Journal of Catalysis, 110(2), 375–387. https://doi.org/10.1016/0021-9517(88)90328-4

LaVopa, V., & Satterfield, C. N. (1988b). Response of Dibenzothiophene Hydrodesulfurization to Presence of Nitrogen Compounds. Chemical Engineering Communications, 70(1), 171–176. https://doi.org/10.1080/00986448808940626

Lecrenay, E., Sakanishi, K., & Mochida, I. (1997). Catalytic Hydrodesulfurization of Gas Oil and Model Sulfur Compounds over Commercial and Laboratory-Made CoMo and NiMo Catalysts: Activity and Reaction Scheme. Catalysis Today, 39(1–2), 13–20. https://doi.org/10.1016/S0920-5861(97)00084-9

Li, D. (2013). Crucial Technologies Supporting Future Development of Petroleum Refining Industry. Chinese Journal of Catalysis, 34(1), 48–60. https://doi.org/10.1016/S1872-2067(11)60508-1

Li, W., Yu, S. Y., & Iglesia, E. (2002). Deuterium Isotopic Tracer Studies of Thiophene Desulfurization Pathways Using Propane or Dihydrogen as Co-reactants. Journal of Catalysis, 207(1), 31–36. https://doi.org/10.1006/JCAT.2001.3504

Liu, B., Chai, Y., Li, Y., Wang, A., Liu, Y., & Liu, C. (2014a). Effect of Sulfidation Atmosphere on the Performance of the CoMo/γ-Al_2O_3 Catalysts in Hydrodesulfurization of FCC Gasoline. Applied Catalysis A: General, 471, 70–79. https://doi.org/10.1016/J.APCATA.2013.11.017

Liu, B., Chai, Y., Li, Y., Wang, A., Liu, Y., & Liu, C. (2014b). Kinetic Investigation of the Effect of H_2S in the Hydrodesulfurization of FCC Gasoline. Fuel, 123, 43–51. https://doi.org/10.1016/J.FUEL.2014.01.055

Liu, Z., Zhang, Q., Zheng, Y., & Chen, J. (2008). Effects of Nitrogen and Aromatics on Hydrodesulfurization of Light Cycle Oil Predicted by a System Dynamics Model. Energy & Fuels, 22(2), 860–866. https://doi.org/10.1021/ef700622q

Logadóttir, Á., Moses, P. G., Hinnemann, B., Topsøe, N.-Y., Knudsen, K. G., Topsøe, H., & Nørskov, J. K. (2006). A Density Functional Study of Inhibition of the HDS Hydrogenation Pathway by Pyridine, Benzene, and H_2S on MoS_2-Based Catalysts. Catalysis Today, 111(1–2), 44–51. https://doi.org/10.1016/J.CATTOD.2005.10.018

M. A. Rodríguez, & J. Ancheyta. (2004). Modeling of Hydrodesulfurization (HDS), Hydrodenitrogenation (HDN), and the Hydrogenation of Aromatics (HDA) in a Vacuum Gas Oil Hydrotreater. Energy & Fuels. https://doi.org/10.1021/EF030172S

Marquardt, D. W. (1963). An Algorithm for Least-Squares Estimation of Nonlinear Parameters. Journal of the Society for Industrial and Applied Mathematics, 11(2), 431–441. https://doi.org/10.2307/2098941

Meille, V., Schulz, E., Lemaire, M., & Vrinat, M. (1997). Hydrodesulfurization of Alkyldibenzothiophenes over a NiMo/Al_2O_3Catalyst: Kinetics and Mechanism. Journal of Catalysis, 170(1), 29–36. https://doi.org/10.1006/JCAT.1997.1732

Mhadeshwar, A. B., Wang, H., & Vlachos, D. G. (2003). Thermodynamic Consistency in Microkinetic Development of Surface Reaction Mechanisms. The Journal of Physical Chemistry B, 107(46), 12721–12733. https://doi.org/10.1021/JP034954Y

Mijoin, J., Pérot, G., Bataille, F., Lemberton, J. L., Breysse, M., & Kasztelan, S. (2001). Mechanistic Considerations on the Involvement of Dihydrointermediates in the Hydrodesulfurization of Dibenzothiophene-Type Compounds over Molybdenum Sulfide Catalysts. Catalysis Letters, 71(3/4), 139–145. https://doi.org/10.1023/A:1009055205076

Miller, J. T., Reagan, W. J., Kaduk, J. A., Marshall, C. L., & Kropf, A. J. (2000). Selective Hydrodesulfurization of FCC Naphtha with Supported MoS2 Catalysts: The Role of Cobalt. Journal of Catalysis, 193(1), 123–131. https://doi.org/10.1006/JCAT.2000.2873

Monteiro-Gezork, A. C. A., Natividad, R., & Winterbottom, J. M. (2008). Hydrogenation of Naphthalene on NiMo- Ni- and Ru/Al_2O_3 Catalysts: Langmuir–Hinshelwood Kinetic Modelling. Catalysis Today, 130(2–4), 471–485. https://doi.org/10.1016/J.CATTOD.2007.10.102

Moreau, C., & Geneste, P. (1990). Factors Affecting the Reactivity of Organic Model Compounds in Hydrotreating Reactions. In Theoretical Aspects of Heterogeneous Catalysis (pp. 256–310). Dordrecht: Springer Netherlands. https://doi.org/10.1007/978-94-010-9882-3_7

Moses, P. G., Grabow, L. C., Fernandez, E. M., Hinnemann, B., Topsøe, H., Knudsen, K. G., & Nørskov, J. K. (2014). Trends in Hydrodesulfurization Catalysis Based on Realistic Surface Models. Catalysis Letters, 144(8), 1425–1432. https://doi.org/10.1007/s10562-014-1279-4

Moses, P. G., Hinnemann, B., Topsøe, H., & Nørskov, J. K. (2007). The Hydrogenation and Direct Desulfurization Reaction Pathway in Thiophene Hydrodesulfurization over MoS_2

Catalysts at Realistic Conditions: A Density Functional Study. Journal of Catalysis, 248(2), 188–203. https://doi.org/10.1016/J.JCAT.2007.02.028

Myung, J. I., Tang, Y., & Pitt, M. A. (2009). Chapter 11 Evaluation and Comparison of Computational Models. Methods in Enzymology, 454, 287–304. https://doi.org/10.1016/S0076-6879(08)03811-1

Nagai, M. (1985). High Activity and Selectivity of a "Poisoned" NiMo/Al_2O_3 Catalyst for a Desulfurization Reaction. Industrial & Engineering Chemistry Product Research and Development, 24(3), 489–491. https://doi.org/10.1021/i300019a031

Nagai, M., Sato, T., & Aiba, A. (1986). Poisoning Effect of Nitrogen Compounds on Dibenzothiophene Hydrodesulfurization on Sulfided NiMo/Al_2O_3 Catalysts and Relation to Gas-Phase Basicity. Journal of Catalysis, 97(1), 52–58. https://doi.org/10.1016/0021-9517(86)90036-9

Nguyen, M.-T., Pirngruber, G. D., Albrieux, F., Chainet, F., Tayakout-Fayolle, M., & Geantet, C. (2019). How Does an Acidic Support Affect the Hydrotreatment of a Gas Oil with High Nitrogen Content? Energy & Fuels, 33(2), 1467–1472. https://doi.org/10.1021/acs.energyfuels.8b04116

Nguyen, M.-T., Pirngruber, G. D., Chainet, F., Tayakout-Fayolle, M., & Geantet, C. (2017). Indole Hydrodenitrogenation over Alumina and Silica–Alumina-Supported Sulfide Catalysts—Comparison with Quinoline. Industrial & Engineering Chemistry Research, 56(39), 11088–11099. https://doi.org/10.1021/acs.iecr.7b02993

Nguyen, M.-T., Tayakout-Fayolle, M., Pirngruber, G. D., Chainet, F., & Geantet, C. (2015). Kinetic Modeling of Quinoline Hydrodenitrogenation over a NiMo(P)/Al_2O_3 Catalyst in a Batch Reactor. Industrial & Engineering Chemistry Research, 54(38), 9278–9288. https://doi.org/10.1021/acs.iecr.5b02175

Parkash, S., & Parkash, S. (2003). Distillate Hydrotreating. Refining Processes Handbook, 29–61. https://doi.org/10.1016/B978-075067721-9/50002-5

Pérez-Martínez, D. J., Eloy, P., Gaigneaux, E. M., Giraldo, S. A., & Centeno, A. (2010). Study of the Selectivity in FCC Naphtha Hydrotreating by Modifying the Acid–Base Balance of CoMo/γ-Al_2O_3 catalysts. Applied Catalysis A: General, 390(1–2), 59–70. https://doi.org/10.1016/J.APCATA.2010.09.028

Pérez-Martínez, D. J., Gaigneaux, E. M., & Giraldo, S. A. (2012). Improving the Selectivity to HDS in the HDT of Synthetic FCC Naphtha Using Sodium Doped Amorphous Aluminosilicates as Support of CoMo Catalysts. Applied Catalysis A: General, 421–422, 48–57. https://doi.org/10.1016/J.APCATA.2012.01.036

Permyakov, E. A., Solkan, V. N., & Kogan, V. M. (2015). Role of SH Groups and Chemisorbed Hydrogen in the Formation of Sulfur Vacancies on an Edge of a Molybdenum Disulfide Crystallite. Kinetics and Catalysis, 56(2), 147–157. https://doi.org/10.1134/S0023158415020081

Pinzón, M. H., Centeno, A., & Giraldo, S. A. (2006). Role of Pt in High Performance Pt-Mo Catalysts for Hydrotreatment Reactions. Applied Catalysis A: General, 302(1), 118–126. https://doi.org/10.1016/J.APCATA.2005.12.024

Prado, G. H. C., Rao, Y., & de Klerk, A. (2017). Nitrogen Removal from Oil: A Review. Energy & Fuels, 31(1), 14–36. https://doi.org/10.1021/acs.energyfuels.6b02779

Prins, R. (2001). Catalytic Hydrodenitrogenation. Advances in Catalysis, 46, 399–464. https://doi.org/10.1016/S0360-0564(02)46025-7

Rabarihoela-Rakotovao, V., Brunet, S., Berhault, G., Perot, G., & Diehl, F. (2004). Effect of Acridine and of Octahydroacridine on the HDS of 4,6-Dimethyldibenzothiophene Catalyzed by Sulfided NiMoP/Al_2O_3. Applied Catalysis A: General, 267(1–2), 17–25. https://doi.org/10.1016/J.APCATA.2004.02.017

Rabarihoela-Rakotovao, V., Diehl, F., & Brunet, S. (2009). Deep HDS of Diesel Fuel: Inhibiting Effect of Nitrogen Compounds on the Transformation of the Refractory 4,6-Dimethyldibenzothiophene Over a NiMoP/Al_2O_3 Catalyst. Catalysis Letters, 129(1–2), 50–60. https://doi.org/10.1007/s10562-008-9777-x

Raghuveer, C. S., Thybaut, J. W., & Marin, G. B. (2016). Pyridine Hydrodenitrogenation Kinetics over a Sulphided NiMo/γ-Al_2O_3 Catalyst. Fuel, 171, 253–262. https://doi.org/10.1016/J.FUEL.2015.12.042

Rana, M. S., Al-Barood, A., Brouresli, R., Al-Hendi, A. W., & Mustafa, N. (2018). Effect of Organic Nitrogen Compounds on Deep Hydrodesulfurization of Middle Distillate. Fuel Processing Technology, 177, 170–178. https://doi.org/10.1016/J.FUPROC.2018.04.014

Rana, M. S., Navarro, R., & Leglise, J. (2004). Competitive Effects of Nitrogen and Sulfur Content on Activity of Hydrotreating $CoMo/Al_2O_3$ Catalysts: A Batch Reactor Study. Catalysis Today, 98(1–2), 67–74. https://doi.org/10.1016/J.CATTOD.2004.07.020

Rangarajan, S., & Mavrikakis, M. (2015). Adsorption of Nitrogen- and Sulfur-Containing Compounds on NiMoS for Hydrotreating Reactions: A DFT and vdW-Corrected Study. AIChE Journal, 61(12), 4036–4050. https://doi.org/10.1002/aic.15025

Rangarajan, S., & Mavrikakis, M. (2016). DFT Insights into the Competitive Adsorption of Sulfur- and Nitrogen-Containing Compounds and Hydrocarbons on Co-Promoted Molybdenum Sulfide Catalysts. ACS Catalysis, 6(5), 2904–2917. https://doi.org/10.1021/acscatal.6b00058

Rangarajan, S., & Mavrikakis, M. (2017). On the Preferred Active Sites of Promoted MoS_2 for Hydrodesulfurization with Minimal Organonitrogen Inhibition. ACS Catalysis, 7(1), 501–509. https://doi.org/10.1021/acscatal.6b02735

Rautanen, P. A., Lylykangas, M. S., Aittamaa, J. R., & Krause, A. O. I. (2002). Liquid-Phase Hydrogenation of Naphthalene and Tetralin on Ni/Al_2O_3: Kinetic Modeling. Industrial & Engineering Chemistry Research, 41(24), 5966–5975. https://doi.org/10.1021/IE020395Q

Rayo, P., Ramírez, J., Torres-Mancera, P., Marroquín, G., & Maity, S. K. (2012). Hydrodesulfurization and Hydrocracking of Maya Crude with P-Modified $NiMo/Al_2O_3$ Catalysts. Fuel, 100, 34–42. https://doi.org/10.1016/J.FUEL.2011.12.004

Research Institute of Economy Trade and Industry (RIETI). (n.d.). Japan's Environmental Policy. Retrieved December 16, 2018, from https://www.rieti.go.jp/en/special/policy-update/059.html

Romero, C. M. C., Thybaut, J. W., & Marin, G. B. (2008). Naphthalene Hydrogenation over a $NiMo/\gamma\text{-}Al_2O_3$ Catalyst: Experimental Study and Kinetic Modelling. Catalysis Today, 130(1), 231–242. https://doi.org/10.1016/J.CATTOD.2007.06.074

Rosenbrock, H. H. (1960). An Automatic Method for Finding the Greatest or Least Value of a Function. The Computer Journal, 3(3), 175–184. https://doi.org/10.1093/comjnl/3.3.175

Sahu, R., Song, B. J., Im, J. S., Jeon, Y.-P., & Lee, C. W. (2015). A Review of Recent Advances in Catalytic Hydrocracking of Heavy Residues. Journal of Industrial and Engineering Chemistry, 27, 12–24. https://doi.org/10.1016/J.JIEC.2015.01.011

Salazar, N., Schmidt, S. B., & Lauritsen, J. V. (2019). Adsorption of Nitrogenous Inhibitor Molecules on MoS_2 and CoMoS Hydrodesulfurization Catalysts Particles Investigated by Scanning Tunneling Microscopy. Journal of Catalysis, 370, 232–240. https://doi.org/10.1016/J.JCAT.2018.12.014

Santacesaria, E. (1997). Kinetics and Transport Phenomena. Catalysis Today, 34(3–4), 393–400. https://doi.org/10.1016/S0920-5861(96)00061-2

Sapre, A. V., & Gates, B. C. (1981). Hydrogenation of Aromatic Hydrocarbons Catalyzed by Sulfided $CoO\text{-}MoO_3/Al_2O_3$. Reactivities and Reaction Networks. Industrial & Engineering Chemistry Process Design and Development, 20(1), 68–73. https://doi.org/10.1021/i200012a010

Šarić, M., Rossmeisl, J., & Moses, P. G. (2017). Modeling the Active Sites of Co-Promoted MoS_2 Particles by DFT. Physical Chemistry Chemical Physics, 19(3), 2017–2024. https://doi.org/10.1039/C6CP06881B

Šarić, M., Rossmeisl, J., & Moses, P. G. (2018). Modeling the Adsorption of Sulfur Containing Molecules and their Hydrodesulfurization Intermediates on the Co-Promoted MoS_2 Catalyst by DFT. Journal of Catalysis, 358, 131–140. https://doi.org/10.1016/J.JCAT.2017.12.001

Schachtl, E., Kondratieva, E., Gutiérrez, O. Y., & Lercher, J. A. (2015). Pathways for H_2 Activation on (Ni)-MoS_2 Catalysts. The Journal of Physical Chemistry Letters, 6(15), 2929–2932. https://doi.org/10.1021/acs.jpclett.5b01217

Schachtl, E., Zhong, L., Kondratieva, E., Hein, J., Gutiérrez, O. Y., Jentys, A., & Lercher, J. A. (2015). Understanding Ni Promotion of $MoS_2/\gamma\text{-}Al_2O_3$ and its Implications for the Hydrogenation of Phenanthrene. ChemCatChem, 7(24), 4118–4130. https://doi.org/10.1002/cctc.201500706

Schulz, H., Böhringer, W., Waller, P., & Ousmanov, F. (1999). Gas Oil Deep Hydrodesulfurization: Refractory Compounds and Retarded Kinetics. Catalysis Today, 49(1–3), 87–97. https://doi.org/10.1016/S0920-5861(98)00412-X

Schwarz, G. (1978). Estimating the Dimension of a Model. The Annals of Statistics, 6(2), 461–464. https://doi.org/10.1214/aos/1176344136

Shafi, R., & Hutchings, G. J. (2000). Hydrodesulfurization of Hindered Dibenzothiophenes: an Overview. Catalysis Today, 59(3–4), 423–442. https://doi.org/10.1016/S0920-5861(00)00308-4

Sharifvaghefi, S., Yang, B., & Zheng, Y. (2018). New Insights on the Role of H_2S and Sulfur Vacancies on Dibenzothiophene Hydrodesulfurization over MoS_2 Edges. Applied Catalysis A: General, 566, 164–173. https://doi.org/10.1016/J.APCATA.2018.05.033

Singhal, G. H., Espino, R. L., Sobel, J. E., & Huff, G. A. (1981). Hydrodesulfurization of Sulfur Heterocyclic Compounds: Kinetics of Dibenzothiophene. Journal of Catalysis, 67(2), 457–468. https://doi.org/10.1016/0021-9517(81)90305-5

Song, C. (2003). An Overview of New Approaches to Deep Desulfurization for Ultra-Clean Gasoline, Diesel Fuel and Jet Fuel. Catalysis Today, 86(1–4), 211–263. https://doi.org/10.1016/S0920-5861(03)00412-7

Song, C., & Ma, X. (2003). New Design Approaches to Ultra-Clean Diesel Fuels by Deep Desulfurization and Deep Dearomatization. Applied Catalysis B: Environmental, 41(1–2), 207–238. https://doi.org/10.1016/S0926-3373(02)00212-6

Song, T., Zhang, Z., Chen, J., Ring, Z., Yang, H., & Zheng, Y. (2006). Effect of Aromatics on Deep Hydrodesulfurization of Dibenzothiophene and 4,6-Dimethyldibenzothiophene over $NiMo/Al_2O_3$ Catalyst. Energy & Fuels, 20(6), 2344–2349. https://doi.org/10.1021/EF060199M

Speight, J. G., & Ancheyta Juárez, J. (2007). Hydroprocessing of Heavy Oils and Residua. CRC Press.

Speight, J. G., & Speight, J. G. (2013). Hydrotreating and Desulfurization. Heavy and Extra-Heavy Oil Upgrading Technologies, 69–94. https://doi.org/10.1016/B978-0-12-404570-5.00004-1

Speight, J. G., & Speight, J. G. (2019). Upgrading by Hydrotreating. Heavy Oil Recovery and Upgrading, 423–465. https://doi.org/10.1016/B978-0-12-813025-4.00010-6

Stanislaus, A., & Cooper, B. H. (1994). Aromatic Hydrogenation Catalysis: A Review. Catalysis Reviews, 36(1), 75–123. https://doi.org/10.1080/01614949408013921

Stanislaus, A., Marafi, A., & Rana, M. S. (2010). Recent Advances in the Science and Technology of Ultra Low Sulfur Diesel (ULSD) Production. Catalysis Today, 153(1–2), 1–68. https://doi.org/10.1016/J.CATTOD.2010.05.011

Sumbogo Murti, S. D., Yang, H., Choi, K.-H., Korai, Y., & Mochida, I. (2003). Influences of Nitrogen Species on the Hydrodesulfurization Reactivity of a Gas Oil over Sulfide Catalysts of Variable Activity. Applied Catalysis A: General, 252(2), 331–346. https://doi.org/10.1016/S0926-860X(03)00468-X

Sun, M., Nelson, A. E., & Adjaye, J. (2004). On the Incorporation of Nickel and Cobalt into MoS_2-edge Structures. Journal of Catalysis, 226(1), 32–40. https://doi.org/10.1016/J.JCAT.2004.05.005

Tao, X., Zhou, Y., Wei, Q., Ding, S., Zhou, W., Liu, T., & Li, X. (2017). Inhibiting Effects of Nitrogen Compounds on Deep Hydrodesulfurization of Straight-Run Gas Oil over a NiW/Al_2O_3 Catalyst. Fuel, 188, 401–407. https://doi.org/10.1016/J.FUEL.2016.09.055

Temel, B., Tuxen, A. K., Kibsgaard, J., Topsøe, N.-Y., Hinnemann, B., Knudsen, K. G., Besenbacher, F. (2010). Atomic-scale Insight into the Origin of Pyridine Inhibition of MoS_2-Based Hydrotreating Catalysts. Journal of Catalysis, 271(2), 280–289. https://doi.org/10.1016/J.JCAT.2010.02.007

Toba, M., Miki, Y., Matsui, T., Harada, M., & Yoshimura, Y. (2007). Reactivity of Olefins in the Hydrodesulfurization of FCC Gasoline over CoMo Sulfide Catalyst. Applied Catalysis B: Environmental, 70(1–4), 542–547. https://doi.org/10.1016/J.APCATB.2005.12.026

Transport Policy. (n.d.). EU: Fuels: Diesel and Gasoline. Retrieved December 16, 2018, from https://www.transportpolicy.net/standard/eu-fuels-diesel-and-gasoline/

Tu, C., Li, M., Li, H., Chu, Y., Liu, F., Nie, H., & Li, D. (2016). Effects of Sulfur Compounds on the Hydrogenation and Isomerization of 1-Hexene over a Sulfided CoMo Catalyst for Hydrodesulfurization. RSC Advances, 6(39), 33177–33183. https://doi.org/10.1039/C5RA27583K

Tuxen, A. K., Füchtbauer, H. G., Temel, B., Hinnemann, B., Topsøe, H., Knudsen, K. G., … Lauritsen, J. V. (2012). Atomic-Scale Insight into Adsorption of Sterically Hindered Dibenzothiophenes on MoS_2 and Co–Mo–S Hydrotreating Catalysts. Journal of Catalysis, 295, 146–154. https://doi.org/10.1016/J.JCAT.2012.08.004

United States Environmental Protection Agency (EPA). (n.d.). Diesel Fuel Standards and Rulemakings. Retrieved December 4, 2018, from https://www.epa.gov/diesel-fuel-standards/diesel-fuel-standards-and-rulemakings#onroad-diesel

United States Environmental Protection Agency (EPA). (n.d.-b). Regulations for Emissions from Vehicles and Engines. Retrieved December 4, 2018, from https://www.epa.gov/regulations-emissions-vehicles-and-engines/final-rule-control-air-pollution-motor-vehicles-tier-3

United States Environmental Protection Agency (EPA). (n.d.-c). What are Hazardous Air Pollutants? Retrieved December 4, 2018, from https://www.epa.gov/haps/what-are-hazardous-air-pollutants

Valencia, D., Klimova, T., & García-Cruz, I. (2012). Aromaticity of Five- and Six-Membered Heterocycles Present in Crude Oils – An Electronic Description for Hydrotreatment Process. Fuel, 100, 177–185. https://doi.org/10.1016/J.FUEL.2012.05.011

Valencia, D., Peña, L., & García-Cruz, I. (2012). Reaction Mechanism of Hydrogenation and Direct Desulfurization Routes of Dibenzothiophene-Like Compounds: A Density Functional Theory Study. International Journal of Quantum Chemistry, 112(22), 3599–3605. https://doi.org/10.1002/qua.24242

van Looij, F., van der Laan, P., Stork, W. H. ., DiCamillo, D. ., & Swain, J. (1998). Key Parameters in Deep Hydrodesulfurization of Diesel Fuel. Applied Catalysis A: General, 170(1), 1–12. https://doi.org/10.1016/S0926-860X(98)00028-3

Vannice, M. A., Hyun, S. H., Kalpakci, B., & Liauh, W. C. (1979). Entropies of Adsorption in Heterogeneous Catalytic Reactions. Journal of Catalysis, 56(3), 358–362. https://doi.org/10.1016/0021-9517(79)90128-3

Vanrysselberghe, V., & Froment, G. F. (1996). Hydrodesulfurization of Dibenzothiophene on a $CoMo/Al_2O_3$ Catalyst: Reaction Network and Kinetics. Industrial & Engineering Chemistry Research, 35(10), 3311–3318. https://doi.org/10.1021/IE960099B

Vanrysselberghe, V., & Froment, G. F. (1996). Hydrodesulfurization of Dibenzothiophene on a $CoMo/Al_2O_3$ Catalyst: Reaction Network and Kinetics. Industrial & Engineering Chemistry Research, 35(10), 3311–3318. https://doi.org/10.1021/IE960099B

Viswanadham, N., Negi, B. S., Garg, M. O., Sundaram, M., Sairam, B., & Agarwal, A. K. (2007). Reformulation of FCC Gasoline. Fuel, 86(9), 1290–1297. https://doi.org/10.1016/J.FUEL.2006.09.016

Vrinat, M. L. (1983). The Kinetics of the Hydrodesulfurization Process - a Review. Applied Catalysis, 6(2), 137–158. https://doi.org/10.1016/0166-9834(83)80260-7

Wang, H., & Prins, R. (2009). Hydrodesulfurization of Dibenzothiophene, 4,6-Dimethyldibenzothiophene, and their Hydrogenated Intermediates over $Ni–MoS_2/\gamma\text{-}Al_2O_3$. Journal of Catalysis, 264(1), 31–43. https://doi.org/10.1016/J.JCAT.2009.03.011

Wang, Y., Sun, Z., Wang, A., Ruan, L., Lu, M., Ren, J., … Yao, P. (2004). Kinetics of Hydrodesulfurization of Dibenzothiophene Catalyzed by Sulfided Co−Mo/MCM-41. Industrial & Engineering Chemistry Research, 43(10), 2324–2329. https://doi.org/10.1021/IE030856N

Wei, Q., Wen, S., Tao, X., Zhang, T., Zhou, Y., Chung, K., & Xu, C. (2015). Hydrodenitrogenation of Basic and Non-Basic Nitrogen-Containing Compounds in Coker Gas Oil. Fuel Processing Technology, 129, 76–84. https://doi.org/10.1016/J.FUPROC.2014.08.001

Weitkamp, A. W. (1968). Stereochemistry and Mechanism of Hydrogenation of Naphthalenes on Transition Metal Catalysts and Conformational Analysis of the Products. Advances in Catalysis, 18, 1–110. https://doi.org/10.1016/S0360-0564(08)60428-9

Wen, Y., Wang, G., Xu, C., & Gao, J. (2012). Study on in Situ Sulfur Removal from Gasoline in Fluid Catalytic Cracking Process. Energy & Fuels, 26(6), 3201–3211. https://doi.org/10.1021/ef300499j

Xiang, C., Chai, Y., Liu, Y., & Liu, C. (2008). Mutual Influences of Hydrodesulfurization of Dibenzothiophene and Hydrodenitrogenation of Indole over $NiMoS/Al_2O_3$ Catalyst. Journal of Fuel Chemistry and Technology, 36(6), 684–690. https://doi.org/10.1016/S1872-5813(09)60004-9

Yamada, M., Saito, A., Wakatsuki, T., & Obara, T. (1987). Effect of H_2S on Hydrogenation Activity of Sulfided $Co/Mo/Al_2O_3$. Chemistry Letters, 16(4), 571–572. https://doi.org/10.1246/cl.1987.571

Yang, H., Chen, J., Fairbridge, C., Briker, Y., Zhu, Y. J., & Ring, Z. (2004). Inhibition of Nitrogen Compounds on the Hydrodesulfurization of Substituted Dibenzothiophenes in Light Cycle Oil. Fuel Processing Technology, 85(12), 1415–1429. https://doi.org/10.1016/J.FUPROC.2003.09.008

Yang, H., Fairbridge, C., & Ring, Z. (2003). Adsorption of Dibenzothiophene Derivatives over a MoS_2 NanoclusterA Density Functional Theory Study of Structure−Reactivity Relations. Energy & Fuels, 17(2), 387398. https://doi.org/10.1021/EF020171K

Yang, H., Wang, Y., Jiang, H., Weng, H., Liu, F., & Li, M. (2014). Kinetics of Phenanthrene Hydrogenation System over $CoMo/Al_2O_3$ Catalyst. Industrial & Engineering Chemistry Research, 53(31), 12264–12269. https://doi.org/10.1021/ie501397n

Yin, C., Zhu, G., & Xia, D. (2002). A Study of the Distribution of Sulfur Compounds in Gasoline Fraction Produced in China: Part 2. The Distribution of Sulfur Compounds in Full-Range FCC and RFCC Naphthas. Fuel Processing Technology, 79(2), 135–140. https://doi.org/10.1016/S0378-3820(02)00108-X

Yu, S. Y., Li, W., & Iglesia, E. (1999). Desulfurization of Thiophene via Hydrogen Transfer from Alkanes on Cation-Modified H-ZSM5. Journal of Catalysis, 187(2), 257–261. https://doi.org/10.1006/JCAT.1999.2668

Zepeda, T. A., Pawelec, B., Obeso-Estrella, R., Díaz de León, J. N., Fuentes, S., Alonso-Núñez, G., & Fierro, J. L. G. (2016). Competitive HDS and HDN Reactions over NiMoS/HMS-Al Catalysts: Diminishing of the Inhibition of HDS Reaction by Support Modification with P. Applied Catalysis B: Environmental, 180, 569–579. https://doi.org/10.1016/J.APCATB.2015.07.013

Zeuthen, P., Knudsen, K. G., & Whitehurst, D. D. (2001). Organic Nitrogen Compounds in Gas Oil Blends, their Hydrotreated Products and the Importance to Hydrotreatment. Catalysis Today, 65(2–4), 307–314. https://doi.org/10.1016/S0920-5861(00)00566-6

Zhang, C., Liu, X., Liu, T., Jiang, Z., & Li, C. (2019). Optimizing Both the $CoMo/Al_2O_3$ Catalyst and the Technology for Selectivity Enhancement in the Hydrodesulfurization of FCC

Gasoline. Applied Catalysis A: General, 575, 187–197. https://doi.org/10.1016/J.APCATA.2019.02.025

Zhao, H. Y., Oyama, S. T., & Naeemi, E. D. (2010). Hydrogen Storage Using Heterocyclic Compounds: The Hydrogenation of 2-Methylthiophene. Catalysis Today, 149(1–2), 172–184. https://doi.org/10.1016/J.CATTOD.2009.02.039

Appendices

Appendix A. Supplementary Information Chapter 1

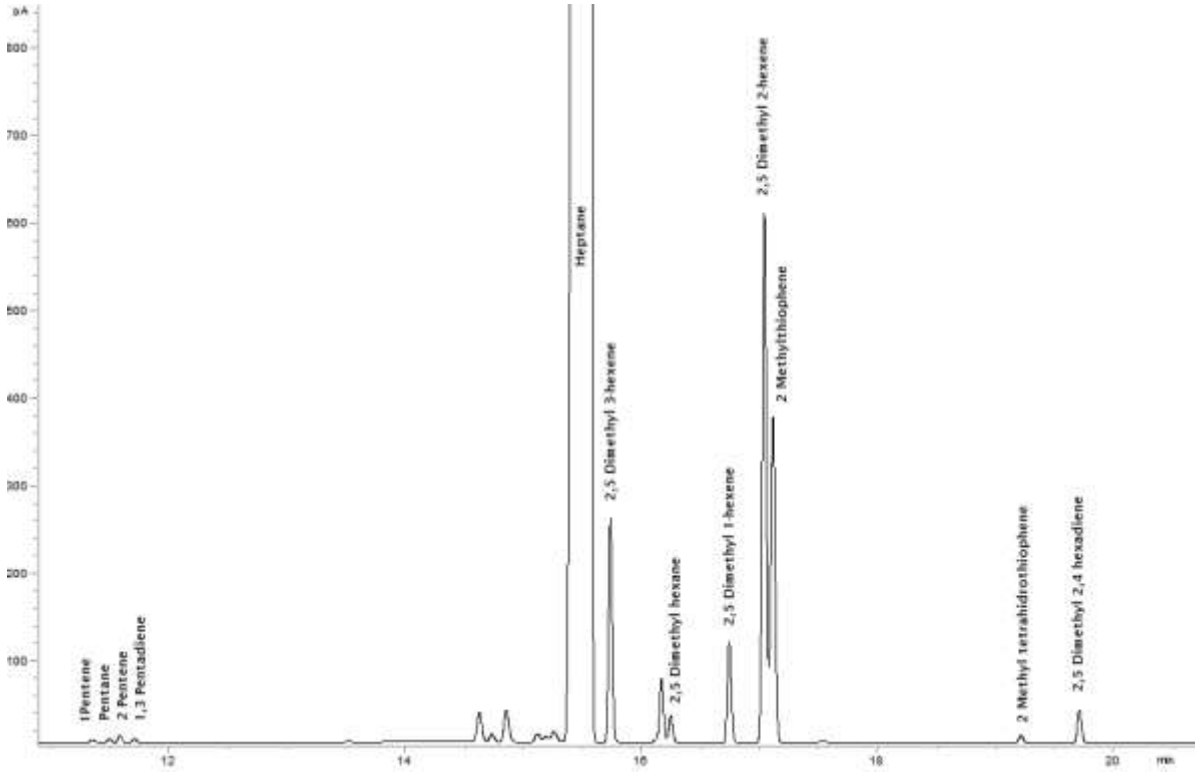

Figure S1.1. GC chromatogram of reaction products from the catalytic test performed for Feed 5 in steady state conditions (T=250°C, P= 50 bar, liquid-flow rate of 20 mLh^{-1} and H_2/liquid feed ratio = 500).

a)

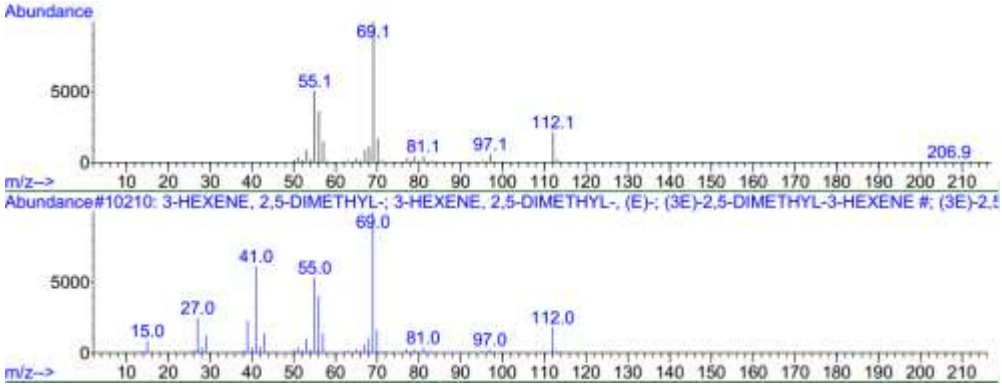

b)

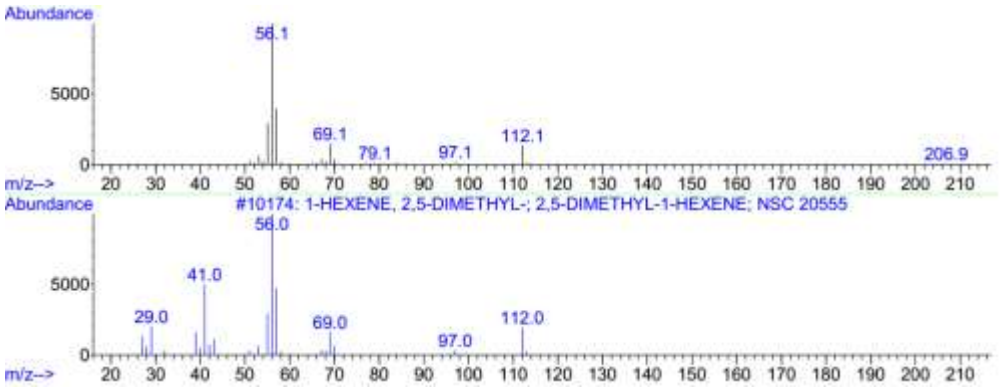

c)

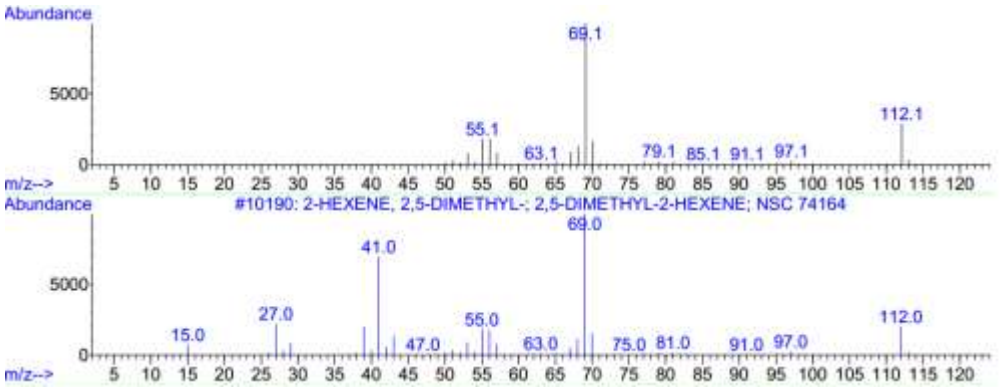

Figure S1.2. Mass spectra of hydrogenation products for of 2,5-dimethyl-2,4-hexadiene (2,4C_6diene) as obtained for a catalytic test performed for Feed 5: a) 2,5-dimethyl-3-hexene (3Hexene), b) 2,5-dimethyl-1-hexene (1Hexene) and c) 2,5-dimethyl-2-hexene (2Hexene).

Appendix B. Supplementary information Chapter 2

Supporting information

Section S2.1. Reaction systems used on catalytic test.

Figure S1 presents a picture of two experimental setups. Catatest (I) consists of a storage tank of 2 L capacity with a flow measurement device, which contains a pump of positive displacement (Eldex AA-100-S, flow range (mL min^{-1}): 0.2-10), responsible for transporting the flow to the reactor at operating pressure. The reaction module accounts for an oven with four heating zones controlled by four Watlow devices (982 series). The temperature in the catalytic bed is monitored by a thermocouple contained in its internal area through a thermowell. The gas flow (H_2, N_2), is added with flow mass controllers (Brooks (SLA5850 series)). Both liquid and gaseous reactants feed to a reactor made of stainless steel 316 with an internal diameter of 1/2 inch. The reaction products go to a separation stage, which consists of a flash separator and an exchanger that is responsible for condensing the vapors. The sampling is carried out using a loop with on-off valves that allows taking samples at defined time intervals to be analyzed through the gas chromatograph.

The system of Catatest (II) is similar to the Catatest (I), the differences are: the pump is a Cole-Parmer 74930-10, flow range (mL min^{-1}): 0.001-12; the pressure of the system is controlled by electronic pressure controller (Brooks SLA5820), and the oven has 2 heating zones.

a) **b)**

Figure S2.1. Reaction systems a) Catatest (I) and b) Catatest (II).

Section S2.2. Error in the carbon balance calculated for the reactions.

Table S2.1. Error in the carbon balance calculated for the reaction of the hydrodesulfurization of dibenzothiophene.

W/F_{DBT}	T [°C]	Carbon loss (%)
182	300	2.1
122	300	1.0
91	300	1.6
74	300	0.9
46	300	0.5
33	300	0.4
122	280	1.3
74	280	0.4
46	280	1.1

W/F_{DBT}	T [°C]	Carbon loss (%)
33	280	1.0
122	260	0.5
74	260	0.6
46	260	2.3
33	260	1.1

Table S2.2. Error in the carbon balance calculated for the simultaneous reaction of the hydrodesulfurization of dibenzothiophene and hydrogenation of naphthalene.

W/F_{DBT}	W/F_{NP}	T [°C]	Carbon loss (%)
122	56	300	1.3
122	56	280	2.8
122	56	260	2.5
122	28	300	2.3
122	28	280	1.3
122	28	260	2.4

Table S2.3. Error in the carbon balance calculated for the simultaneous reaction of the hydrodesulfurization of dibenzothiophene and hydrogenation of fluorene.

W/F_{DBT}	W/F_{FL}	T [°C]	Carbon loss (%)
122	73	300	3.6
122	73	280	1.7
122	73	260	1.8
122	37	300	2.2
122	37	280	0.7
122	37	260	3.2

Table S2.4. Error in the carbon balance calculated for the simultaneous reaction of the hydrodesulfurization of dibenzothiophene and hydrogenation of phenanthrene.

W/F_{DBT}	W/F_{PHE}	T [°C]	Carbon loss (%)
122	73	300	4.8
122	73	280	1.7
122	73	260	4.3
122	37	300	4.2
122	37	280	3.2
122	37	260	4.7

Section S2.3. Surface coverage of σ and π sites on the reaction of hydrodesulfurization of dibenzothiophene in the absence and presence of aromatic compounds.

a) **b)**

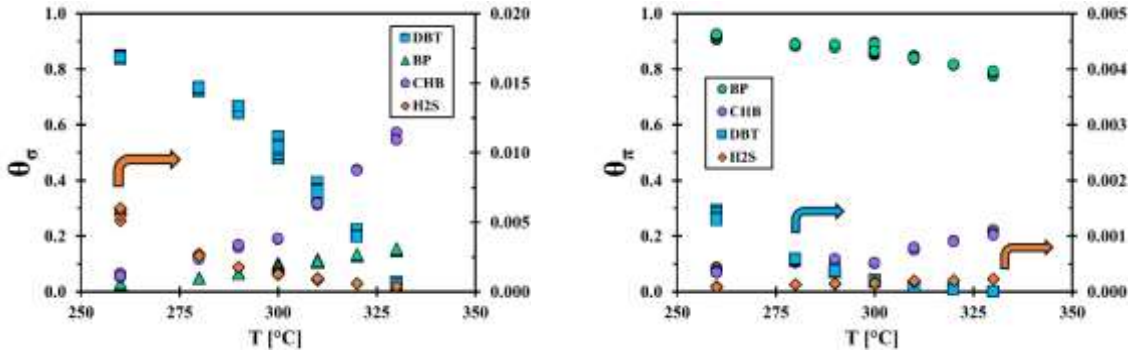

Figure S2.2. Surface coverage of a) σ sites and b) π sites on the reaction of HDS of DBT at 122 $kg_{cat}kmol_{DBT}^{-1}h$.

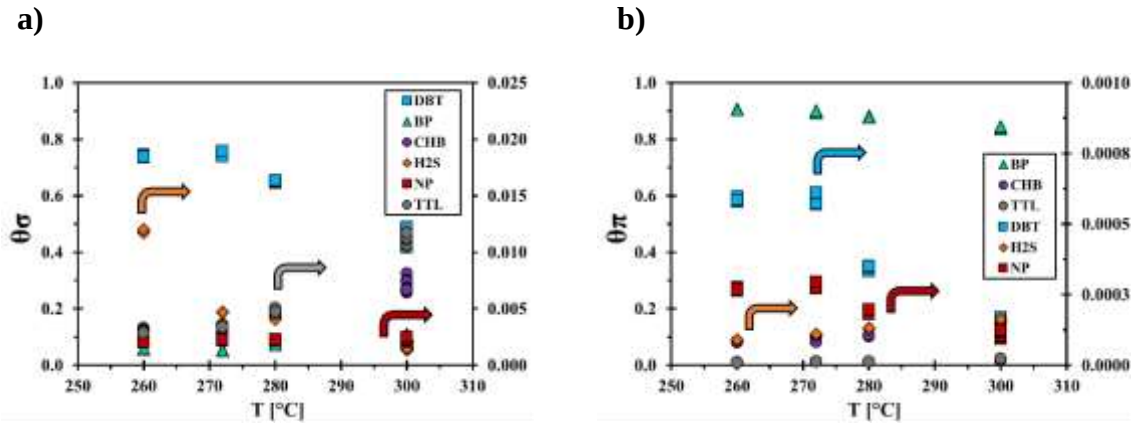

Figure S2.3. Surface coverage of a) σ sites and b) π sites on the reaction of HDS of DBT (122 $kg_{cat}kmol_{DBT}^{-1}h$) and hydrogenation of naphthalene (56 $kg_{cat}kmol_{NP}^{-1}h$).

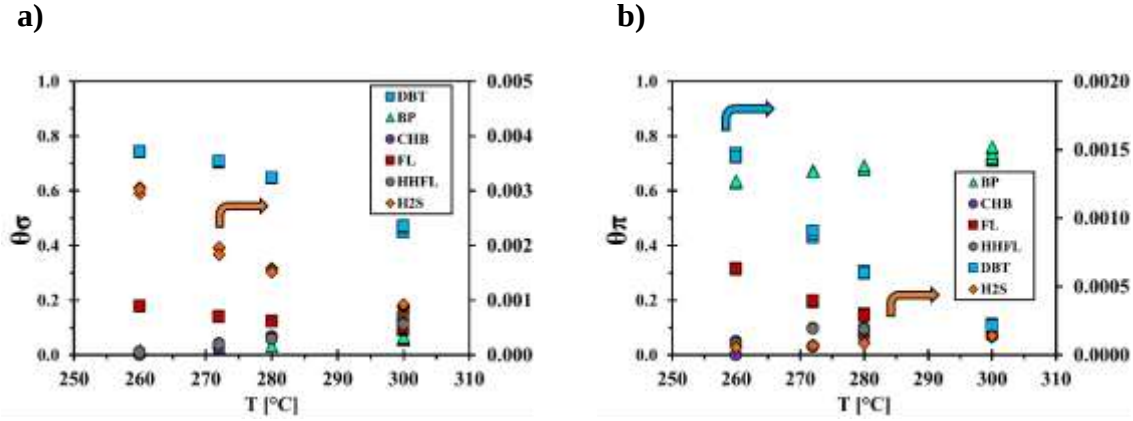

Figure S2.4. Surface coverage of a) σ sites and b) π sites on the reaction of HDS of DBT (122 $kg_{cat}kmol_{DBT}^{-1}h$) and hydrogenation of fluorene (73 $kg_{cat}kmol_{FL}^{-1}h$).

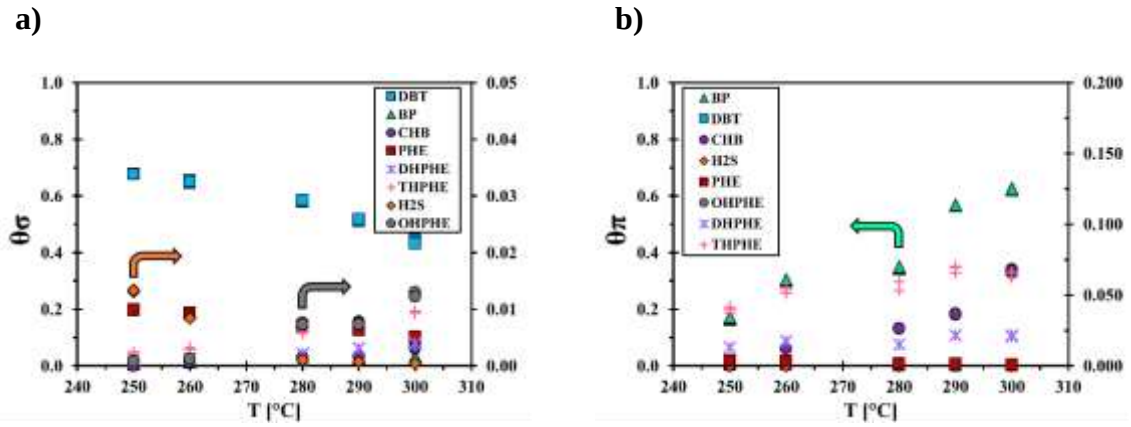

Figure S2.5. Surface coverage of a) σ sites and b) π sites on the reaction of HDS of DBT (122 $kg_{cat}kmol_{DBT}^{-1}h$) and hydrogenation of phenanthrene (59 $kg_{cat}kmol_{FL}^{-1}h$).

Section S2.4. Kinetic model selection.

Statistical methods have been implemented in literature to evaluate and select competing models accounting for different sets of parameters. The most widely used are: the statistical F-test, the Akaike Information Criteria (AIC), and the Bayesian Information Criterion (BIC). Currently, BIC is preferred because it includes a penalty term greater than AIC for the number of parameters involved in the models (Kass & Raftery, 1995; Myung, Tang, & Pitt, 2009; Schwarz, 1978). BIC is calculated according to the equation:

$$BIC = N\,Ln\left(\frac{RSS}{N}\right) + p\,Ln(N)$$

Where, N is the number of data points, RSS is the sum of squared residuals, and p the number of model parameters. When evaluating a set of competing models, a model with the lowest BIC value is preferred. To corroborate the selection of the model ΔBIC = (BIC of a competing-model) – (BIC of the selected-model) is calculated to validate model selection[3] Table S5 is normally used as guidance:

Table S2.5. Evidence against high BIC.

Δ BIC	**Evidence against high BIC**
1 to 3	Not worth more than a bare mention
3 to 20	Positive
20 to 150	Strong
> 150	Very strong

Table S6 presents the BIC of the three kinetic models evaluated for the hydrodesulfurization of dibenzothiophene, i.e. DBT1S, DBT2S, and DBTBP2S. Among these models, DBTBP2S showed the lowest BIC. DBTBP2S was also found to have ΔBIC = 17 in comparison to DBT2S. These results justify choosing DBTBP2S over the other models.

Table S2.6. Bayesian Information Criterion (BIC) for the kinetic models of the hydrodesulfurization of dibenzothiophene.

Model	**Adsorption**		**Reaction**		**Number of Parameters**	**BIC**	**Δ BIC**
	Sites σ	**Sites π**	**Sites σ**	**Sites π**			
DBT1S	X		$DBT \rightarrow BP$ $DBT \rightarrow CHB$		12	1468	171
DBT2S	X	X	$DBT \rightarrow BP$	$DBT \rightarrow CHB$	20	1314	17
DBTBP2S	**X**	**X**	$\boldsymbol{DBT \rightarrow BP}$ $\boldsymbol{DBT \rightarrow CHB}$ $\boldsymbol{BP \rightarrow CHB}$		**22**	**1297**	**---**

For the simultaneous hydrodesulfurization of dibenzothiophene and hydrogenation of fluorene, the Model 4 having the largest number of parameters, i.e. 36 parameters, did not lead to the lowest BIC. Instead the model DBTFL having 32 parameters presented the lower BIC, vide Table S7. For the hydrodesulfurization of dibenzothiophene in the presence of phenanthrene a similar result was obtained. The model DBTPHE with 46 parameters presented the lowest BIC, while the Model 3 with 54 parameters led to the worst fit, vide Table S8.

Table S2.7. Bayesian Information Criterion (BIC) for the kinetic models for the simultaneous hydrodesulfurization of dibenzothiophene and hydrogenation of fluorene.

Model	Adsorption		Reaction		Number of Parameters	BIC	Δ BIC
	Sites σ	**Sites π**	**Sites σ**	**Sites π**			
1	X		$FL \rightarrow HHFL$		28	1200	375
2		X		$FL \rightarrow HHFL$	28	943	118
3	X	X	$FL \rightarrow HHFL$		32	1225	400
DBTFL	**X**	**X**		$\boldsymbol{FL \rightarrow HHFL}$	**32**	**825**	**---**
4	X	X	$FL \rightarrow HHFL$	$FL \rightarrow HHFL$	34	1235	409

Table S2.8. Bayesian Information Criterion (BIC) for the kinetic models for the simultaneous hydrodesulfurization of dibenzothiophene and hydrogenation of phenantrene.

Model	**Adsorption**		**Reaction**		**Number of Parameters**	**BIC**	**Δ BIC**
	Sites σ	**Sites π**	**Sites σ**	**Sites π**			
1		X		$PHE \rightarrow DHPHE$ $PHE \rightarrow THPHE$ $DHPHE \rightarrow OHPHE$ $THPHE \rightarrow OHPHE$	38	1637	138
DBTPHE	**X**	**X**		$\boldsymbol{PHE \rightarrow DHPHE}$ $\boldsymbol{PHE \rightarrow THPHE}$	**46**	**1499**	**---**

Model	Adsorption		Reaction		Number of Parameters	BIC	Δ BIC
	Sites σ	Sites π	Sites σ	Sites π			
				$DHPHE \rightarrow OHPHE$ $THPHE \rightarrow OHPHE$			
2	X	X	$PHE \rightarrow DHPHE$ $PHE \rightarrow THPHE$ $DHPHE \rightarrow OHPHE$ $THPHE \rightarrow OHPHE$	$PHE \rightarrow DHPHE$ $PHE \rightarrow THPHE$ $DHPHE \rightarrow OHPHE$ $THPHE \rightarrow OHPHE$	54	1711	212

Finally, in the case of the simultaneous reaction of dibenzothiophene and hydrogenation of naphthalene, the model DBTNP that contains more parameters than the competing models showed the lowest BIC, vide Table S9.

Table S2.9. Bayesian Information Criterion (BIC) for the kinetic models for the simultaneous hydrodesulfurization of dibenzothiophene and hydrogenation of naphthalene.

Model	Adsorption		Reaction		Number of Parameters	BIC	Δ BIC
	Sites σ	Sites π	Sites σ	Sites π			
1	X		$NP \rightarrow TTL$		28	1437	36
2		X		$NP \rightarrow TTL$	28	1533	132
3	X		$NP \rightleftarrows TTL$		30	1536	135
4		X		$NP \rightleftarrows TTL$	30	1547	146
5	X	X	$NP \rightarrow TTL$		32	1463	62
6	X	X		$NP \rightarrow TTL$	32	1447	46
7	X	X	$NP \rightleftarrows TTL$		34	1632	231
8	X	X		$NP \rightleftarrows TTL$	34	1608	207
9	X	X	$NP \rightarrow TTL$	$NP \rightarrow TTL$	34	1580	179
DBTNP	**X**	**X**	$\boldsymbol{NP \rightleftarrows TTL}$	$\boldsymbol{NP \rightleftarrows TTL}$	**38**	**1401**	**---**

Section S2.5. Reaction of the hydrogenation of biphenyl to cyclohexylbenzene.

Two different catalytic tests were carried out to verify the hydrogenation of biphenyl to cyclohexylbenzene. The first reaction was the hydrodesulfurization of dibenzothiophene (1 wt.%) under equilibrium conditions; i.e. with a conversion of DBT higher that 95%. The second test consisted on adding biphenyl (0.5 wt.%) to a DBT feed (1 wt.%). Both tests were performed at 300°C. For the first test, the yield to CHB was ca. 20% whereas for the second test the yield to CHB was ca. 26%. The latter represented a conversion of BP of ca. 10% as in regard to the 0.5 wt.% of added biphenyl, vide Figure S6. Therefore, we concluded that biphenyl hydrogenation to cyclohexylbenzene is kinetically slow yet significant under our reaction conditions.

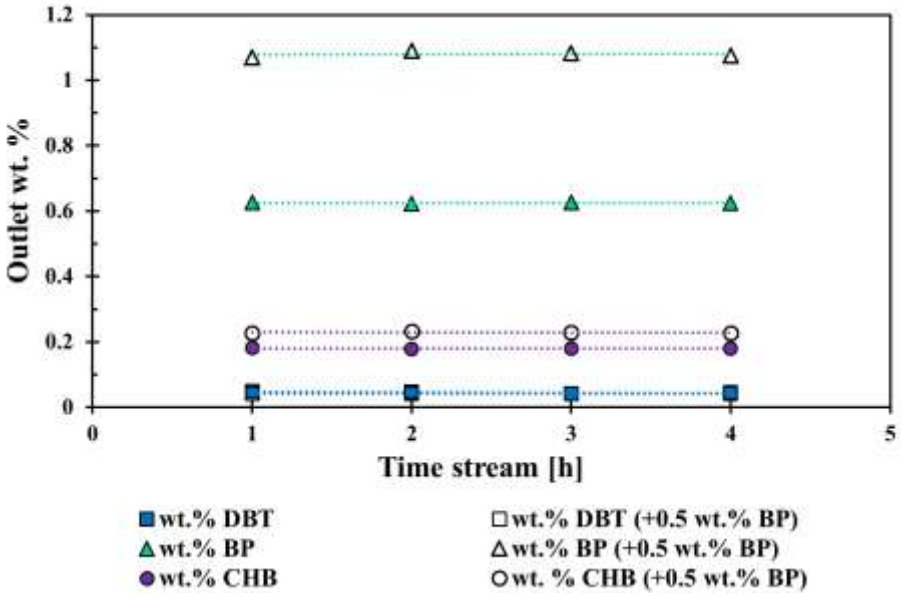

Figure S26. Catalytic tests for the hydrogenation of biphenyl to cyclohexylbenzene in the presence of dibenzothiophene over sulfided NiMo/γ-Al_2O_3. p = 5 MPa, T = 300 °C.

Section S2.6. Adsorption equilibrium constants and rates coefficients at 280°C for the reactions of hydrodesulfurization of dibenzothiophene, hydrogenation of naphthalene, fluorene, and phenanthrene.

Table S2.10. Parameter values derived from the data of HDS of DBT at 280°C.

Parameter	Value
$K_{DBT,\sigma}, kPa^{-1}$	0.3006
$K_{BP,\sigma}, kPa^{-1}$	0.0275
$K_{CHB,\sigma}, kPa^{-1}$	0.4271
$K_{H_2S,\sigma}, kPa^{-1}$	0.0012
$K_{DBT,\pi}, kPa^{-1}$	0.0047
$K_{BP,\pi}, kPa^{-1}$	9.7120
$K_{CHB,\pi}, kPa^{-1}$	7.3578
$K_{H_2S,\pi}, kPa^{-1}$	0.0011
$k_{DBT,\sigma}, kmol_{DBT}(kg_{cat}h)^{-1}$	1.1918
$k_{DBT,\pi}, kmol_{DBT}(kg_{cat}h)^{-1}$	0.4393
$k_{BP,\pi}, kmol_{DBT}(kg_{cat}h)^{-1}$	0.2950

Table S2.11. Parameter values derived from the data of the hydrogenation of naphthalene in the presence of DBT at 280°C.

Parameter	Value
$K_{NP,\sigma}, kPa^{-1}$	0.0003
$K_{TTL,\sigma}, kPa^{-1}$	0.0026
$K_{NP,\pi}, kPa^{-1}$	0.0008
$K_{TTL,\pi}, kPa^{-1}$	0.1957
$k^{F}_{NP,\sigma}, kmol_{NP}(kg_{cat}h)^{-1}$	0.6074
$k^{F}_{NP,\pi}, kmol_{NP}(kg_{cat}h)^{-1}$	0.7334
$k^{R}_{NP,\sigma}, kmol_{TTL}(kg_{cat}h)^{-1}$	0.5261
$k^{R}_{NP,\pi}, kmol_{TTL}(kg_{cat}h)^{-1}$	0.4452

Table S2.12. Parameter values derived from the data of the hydrogenation of fluorene in the presence of DBT at 280°C.

Parameter	Value
$K_{FL,\sigma}, kPa^{-1}$	0.0222
$K_{HHFL,\sigma}, kPa^{-1}$	0.4037
$K_{FL,\pi}, kPa^{-1}$	0.4415
$K_{HHFL,\pi}, kPa^{-1}$	10.8379
$k_{FL,\pi}, kmol_{FL}(kg_{cat}h)^{-1}$	0.6058

Table S2.13. Parameter values derived from the data of the hydrogenation of phenanthrene in the presence of DBT at 280°C.

Parameter	Value
$K_{PHE,\sigma}, kPa^{-1}$	0.0329
$K_{OHPHE,\sigma}, kPa^{-1}$	0.0210
$K_{DHPHE,\sigma}, kPa^{-1}$	0.0790
$K_{THPHE,\sigma}, kPa^{-1}$	0.2002
$K_{PHE,\pi}, kPa^{-1}$	0.0072
$K_{OHPHE,\pi}, kPa^{-1}$	29.9172
$K_{DHPHE,\pi}, kPa^{-1}$	0.5323
$K_{THPHE,\pi}, kPa^{-1}$	1.7570
$k_{PHE-THPHE,\pi}, kmol_{PHE}(kg_{cat}h)^{-1}$	2.855
$k_{PHE-DHPHE,\pi}, kmol_{PHE}(kg_{cat}h)^{-1}$	0.838
$k_{DHPHE-OHPFE,\pi}, kmol_{DHPHE}(kg_{cat}h)^{-1}$	0.221
$k_{THPHE-OHPHE,\pi}, kmol_{THPHE}(kg_{cat}h)^{-1}$	14.901

References

Kass, R. E., & Raftery, A. E. (1995). Bayes Factors. *Journal of the American Statistical Association*, *90*(430), 773–795. https://doi.org/10.1080/01621459.1995.10476572

Myung, J. I., Tang, Y., & Pitt, M. A. (2009). Chapter 11 Evaluation and Comparison of Computational Models. *Methods in Enzymology*, *454*, 287–304. https://doi.org/10.1016/S0076-6879(08)03811-1

Schwarz, G. (1978). Estimating the Dimension of a Model. *The Annals of Statistics*, *6*(2), 461–464. https://doi.org/10.1214/aos/1176344136

Appendix C. Supplementary Information Chapter 3

Table S3.1. Kinetic models for the simultaneous hydrodesulfurization of dibenzothiophene and hydrodenitrogenation of quinoline.

Model	**Adsorption**		**Reaction**	
	Sites σ	**Sites π**	**Sites σ**	**Sites π**
1	X	X	$Q \rightarrow 14THQ$	$Q \rightarrow 14THQ$
	X	X	$14THQ \rightarrow DHQ$	$14THQ \rightarrow DHQ$
	X	X	$14THQ \rightarrow OPA$	$14THQ \rightarrow OPA$
2		X		$Q \rightarrow 14THQ$
		X		$14THQ \rightarrow DHQ$
		X		$14THQ \rightarrow OPA$
DBTQ	X	X	$Q \rightarrow 14THQ$	$Q \rightarrow 14THQ$
	X	X	$14THQ \rightarrow OPA$	$14THQ \rightarrow DHQ$

Table S3.2. Kinetic models for the simultaneous hydrodesulfurization of dibenzothiophene and hydrodenitrogenation of indole.

Model	**Adsorption**		**Reaction**	
	Sites σ	**Sites π**	**Sites σ**	**Sites π**
DBTIND	X	X	$IND \rightarrow HIN$	$IND \rightarrow HIN$
	X		$HIN \rightarrow OEA$	
1		X		$IND \rightarrow HIN$
	X		$HIN \rightarrow OEA$	
2	X		$IND \rightarrow HIN$	
	X		$HIN \rightarrow OEA$	